POLITECNICO DI MILANO

School of Industrial Engineering and Information
Department of Aerospace Science and Technology
Master of Science in Aeronautical Engineering

ANTROPOMORPHIC TEST DEVICE AND TOTAL HUMAN MODEL HEAD AND NECK INJURY ANALYSIS BASED ON EXPERIMENTAL AND NUMERICAL ACTIVITY

Advisor: **Prof. Marco Anghileri**

Coadvisors: **Ing. Davide Benetton**
Dr. Mario Mongiardini

M.Sc. Thesis by:
Benedetta Arosio - ID: 803740

Academic Year 2014/2015

To my grandmother Dora.

"Il giorno fu pieno di lampi;
ma ora verranno le stelle,
le tacite stelle."

G. Pascoli

Sommario

La prima parte di questo lavoro è stata la ricerca di correlazione tra il modello reale di manichino Hybrid III e il corrispondente numerico. Per fare questo si sono effettuati test sperimentali sul manichino, i cui risultati sono poi stati confrontati con gli esiti delle simulazioni numeriche. La prima categoria di test è stata condotta facendo impattare un pendolo di 23.1 kg a una velocità di 1.428 m/s sulla testa del modello sperimentale in tre direzioni: frontale, laterale, dall'alto; la seconda categoria di test è stata effettuata sul manichino completo: test di caduta verticale a tre diverse altezze (0.08 m, 0.16 m e 0.24 m), contro una superficie prima orizzontale poi inclinata di 15°.
I dati ottenuti dai test sperimentali sono stati confrontati con i risultati numerici grazie alla riproduzione in LS-DYNA degli scenari sperimentali. La seconda parte del lavoro ha riguardato l'analisi del modello di corpo umano THUMS (Total HUman Model for Safety) di nuova generazione, con particolare attenzione al comportamento di collo e testa, come fatto per Hybrid III. L'analisi si è poi incentrata sulla ricerca di criteri di lesione che possono essere ritenuti validi nell'ambito della crashworthiness.

Parole chiave: THUMS, Hybrid III, HIC, ATD, criteri di lesione alla testa, drop test, FEM, LS-DYNA.

Abstract

The first aim of this study is to determine the level of correlation between the Hybrid III ATD (Antropomorphic Test Device) and its numerical model. This has been achieved by impacting a Hybrid III head-form with a 23.1 kg impactor at 1.428 m/s. Three different directions were selected for the impactor (frontal, lateral and upper direction with respect to the dummy head), and two different configuration for the neck stiffness.
A second scenario was analysed: inverted drop tests of the 50th percentile Hybrid III ATD at three different heights (0.08 m, 0.16 m and 0.24 m) against an horizontal plate first and, subsequently, a 15°inclined plate. The kinematic data obtained was then compared to the results obtained from simulations with the finite element model of the Hybrid III head and neck.
The second objective of this thesis was to analyse the Total HUman Model for Safety (THUMS) with particular attention to its head and neck behaviour. The study was focused on the comparison between THUMS and Hybrid III with the objective to understand whether THUMS good biofidelity could be useful in the study of crashworthiness situations as low speed frontal and side impact, and inverted drop tests.

Keyword: THUMS, Hybrid III, HIC, ATD, head injury, drop tests, Finite Element simulations LS-DYNA.

Acknowledgements

I would like to acknowledge and thank all the people that has supported me throughout the path of my study and in particular the process of writing this thesis.
I would first like to thank my supervisor Prof. Marco Anghileri for giving me the possibility to know the fascinating world of manikin and human model and for giving me the opportunity to go upside-down. Thanks to Mario Mongiardini who greatly helped me in Sydney with his expert technical advice and not only. Great thanks also to Garrett, the THUMS expert, and his wife Jacqueline, who opened their house for me and welcoming me from the very beginning. Thanks also to the entire TARS staff at UNSW.
A special thanks to everyone working at LaST: Davide, who always answered with great patience to me, Sergio, Matteo and Michele, thanks for your knowledge and your time; thanks also to Alessia, Silvia, Adriano, Andrea, Mirko.
Thanks to all my "collegues": Gabriele, Andrea, Cristina, Maria, Edoardo, Chris, Matteo, Giulia; thanks for the help, the reciprocal support and the sweets. Thanks to Pat. I think I would not be here without your great help and your patience...but now it's time for my flower! Thanks to Exoco, each of you taught me something. Thanks to Matteo, Riccardo and Federica.
Thanks to Paolo, Giacomo, Lorenzo, Arianna (yes, you are here!) and Veronica and to our Sunday night. Thanks to Federica: you taught me to take notes!
Thanks twice to Veronica. No need to explain.
Thanks to my grandmother Dora. You are always here with me. Thanks to my uncle Rorro. Your teaching and your passion guided me here.

Thanks to my Mum –Mum, I love you till the Moon and beyond– and my Dad. Thanks for your great constant love and support. I know I can always count on you. Thanks to my little big sister. You are my best half and I'm so proud to be copied by you!
Thanks to my super best friend, Marco. You are my strength, my (BB) lighthouse, my Space man. Thank for your never ending love.

Contents

List of Figures

List of Tables

Chapter 1

Introduction

This chapter aims at briefly introducing the reader to what has been analysed in this work. It also gives basic description of the Anthropomorphic Test Device (ATD) used for the experimental tests, the tests configurations, the numerical FE models analysed in the simulation and the motivation of the tests choices.

1.1 Work objectives

Cervical spine and head injuries –in particular Traumatic Brain Injury (TBI)– can occur in various circumstances. For this reason and because of the severity of their consequences, head and neck injuries have been studied extensively using animals [7], human cadavers [4, 6, 8, 9] and live volunteers [7]. Starting from the late 1940s, the introduction of Anthropomorphic Test Device increased the repeatability of the tests and started a new method to investigate crash situations and fatalities suffered by occupants of vehicles involved in collisions.
Recent advances in computer technology allowed the use of numerical simulation in crashworthiness research and offer an invaluable engineering tool, as much as experimental tests. The computational model can be run repeatedly, with the possibility of changing parameters without a huge amount of costs and time, as happens with the experimental tests.
The development of Finite Element model of Anthropomorphic Test Devices rapidly increased during the last decades also due to the appli-

cability in automotive safety: the simulations with ATD dummies are very useful to understand how injuries of occupants and pedestrian occur. In addition, computer simulations can directly predict the injuries outcome from virtual crash situations. However, computational models are useless unless it has been proven that they can accurately replicate results from experimental testing. This is the motivation of the first part of this work, which compares the experimental test conducted on a Hybrid III head-form with the Hybrid III dummy model improved at LaST (LAboratorio per la Sicurezza dei Trasporti[1]) at Politecnico di Milano on the base of the *LSTC H3 103008 V1.0 Rigid FE.50th*, downloadable from *LSTC* website [10].

Even if real world dummies are based on the human being structure, they have limited biofidelity because of the necessity to implement a durable platform for repeatable testing. In fact, kinematics of humans are different compared to dummy behaviour in a collision [7]. To overcome this obstacle and to better predict the response of a human body, finite element human body models have recently been developed: THUMS is one of those. Since THUMS is relatively new, there have been limited studies to establish its kinematic performances. The aim of this activity is to evaluate and compare the behaviour of the THUMS model with the Hybrid III FE Model. The comparison consists in both a numerical and experimental approach. In particular, the study focused on the investigation of the head and neck responses. Two test setups have been analysed in the activity: the first test seriess can be labelled as *head test* (or *impactor test*), in which only head and neck components have been considered; the second one is the *drop test* involving the whole dummy. The experimental tests were conducted on a Hybrid III 50^{th} percentile male dummy and have been modelled and simulated with both a Hybrid III[2] model and THUMS, *Academic Version 4.02*.

Simulation with THUMS has been performed at the University of New South Wales (UNSW, Sydney, Australia) at Transportation and Road Safety (TARS) department.

Numerical models are ideal for use in studies which investigate the effects of multiple parameters on one or many different outcomes. They

[1] Lab for Transport System Safety

[2] In particular, the HIII model improved at LaST

have been used increasingly to study the response of the human body, as they provide an efficient and cost-effective method of performing many virtual tests without the challenges associated with physical experimentation such as variation in specimen characteristics and test conditions. In the case of finite element human body models there is the benefit that internal response measurements, i.e. bony fracture, ligament rupture, internal organ injury, can be evaluated. Additionally, the response of the body is typically not affected by these measurements as they do not require mounting physical sensors to the parts of interest such as in the case of physical specimens, i.e. force transducers and accelerometers. However, the use of numerical methods requires a highly detailed and accurate model to ensure valid results. The THUMS, which has been continually improved since 1997, is one of the most detailed human body models commercially available. Starting with Version 4, it is possible to simulate not only bone fracture and internal organ injuries but also head injuries. High-resolution CT scans were used to accurately represent the geometry of the human body and the internal organs.
Version 4.02 was released for AM50 in May 2015. The number of elements were increased and the stability of calculation were improved.

1.2 Main purpose and problem definition

In the first phase of the present work, the behaviour of the head and neck Hybrid III numerical model has been compared and validated with the results of experimental tests performed at LaST on the Hybrid III dummy. Then, the same test configurations have been reproduced with THUMS; different strategies to evaluate the values of interest –such as linear acceleration and forces– have been investigated since THUMS has no instrumentations. Eventually, the results obtained with THUMS has been correlated to the same data derived from Hybrid III.
The comparison has been performed looking in particular at:

- head linear acceleration;
- neck forces and moments.

Those parameters measurements were the base for calculating the main injury criteria of interest in this study:

- HIC_{15}: Head Injury Criterion;
- NIJ: Normalized Neck Injury Criterion;
- MOC: Total Moment about Occipital Condyle.

1.3 Injury Criteria

Accelerations, forces and moments in head and neck are measured during both the experimental tests and the simulations, and are compared with human injuries via so-called *injury criteria*. These are mostly of statistical nature and are often based on evaluations and observations of real-life accidents. Nevertheless, injury criteria relate the mechanical responses of crash test dummies in terms of risk to life or injury to a human being. Therefore, calculating head accelerations and neck loadings is essential to understand and predict head and neck injury and the consequences of the crash situation on a living human.
Injury criteria are based on the engineering principle that the internal responses of a mechanical structure are uniquely governed by the structure's geometry and material properties and the forces and motions applied to its surface [11]. They have been derived from experimental efforts using human surrogates where both measurable engineering parameters and trauma consequences are observed and the most meaningful relationship between forces/motions and resulting injuries are determined using statistical techniques.
In addition with the differences between human beings, the level of tolerance evaluation is difficult because that information is obtained through indirect methods, such as animal and cadaver testing, human volunteers below the injury level, crash tests dummies and computer simulations.
A brief description of the crash analysis criteria of interest is hereby presented. The descriptions show the name and the equations used to compute the criteria [12], [11], which are compliant with ISO TS 13499 norm and SAE J1733 Sign Convention [1] (Figure 1.1).

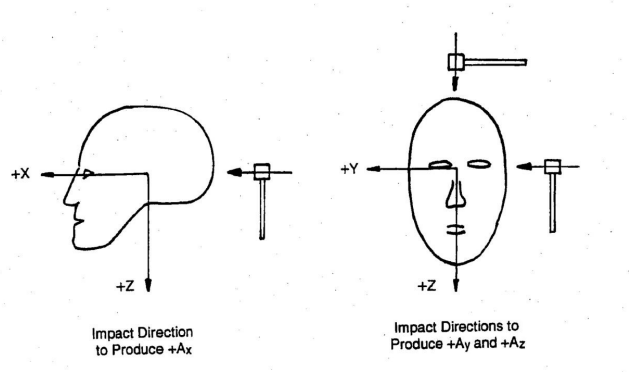

Figure 1.1: Head impact directions that produce positive head accelerations relative to the head coordinate system [1].

HIC

Head Injury Criterion is the standardized parameter to evaluate head acceleration. It is based on the time history of the resultant acceleration from the three spatial directions and its time duration. High head accelerations developed in short period of time will can be tolerated by the human brain, and the longer the period an acceleration is applied, the lower is the safe threshold.

HIC has been developed taking into account the Wayne State Tolerance Curve (WSTC). The WSTC was developed at the Wayne State University during the fifties. A variety of different experiments were performed with heads from human cadavers and dogs in conditions similar to those found in the automobile environment. It was found that head injury –defined as the occurrence of a linear fracture– is correlated with the magnitude of linear acceleration and pulse duration –angular acceleration was not measured–. These data and data from tests with volunteers for low–g long–duration exposure were plotted in the same graph and the Wayne State curve was drawn up (Figure 1.2). The equation for the WSTC curve is [13]:

$$a^{2.5}t = 1000 \tag{1.1}$$

where

a = average acceleration in g;

t = duration of the phenomenon in s.

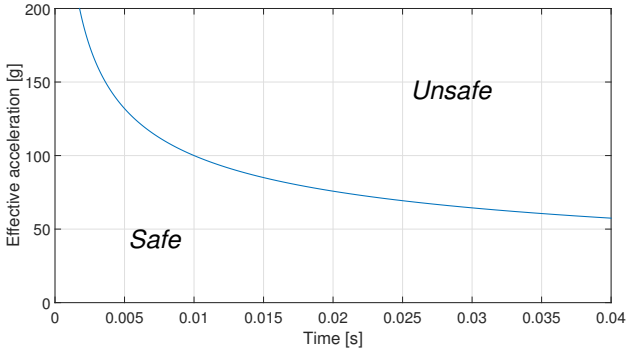

Figure 1.2: Wayne State Curve.

After many alteration and lots of discussion between the scientific and legal communities, the Formula 1.3 was finally adopted.

$$HIC_{15} = max\left[(t_2 - t_1)\left(\frac{1}{(t_2 - t_1)}\int_{t_1}^{t_2} a(t)dt\right)^{2.5}\right] \tag{1.2}$$

$$a(t) = \sqrt{a_x^2 + a_y^2 + a_z^2} \tag{1.3}$$

where:

a(t) is the resultant acceleration of the Centre of Gravity (CG) of the head in units of acceleration of gravity, 1g = 9.81 m/s^2;

t_1, t_2 are two arbitrary times during the acceleration pulse; the time interval over which HIC_{15} is calculated was limited to 0.015 seconds.

A HIC_{15} value of 700 is the maximum allowed: it is estimated to represent a 5 percent risk of a severe injury; a *severe* injury has a score of 4+ on the Abbreviated Injury Scale (AIS)[3].
All head acceleration signal are filtered in accordance to the regulation, SAE J211 [14] with CFC 1000 (for CFC filter description, look at Appendix A).

MOC

MOC is the acronym for *total Moment about Occipital Condyle*:

[3]the Abbreviated Injury Scale (AIS) is an index which is intended to give a measure of the severity of injuries. AIS score goes from 1 to 6, with 1 being minor, 5 severe and 6 a deadly injury

- MOC_x = total lateral bending moment about Occipital Condyle;
- MOC_y = total flexion/extension moment about Occipital Condyle.

It deals with forces and moments measured with the *upper neck load cell*, and evaluates the total moment at the Occipital Condyle:

$$MOC_x = M_x + DF_y$$
$$MOC_y = M_y - DF_x$$

where:

$\mathbf{M}_i$ represents the neck moments in i direction [Nm];

$\mathbf{F}_i$ represents the neck forces in i direction [N];

D represents the distance between the upper neck load cell and the condyle axis. It depends on the load cell type. In this case $D = 0.01778\ m$ [12], related to the *Denton Load Cell*, model IF-205.

The maximum admissible values for MOC are presented in Table 1.1.

MOC	Maximum admissible value [Nm] [15]
MOC_x	134
$MOC_{y_{extension}}$	57
$MOC_{y_{flexion}}$	190

Table 1.1: MOC maximum admissible values.

The forces and moments are filtered in accordance with the regulation SAE J211 [14] with filter CFC 600 (Appendix A).

NIJ

The Normalized Neck Injury Criterion (NIJ) consists of individual tolerance limits for compression, tension (force stretching the neck), flexion and extension moment (forward and reward bending of the neck). The tolerance values are based on volunteers, cadavers and dummy tests. NIJ can not exceed 1.0 at any point in time. NIJ is a linear combination of the normalized neck axial load (tension or compression) and normalized neck moment about occipital condyle. The criteria are named N_{ij} with the i and j as indices for the four injury mechanism:

- N_{TE}: tension-extension;
- N_{TF}: tension-flexion;
- N_{CE}: compression-extension:
- N_{CF}: compression-flexion.

The NIJ are evaluated as the sum of the normalized loads and moments with respect to the critical values defined for tension, compression, extension and flexion [11], [16], [15].

$$N_{ij} = \frac{F_z}{F_{crit}} + \frac{M_y}{M_{crit}} \tag{1.4}$$

where:

$\mathbf{F}_z$ is the axial load, tension or compression;

$\mathbf{F}_{crit}$ represents the critical value of load used for normalization:

- Tension load critical value: F_{Tcrit} = 6806 N;
- Compression load critical value: F_{Ccrit} = -6160 N.

$\mathbf{M}_y$ represents the bending moment, flexion or extension;

$\mathbf{M}_{crit}$ is the critical value for moment used for normalization:

- Flexion moment critical value: M_{Fcrit} = 310 Nm;
- Extension moment critical value: M_{Ecrit} = -135 Nm.

Both the forces and moments have to be filtered in accordance to the regulation, SAR J211 [14], with CFC 600 (Appendix A).

1.4 Thesis structure

The thesis is organized in the following chapters:
Chapter 1: brief introduction to the activity;
Chapter 2: literature review;
Chapter 3: experimental tests performed;
Chapter 4: numerical analysis: Hybrid III and THUMS;
Chapter 5: conclusion, discussion and future developments.

Chapter 2

State of the Art

A brief historical overview on dummies, Anthropomorphic Test Devices and their numerical models, is here presented to show their development from humans to mannequins to human-like mannequins and to introduce the reader to the starting point of the activity.
The main reason that pushed the development of dummy models (real-world and numerical) was the integration of the human aspect into automotive crash situations, to develop and size protective safety systems in accordance with the more stringent safety requirements and, most important, to reduce the injury risk in real-life accident situations.

2.1 Crash Tests Dummy history

The first crash test dummies may have been the best, most responsive and most lifelike dummies in history: they were actual people. Colonel John Paul Stapp [1], can be considered as the crash test pioneer. He began a crash test study program to test the efficacy of seat belts, of doors with safety locks –innovation introduced by Stapp himself in car safety– , of dashboards with energy-absorbing padding and other several innovative features. To evaluate the innovation, he put dummies into salvage cars and crashed them into wood or concrete barriers. The

[1] Colonel John Paul Stapp (11 July 1910, 13 November 1999) was an American career U.S. Air Force officer, flight surgeon, physician, biophysicist, and pioneer in studying the effects of acceleration and deceleration forces on humans. Because of his work, he became famous as *the fastest man on earth*. He studied human tolerances to extreme environments and the related limit of survivable.

dummies were nothing else than humans volunteer and –usually for the highest conditions– Col. Stapp himself. While his insight was crucial to developing safety tests and procedures for the automotive industry, having human volunteers proved to be unfeasible, so they have been replaced with the inanimate crash test dummies still in use today.
Before the introduction of crash test dummies, cadavers, chimpanzees, pigs and other animals were often used in tests.

Figure 2.1: Sierra Sam.

It was 1949 when *Sierra Sam*, shown in Figure 2.1, was created by Samuel W. Alderson, at his Alderson Research Labs (ARL), together with Sierra Engineering Co., under a contract with the United States Air Force (USAF). It was used for evaluation of aircraft ejection seats on sled tests, and to test aviation helmets and pilot restraint harnesses.

Its construction has been possible thanks to the information derived from cadaver tests and researches on animals performed in the previous years.
The dummy was a 95^{th} percentile male dummy, which means that it represented a man heavier and taller than 95% of human males; the dummy was built on anthropometric data based on *"Anthropometry of USAF Personnel"*. The *Sierra Sam* biofidelity was limited to its human-like exterior shape, its weight and height and, partially, the ranges of motion of its articulated limb joints. Neither the instrumentation installed was particularly comprehensive: it was possible to measure only orthogonal linear head acceleration components. As a consequence, it became rapidly quite useless.
In the early 1950s *Sierra Sam* was improved and became suited to conduct crash tests in both motor vehicles and aircraft; it was produced again by Alderson with the collaboration of Grumman. It was called *Gard Dummy*.
The first Hybrid model was born in 1971 from the needs of General Motors to have a reliable and durable dummy. The model was a combination of the best features of the VIP (Very Important People) series (the one produced by Alderson) and Sierra Stan (the rival model produced by Sierra Engineering).
The Hybrid I is known also as the 50^{th} percentile Male Dummy: it represents a man heavier and taller than 50% of human males. However, as for the Sierra Sam and every other dummy, the data from which its anthropometric values are obtained came from the soldiers of the U.S. Air Force. This first Hybrid model has been rapidly surpassed by two new models developed one after another in few years, at the end of the '70s: in 1972 the General Motors introduced the Hybrid II and in 1976 the Hybrid III born. It is explained in detail in the following section.
The technology of these early dummies provided the foundation to create automotive crash test dummies in the early 1960s. Since then, technological advances have contributed to constant improvements in the capabilities, quality and accuracy of crash test dummies.

2.1.1 Hybrid III

Figure 2.2: Hybrid III-50th percentile male crash test dummy.

The Hybrid III-50th percentile male crash test dummy is the most widely used crash test dummy in the world, mainly for the evaluation of frontal crash testing. Originally developed by *General Motors*, the Hybrid III 50th design is now maintained and developed by *Humanetics* in conjunction with the *Society of Automotive Engineers' (SAE) Biomechanics Committees* and the *National Highway Transport and Safety Administration (NHTSA)*.
The dummy is a regulated test device in the USA Code of Federal Regulations (Part 572, Subpart E [17]) and also in the European ECE Regulations. It is considered to have excellent biofidelity and instrumentation capability.
The main difference between Hybrid III and the previous Hybrid II is the improvement in some details: a curved lumbar spine was used in the Hybrid III to achieve a more human-like automotive seating posture, the shoulder structure was designed to improve belt-to-shoulder interfacing, which was a problem with the Hybrid II. Also the neck design was changed to improve the impact response biofidelity and the same

has been done for the chest and knees.
It is important to highlight the measurement capacity of the fully instrumented Hybrid III. It provides 44 response measurements [3]. As an example, in Table 2.1 a list of the main instrumentation of the Hybrid III used in this work is reported:

Measurement	Data Channel
Head:	6
Accelerometers	a_x, a_y, a_z
Gyroscopes	ω_x, ω_y, ω_z
Neck:	6
Upper Neck Load Cell	F_x, F_y, F_z, M_x, M_y, M_z

Table 2.1: Measurement capacity in head and neck.

Figure 2.3: Hybrid III family.

To enhance the results spectrum, Hybrid III-50^{th} percentile was joined by a whole family, shown in Figure 2.3:

- 5^{th} percentile female dummy;
- 10-year old child;
- 6-year old child;
- 3-year old child.

In order to be able to analyse the dynamic response of a larger size person and compare the crash effects onto persons of different build and sizes, the 95^{th} percentile were introduced, thus including the 95% of the population height and weight under the ones of this dummy model. In Table 2.2 some anthropomorphic data regarding the Hybrid III family models and the 95^{th} percentile dummy are listed.

Hybrid Model	**Anthropometric data**		
	Mass [kg]	Stature [m]	Total sitting hight [m]
5^{th}	49	1.4986	0.7874
50^{th}	77.70 $\pm$ 1.18 [a]	1.7458	0.8839
95^{th}	101.15	1.8502	0.9347
3-year old	16.17	0.94488	0.5461
6-year old	23.4	1.1405	0.635
10-year old	35.2	1.2014	0.7239

Table 2.2: Anthropometric data for different Hybrid III models [3].

[a] The weight variation is related to the presence or not of the complete instrumentation

The dummies can also be used in many non-automotive applications such as wheelchairs, medical and sport equipment.
According to [18], dummies must be capable to meet at least five requirements in order to be practical and useful:

1. reproducibility: two identical ATDs should respond in the same way under the same conditions and they should generate the same measurement values;

2. repeatability: the ATD should generate the same responses when repeated tests are conducted under the same initial conditions;

3. biofidelity and anthropometry: how faithfully the ATD simulates the physical characteristics of a human being (mass, heigh, body inertia) and its response to specific condition tests;

4. durability: due to cost and sustainability reasons, a dummy model is required to endure multiple crash test situations, maintaining its integrity;

5. measurement accuracy: calibration standards are defined in order to insure that the measurements made by an ATD are accurate.

2.2 Finite Element Models

Finite Element model of Anthropomorphic Test Device (ATD), commonly known as crash test dummies, have become increasingly applicable in automotive safety. Lots of ATDs models are widely used in many crashworhtiness areas. With huge computational capability and the increasing acceptance of numerical simulations, the ATDs FE models have been improved, becoming more realistic and complex. There are lots of advantages in the use of a numerical ATD: numerical sensors allow the collection of the same data as in a real test but with the possibility of measuring them during the phenomena. Furthermore, experimental tests are difficult and expensive to arrange and numerical simulations represent a convenient way to reduce time and costs.
Nevertheless, experimental tests are essential because they represent the necessary reference to develop and validate the numerical models. The present work has dealt with the development process of two highly detailed frontal impact ATD models: Hybrid III 50^{th} percentile (LaST model) and THUMS 50^{th} percentile both for LS-DYNA FE code. Both these dummy models represent anthropometry of a 50^{th} percentile adult male. The main difference between the two is that the first is a dummy model, and the second is a human model.

2.2.1 Hybrid III: LSTC and LaST modified models

Livermore Software Technology Corporation (LSTC) offers LSTC dummy models, which are easily integrable with LS-DYNA®software. The Hybrid III numerical model is a finite element model of the real Hybrid III dummy. The original LSTC-H3.103008_v1.0 model has been modified at LaST at Politecnico di Milano. The developed model meant to assess aircraft seat crash performances and consists of the same component assemblies defined for the physical ATD: 103 parts and 5819 elements (1800 shells, 26 beams, 3984 solids and 9 discrete elements). The body joints of the ATD, which are a convenient approximation of

the body joints of the human body, are reproduced by numerical constraints (revolute and spherical joints). The interactions between parts are taken into account by defining the proper contact interfaces. The most evident difference with the original model is in the lumbar spine elements. Another important modification concerned the geometry of the cervical area.

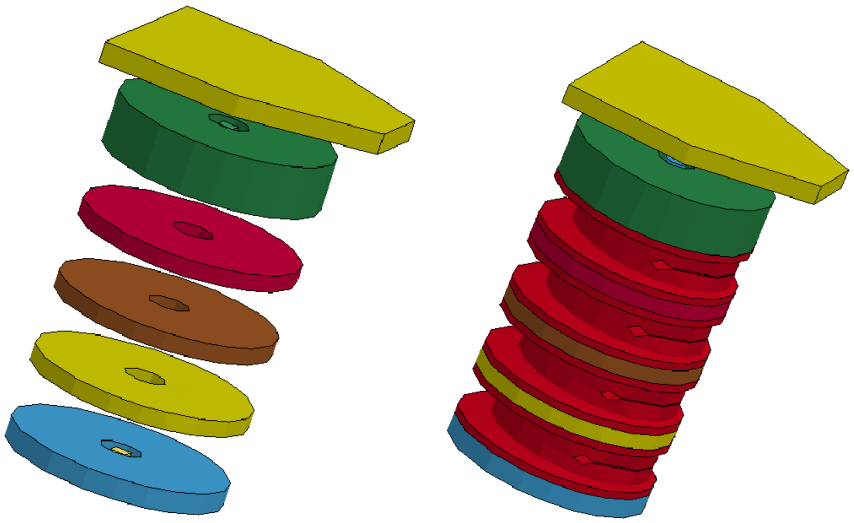

Figure 2.4: Comparison between Hybrid III cervical area: the LSTC original version and the LaST developed version.

Figure 2.4 shows the cervical details: the covering shell of the neck has been removed in order to allow the view of the internal neck structure. However, the differences are not totally visible: in the inner neck of the LaST Hybrid III model, a beam runs from the base of the neck until the upper neck; in the original LSTC model there is no beam through the inner neck (Figure 2.4, left), but there are some points with mass to replace the realistic neck inertial characteristics.

2.2.2 THUMS

Various numerical models of crash test dummies have been developed from the last decade of the 90s. Since the Hybrid III model (and its precursors) are related with the same class ATD real dummy, the newest

numerical model correlate themselves directly with the human being. THUMS is a finite element model of a human being. The model is produced by Toyota Central R& D Labs. The model includes skeletons, muscles, organs and other internal structures.

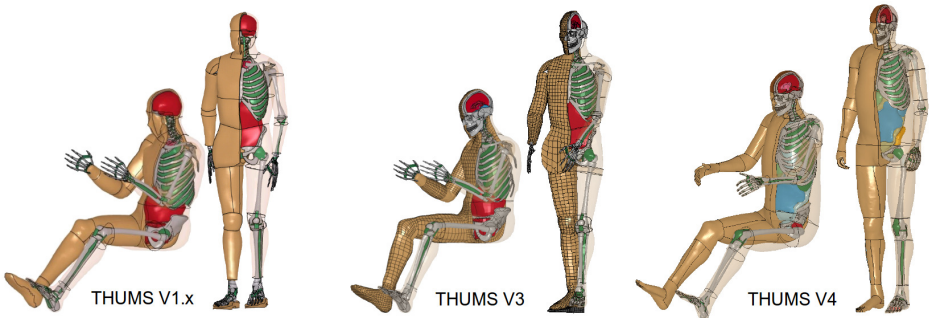

Figure 2.5: THUMS, Total HUman Model for Safety.

THUMS aims to simulate human body kinematics and injury responses in particular in car crashes. The geometries of the human body parts are represented by Finite Element meshes and their material properties are defined assuming constitutive laws. The THUMS version used in this work is the AM 50^{th} percentile model, which has a height of 1.75 m and a weight of 77 kg. There are also other versions and variations of THUMS: a small size female, AF 05%ile model and a large size male, AM 95^{th} percentile model. Each model has two postures: one is the sitting posture, representing the car occupant, and the other –the one used here– is a standing posture, representing a pedestrian. The first version of THUMS was completed in 2000. In this version the brain and internal organs were simplified as solid parts but the major bones and ligaments were modelled. The motion between bones were simulated as relative motion without the use of kinematic joint elements. The total number of elements was around 80000 with an average mesh size of 15 mm.

The second 2004 version introduces some modification in the facial bone parts to simulate fracture.

The third version was generated in 2008 and a detailed brain model was introduced for simulating brain injury. The total number of element was around 130000.

The forth version is the latest model; it was released in 2010. The

model has internal organ parts to simulate their injuries. The total number of elements is around 2000000.
The precise geometrical data for the internal organs of THUMS have been generated from high-resolutions CT (computer technology) scans. The CT scans were originally performed for medical purpose. A data set of a 39-year old male [2] was selected for the AM50 model. It had a weight of 77.3 kg, a height of 173 cm, and a BMI (body mass index) of 25.8. The scanned data –Figure 2.6 shows images of the skin, skeleton and soft tissues included in the scanned data– only included the torso part.

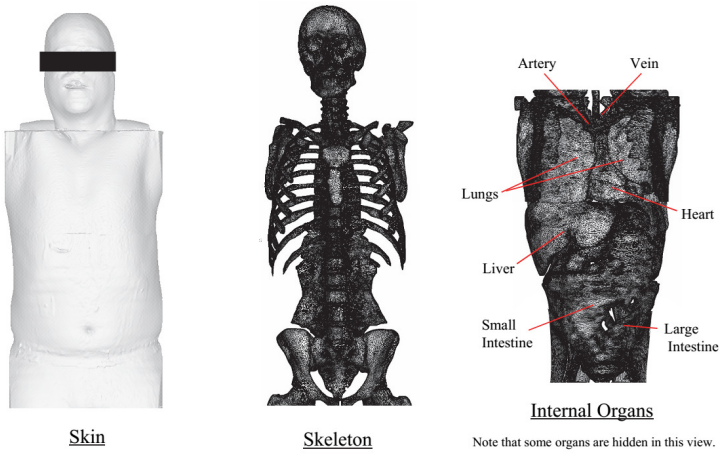

Figure 2.6: Digitized Human Body Data.

Chapter 3

Experimental Tests

"Don't you be a dummy, buckle your safety belts...
and leave the crashing to us!"

The Incredible Crash Dummies

At present, the Hybrid III dummy is the most used available human surrogate for dynamic tests. Loading is measured and specified only at the occipital condyles. The Hybrid III neck bending stiffness, peak injury measures, and onset criteria are based on tensed volunteer musculature.
The experimental tests conducted took entirely place in the Laboratory of Transport Safety, LaST, at Politecnico di Milano; they consisted in two completely different tests: the first set regards the only head and neck components, the second one involve the complete Hybrid III ATD. Both these series of tests were conducted to evaluate the behaviour of the Hybrid III dummy available at LaST, and, in particular, of its neck. The dummy was instrumented with head accelerometer and upper neck load cell in order to record accelerations, forces and moments. Those were collected for the following comparison with the numerical simulation results.

3.1 Tests introduction

The experimental tests were conducted using the Hybrid III dummy, which is firmly established as a device for estimating the human response

to inertial and, more recently, axial loadings [19]. The experimental tests conducted had the main purpose of creating a collection of data regarding the dummy response in some simple impact configurations in order to evaluate the level of reliability of the Hybrid III used in simulations. The second aim of this activity is to evaluate the THUMS reaction in comparison with the Hybrid III model, which is widely used since the 1970s and is currently used in standards for evaluating the safety of cars.
The tests performed can be divided in two groups:

- impactor tests on the head and neck;
- drop test on the complete Hybrid III body.

A total of 18 head tests with head and neck and 36 drop tests with the whole dummy has been performed. The two set-ups are hereby described in details.

3.2 Instrumentations

In both test series, a Hybrid III 50^{th} percentile male (Figure 2.2) has been used. Its head was instrumented according to the Code of Federal Regulation, Part 572E [17]. The Hybrid III instrumentation used allowed the measurement of three linear accelerations at its head centre of gravity, six upper neck forces and moments and three angular displacements.

3.2.1 Upper Neck load cell and accelerometers

Inside the aluminium skull three accelerometers measure the three linear accelerations of the ATD's head center of gravity (CG), whereas a 6-Axis Upper Neck Load Cell (model IF-205, Figure 3.1) evaluates three upper neck forces and three upper neck moments about the load cell position.

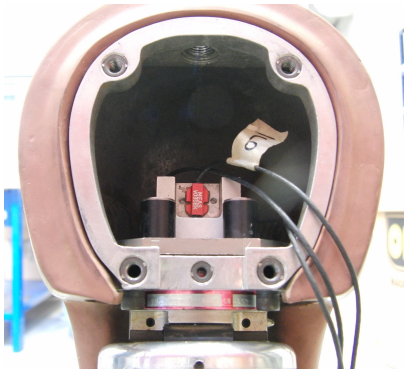

Figure 3.1: Head Load cell, IF-205.

Nine data channels were recorded using a Data Acquisition System (DAS) sampling at the frequency of 12500 Hz:

- x-force, y-force, z-force, [N];
- x-moment, y-moment, z-moment, [Nm];
- x-acceleration, y-acceleration, z-acceleration, [g].

Data was recorded using a TDAS Pro data acquisition system, processed according to SAE J211 standards [14]. The DAS was connected to a personal computer in order to set the acquisition configuration for each test and to save the measurements in ascii format. In Table 3.1 the general configuration of the DAS are presented.

Sampling frequency	12500 Hz
Filter	Low-pass filter, 2500 Hz

Table 3.1: Configuration of the acquisition system.

3.2.2 Impactor

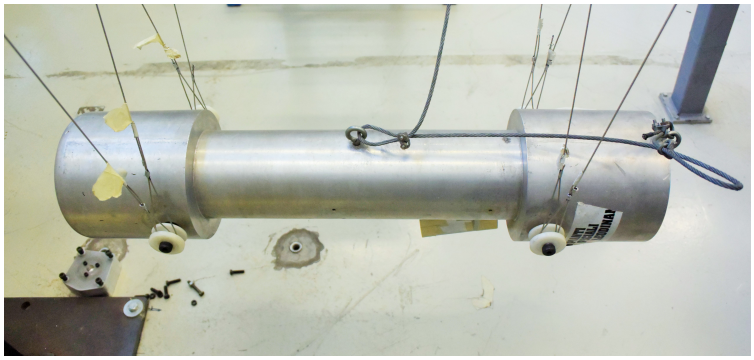

Figure 3.2: Impactor used in the head tests.

Mass [kg]	23.1
Radius [m]	0.075
Length [m]	0.7
Height from ground[a] [m]	0.737

Table 3.2: Impactor geometry.

[a]Measured in the pendulum equilibrium position

The impactor is hung on a frame through eight cables pinned on it in a manner that the impactor can remain horizontal during the motion. The complete frame is 4.5 $\times$ 1.6 $\times$ 1.6 m.
The head and neck assembly was housed on a basement 0.485 m high and it allows to have the three desired configurations for the frontal, lateral and upper impactor scenarios. It has been used as a reference to describe the point where the impactor hits the head.

3.2.3 High-speed camera

Figure 3.3: Phantom v5 used to acquire video frame.

A high-speed camera –Phantom v5 (Figure 3.3)– was used to acquire videos of each impact test at 400 frames per seconds. The videos were used to evaluate the pendulum velocity and the condyle plane rotation during each impact to evaluate the impact event from a global and qualitative point of view. The velocity measurement was possible thanks to a graduated ruler mounted behind the head-neck assembly. The video allowed to fix two different instants during the impact motion and to evaluate the distance in space (looking at the graduated ruler) and time between them. Using the basic equation for the velocity calculation (variation of space over variation of time), an impact velocity of 1.428 m/s has been obtained for every impact.

3.2.4 Gyro

Three single axis DTS ARS- rate gyro was added at the Hybrid III dummy head centre of gravity. As a first approach, the angular displacement of the head was determined by video analysis; however, in addition, it was obtained through numerical integration of the data from the rate gyro.

3.3 Head and neck tests

The purpose of these tests was to investigate the response of Anthropomorphic Hybrid III head and neck components in frontal, lateral and upper impact and to evaluate the Injury Criteria. The collection of those data made possible the comparison of them with the one coming out of the numerical simulations.
The Hybrid III 50^{th} percentile male head-form mounted on the corresponding neck was used. The geometry characteristics are collected in Table 3.3 for the head and in Table 3.4 for the neck.

Head			
Mass [kg]	Circumference [mm]	Width [mm]	Length [mm]
4.54	597	155	203

Table 3.3: Head geometric characteristics.

Neck		
Mass [kg]	Diameter [mm]	Length [mm]
1.54	82.3	123.8

Table 3.4: Neck geometric characteristics.

The head is composed by a single-piece anthropomorphic skull and a monolithic cap, both aluminium made and covered by vinyl skin. The two parts are separated to allow easy access for instrumentation [3].
The Hybrid III neck is composed of rubber and aluminium discs which simulate the human vertebrae and which have anthropomorphic response in dynamic flexion and extension. Inside the neck, a steel cable runs through the central axis of the neck and limits stretching. One of the aim of this activity is to understand the influence of this cable on neck behaviour. For this reason, two different scenarios of axial tensile strength were analysed, changing the configuration of the cable.
The two configurations of the steel cable inside the neck have been evaluated in two different ways:

- looking at the initial position of the black line drown on the neck (as shown in Figure 3.4): in the first configuration the line is horizontal. In the second one the angle is about 7°;

- measuring the length of the axial cable thread which remains out of the hex nut:

  first configuration: 10.1 mm;

  second configuration: 14.4 mm.

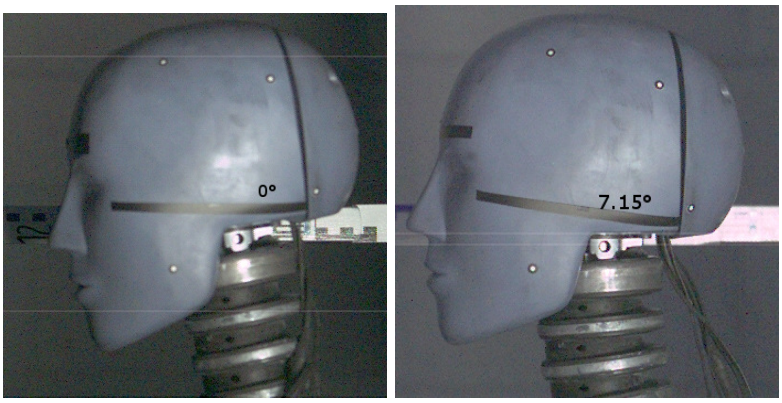

Figure 3.4: Initial head-neck configuration with different angles.

The neck attaches to the head through an aluminium nodding joint, rubber nodding blocks and a stainless steel condyle pin, as shown in Figure 3.5. Thanks to the pin, the head is allowed to nod in the condyle and sagittal plane.

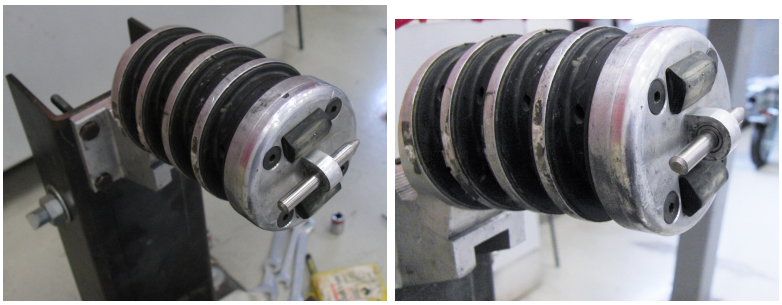

Figure 3.5: Nodding joint between the neck and the head.

3.3.1 Test procedure

The test procedure has been always the same: the pendulum was released in order to impact the target, with a velocity dependent from its initial position; to perform tests with constant impact velocity, the

initial position of the pendulum has always been the same. The pendulum velocity was measured through high speed videos and the ruler behind the neck (Figure 3.10): the impact tests were all conducted with an impactor velocity of 1.428 m/s. The 400 fps video allowed to evaluate the number of frames during which the pendulum covers 0.1 m, measured with the ruler. The head-form was hit three times per position (frontal, lateral, up), in both the two cable configurations in order to confirm the repeatability of the tests. As a first proof of that, the measured value of velocity was always 1.428 m/s for each test. However, in order to be sure of the repeatability, the data from the tests were post-processed in Matlab® and compared. In Figure 3.6 the three x-accelerations measured in the frontal impact, with the same configuration of the neck cable are shown. The same has been done with y-acceleration in the lateral impact (Figure 3.7) and for z-acceleration in upper impact (Figure 3.8). These comparison analysis have been done for every DAS output (three forces, three moments and three accelerations) in either frontal, lateral and upper impact for both cable positions. The signals have all been filtered in accordance to the regulation, SAR J211 [14]. Acceleration signals are filtered with CFC1000, forces and moments with CFC600; CFC filters are described in Appendix A.

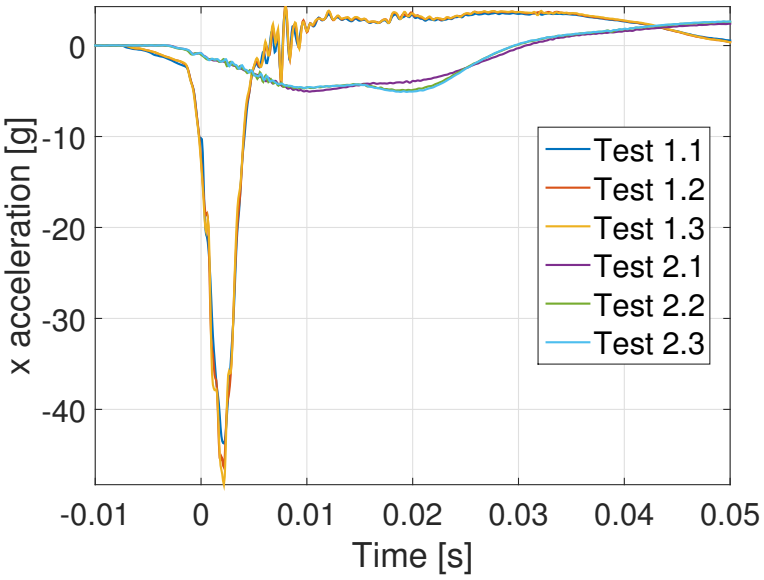

Figure 3.6: x-acceleration of three repeated frontal tests: first cable configuration (1.1, 1.2 and 1.3) and second cable configuration (2.1, 2.2 and 2.3).

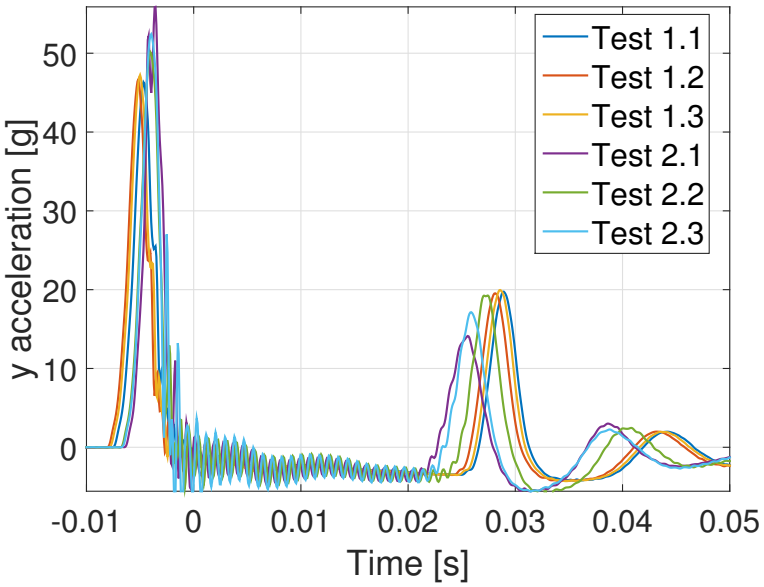

Figure 3.7: y-acceleration of three repeated lateral tests: first cable configuration (1.1, 1.2 and 1.3) and second cable configuration (2.1, 2.2 and 2.3).

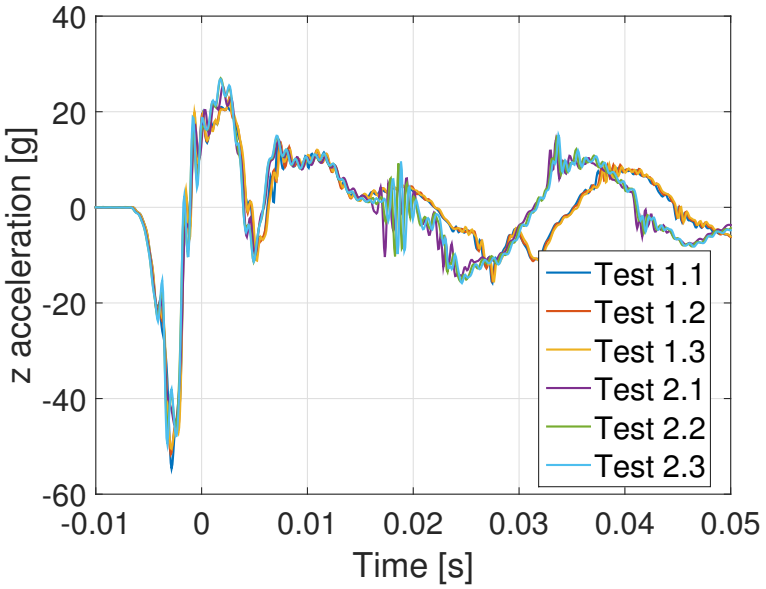

Figure 3.8: z-acceleration of three repeated upper tests: first cable configuration (1.1, 1.2 and 1.3) and second cable configuration (2.1, 2.2 and 2.3).

Looking at the maximum and the minimum acceleration values of each one of the three repeated tests, it is possible to evaluate the scatter factor with respect to the average value. The values of the three tests for the frontal impact in both the cable configurations are collected in Table 3.5 as an example, whereas the complete test session is reported in Appendix B. The reported data show the repeatability of the test results.

Test number	First cable configuration		Second cable configuration	
	Max(a_x)[g]	Scatter factor	Max(a_x)[g]	Scatter factor
1	43.7376	5.1	10.4889	6.26
2	46.3631	0.51	9.6981	1.75
3	48.2775	4.6	9.4259	4.5

Table 3.5: Comparison of maximum acceleration values for frontal impact tests.

The impact location remains always the same in every test: the base of the head-form is used as a reference. The impact points on the head with respect to the head-form basement in the three directions are (Figure 3.9):

- frontal impact: 260 mm in z-direction, aligned with the CG in

y-direction;

- lateral impact: 260 mm in z-direction, 145 mm from the back edge of the neck base in x-direction (aligned with the CG);
- upper impact: 260 mm in z-direction, 10 mm from the upper point of the nose, aligned with the CG in y-direction.

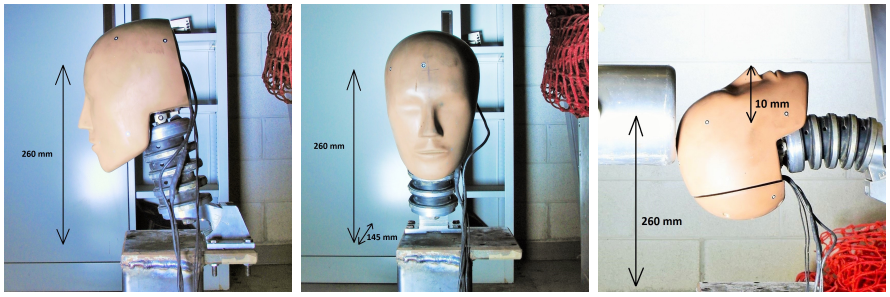

Figure 3.9: Impact location in frontal (left), lateral (center) and upper (right) impact.

The distance between the basement of the head-form and the pendulum impact location is always the same: the position of the pendulum has maintained always the same, independently of the impact test performed.
The condyle plane rotation has been measured looking at the difference between initial and final position of the black line drown on the head as reference. Because of the interest in occipital condyle rotation for every head configuration, three black lines were placed on the head, one per position, as shown in Figure 3.10.

Figure 3.10: Black line in frontal impact test, configuration 1 of the inner neck cable.

The three images in Figure 3.10 refer to the initial condition of the head-form (before the impact) in the *first cable configuration* (10.1

mm of the threaded screw off the nut) for frontal impact. In this configuration they can be considered all horizontal. These images are an example of the initial configuration photo-frame saved for every impact test performed. The initial condition of the head has been compared with the with the one with the largest displacement. The photo-frames corresponding to the initial configuration and the one with the maximum plane rotation, have been saved and rearranged through an image editor: the two images were merged in order to be able to measure the angle between the two conditions. As an example, Figure 3.11 shows the edited images that allowed the measurement of the angle. This procedure has been done for every test performed.

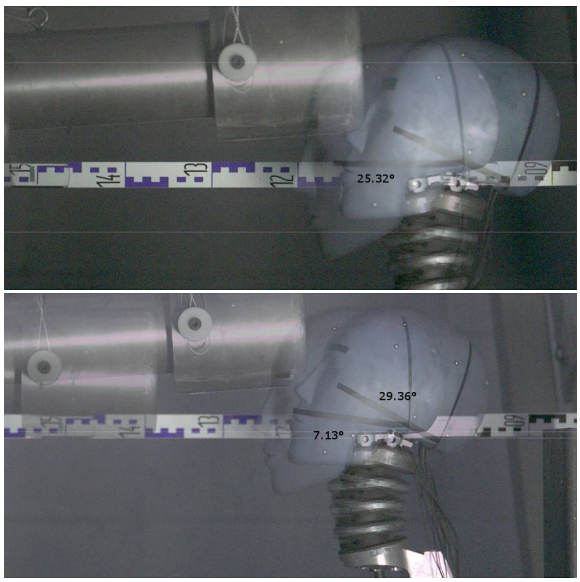

Figure 3.11: Merged images of initial and final configuration in both neck cable configurations.

The maximum angle values are collected in Table 3.6 for the first and second neck cable configuration, both in the frontal impact tests.

Test number	Angle [°]	
	First cable configuration	Second cable configuration
1	25.32	30.31
2	25.32	29.36
3	25.30	29.36

Table 3.6: Maximum rotation angle of the condyle plane in frontal impact tests.

The angle value in this *second cable configuration* is evaluated with respect to the horizontal; in order to know the maximum angle rotation with respect to the initial configuration, the value of the angle of the initial position has to be subtracted to the value in the table. In this case, the initial configuration angle is 7.13° with respect to the horizontal direction.

Acceleration peak, HIC, MOC and NIJ were calculated for each head impact. The linear acceleration peaks were evaluated because this parameter is worldwide accepted as one of the best predicted measurement [20], for the main reason that research in head injury started at a time when measurement techniques were limited. As a consequence, it was difficult to measure the effects of an impact on the brain directly. The acceleration peaks are collected in Appendix B. The mean peak values have been used as a comparison to verify the results of the numerical simulation.
HIC_{15} was calculated for every impact, thanks to the acceleration data collected by the DAS.

$$HIC_{15} = (t_2 - t_1)\left(\frac{1}{(t_2 - t_1)}\int_{t_1}^{t_2} a(x)dx\right) \tag{3.1}$$

Impact direction	Test number	HIC_{15}	
		First cable configuration	Second cable configuration
Frontal	1	19.87	1.4
	2	21.75	1.19
	3	22.35	1.13
Lateral	1	17.12	24.60
	2	17.03	20.83
	3	17.47	22.63
Upper	1	21.45	19.34
	2	21.64	20.36
	3	21.89	21.81

Table 3.7: HIC_{15} values of experimental head tests in first (left) and second (right) cable configuration.

The values of HIC_{15} change significantly from one cable configuration to the other.
In frontal impact, both the a_x and a_z signals are lower in the second cable configuration then in the first: the HIC values are lower too. The influence of a_y is negligible because it is lower than the others.
In lateral impact the most important acceleration value used for the HIC calculation comes from the *lateral acceleration, a_y*. In Figure 3.7 the y-axis acceleration time-histories in lateral impact tests can be analysed: they increase in the second cable configuration with respect to the first one. The cable influence in upper impact test is not so significant as in the two previous configurations. Thanks to the *upper neck load cell*, all the forces and moments have been measured; they allowed the calculation of two important criteria used for the evaluation of neck response in crash: MOC and NIJ [11]. They have been evaluated for every impact situation due to control whether their values exceeded the limit. Thanks to the low velocity of the pendulum, the injury thresholds have never been overtaken: the maximum admissible value for MOC_x is 134 Nm, for MOC_y is 57 Nm in extension (positive moment) and 190 Nm in flexion (negative moment). In Appendix B, B.3 the MOC time history both in x and y directions for every head impact test are shown. All the NIJ graphs are collected in Appendix B as well. The NIJ values have never reached the unity (maximum admissible value) in any point

in time.

3.4 Drop test

The drop test were conducted in three different configurations with respect to the height of impact and three different configurations with respect to the angular inclination of the surface of impact and, when the plane of impact was not horizontal, three different scenario were made up with respect to the orientation of the dummy about its z-axis (Figure 3.12). Also the *drop test*, like the *head tests*, has been performed three times in every scenario. Thus, 36 free fall tests were conducted with the whole dummy as summarised in Table 3.8.

Plane inclination	Drop height [m]	Dummy orientation (Figure 3.12)
0°	0.08 0.16 0.24	a, b and c are equivalent
15°	0.08 0.16 0.24	a, b, c a, b, c a, b, c

Table 3.8: Experimental drop tests configuration.

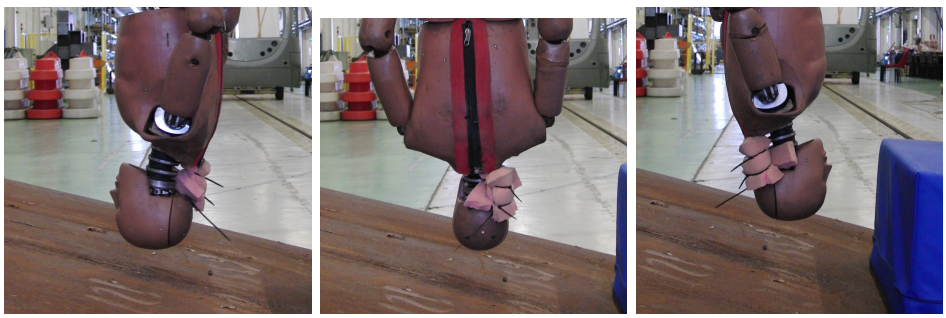

Figure 3.12: The a (left), b (middle) and c (right) direction of the dummy in the inclined plane configuration.

The dummy was hung by its feet at the desired heights. A *quick release mechanism* gave the start of the fall in every drop tests.

3.4.1 Test procedure

The dummy arms and legs were tied with tape respectively to the torso and to themselves. Hence, the asymmetry related to arms or legs movements far from the z-axis has been avoided as much as possible. Videos recorded with the camera –described in the 3.2.3 section– have shown the verticality of the dummy until the impact. Different positions have been assumed by the Hybrid III after the fall: it is related to the x-axis (related to the Hybrid III head coordinate system in Figure 1.1) orientation with respect to the impact plane. The dummy was hung from its feet such as the head would be the first point of impact. A quick release hook was used to give the start to the drop phenomena.
The accelerometer in the neighbourhood of the head CG measure the linear acceleration, the load cell placed at the occipital condyle measured the neck forces. The z-axis linear acceleration and the z-axis neck forces in the three angular inclination of the impact plane with the three different x-axis orientation are depicted in Figure 3.13 for the 0°tests at different heights and in Figure 3.15 for the inclined plane configuration.

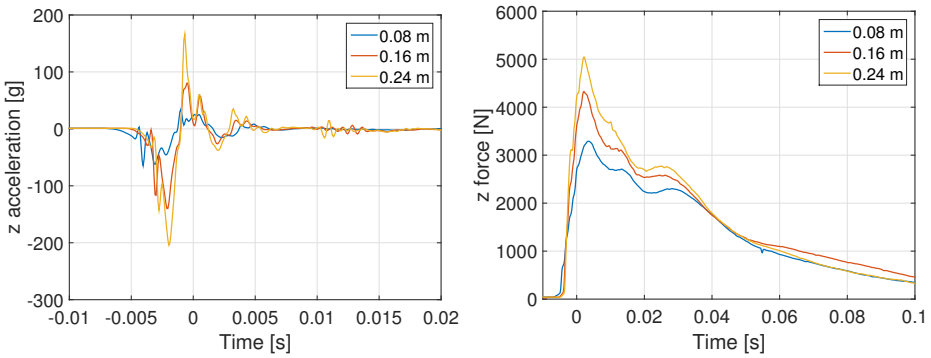

Figure 3.13: z-axis acceleration (left) and force (right) for 0° drop test, experimental.

As the drop heights increased, the head acceleration increased. In addition, the maximum acceleration peak is reached later in time with the augmentation of height.
The same happened with the force in the dummy neck: the lower force is registered at 0.08 m and the highest is recorded at 0.24 m.
As an example, the Figure 3.14 reported the z-axis acceleration time history and z-axis force time history to proof the repeatability of the tests. This aspect has been analysed for every impact scenario and

then confirmed.

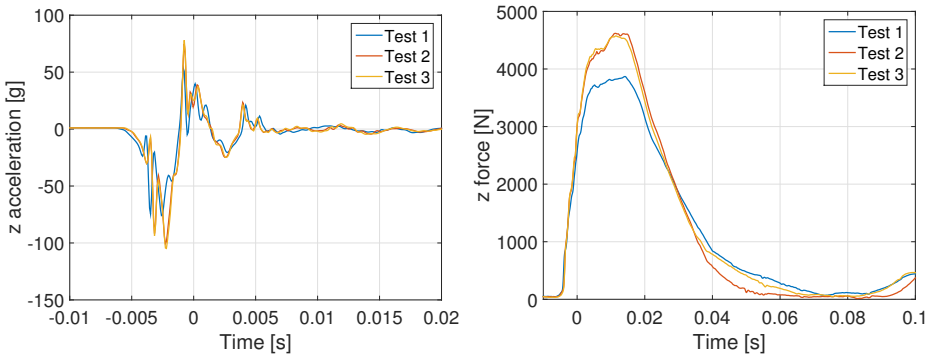

Figure 3.14: z-axis acceleration (left) and force (right) for 15° drop test, experimental test, repeatability.

The inclined plate drop tests were conducted with three different orientations of the whole dummy, as depicted in Figure 3.12. The main difference was measured in z-axis neck force: in *a* orientation were observed the highest force. The time-history acceleration were similar in every dummy orientation.

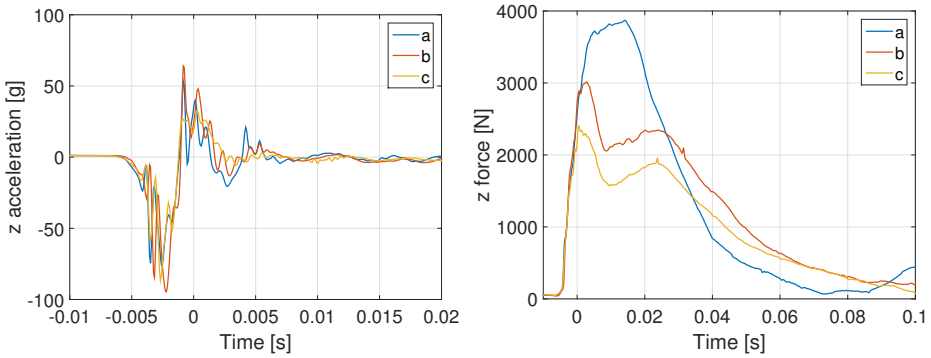

Figure 3.15: z-axis acceleration (left) and force (right) for 15° drop test, experimental test, different orientation.

Chapter 4

Numerical Simulations

The predictive capabilities of Finite Element Analysis allow to understand in detail a crash event in a virtual environment, limiting the number of physical tests that are needed to be executed. This means reduction of costs and time.
Throughout the research proposed in this thesis, the numerical analysis were all conducted with LS-DYNA 971 as solver and Ls-PrePost 3.2 as pre and post processor, both for the Hybrid III simulations and for THUMS simulations.
This Chapter explains how the experimental tests has been reproduced in a numerical environment and the comprehensive sensitivity analysis carried out to identify the optimal set-up of the FE model.

4.1 Hybrid III

The physical Hybrid III adult dummy used in the experimental tests is the base for the Hybrid III dummy FE model used in the simulations. Hence, they should have the same responses under the same initial conditions. As for the real dummy, in the FE Hybrid III an accelerometer is positioned in the head center for the linear head accelerations evaluation, a load cell in the upper neck can be used to evaluate the forces and moments at the occipital condyle. Looking at Figure 4.1 and bearing in mind Figure 3.1, it is easy to see the analogy between the real dummy Hybrid III and the FE one.

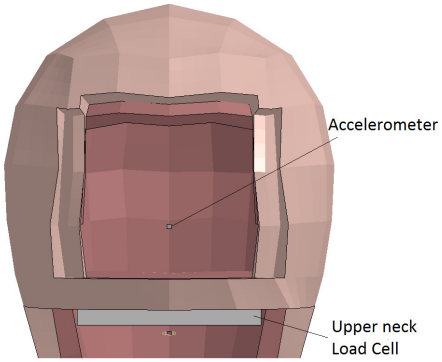

Figure 4.1: FE Hybrid III head instrumentation.

Thanks to the documentation [21] associated with the FEM Hybrid III, the post-processing analysis resulted quite easy. In the document the recommended procedures to follow for performing dummy post-processing using LS-PrePost are explained.

4.1.1 Head tests

The Hybrid III model comes from a previous research activity performed at LaST, Politecnico di Milano[22]. It has been developed starting from the original LSTC Hybrid III numerical model. The first step of the numerical procedure consisted in the separation of the head plus neck component from the rest of the Hybrid III body.
The tests set-up were partially reproduced, replacing the basement of the head with a boundary condition on the neck base. The frame to which the pendulum was hung through eight cables was reproduced with four cables and boundary conditions at the top end of them. The pendulum was modelled with the same characteristics of the real one concerning mass, geometrical dimensions and velocity.

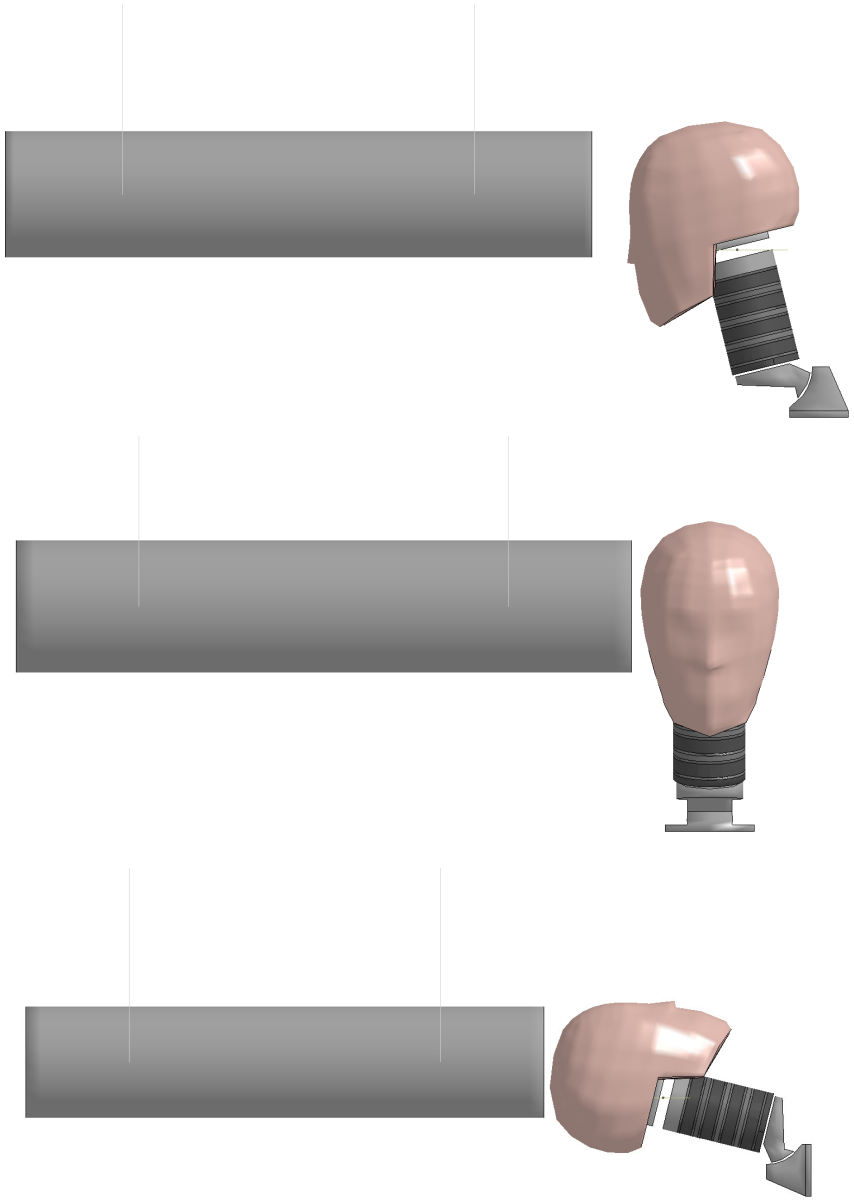

Figure 4.2: LS-DYNA head simulation with Hybrid III.

The cables were modelled with 100 beams each, modelled with the same material: Cable Discrete Beam [23], with density and Young modulus of steel. In the simulations the length of the cables was the same as in experimental tests. This has been done in order to simulate the

correct pendulum motion. The cables had an angular velocity related to the known pendulum linear velocity. They are pinned at the cylinder thanks to spherical joints; the spherical joints make possible the connection between two rigid bodies; for this reason, the last beams of the wires, the nearest to the cylinder, were modelled with rigid material, as the cylinder.
The comparison between numerical simulation and experimental tests was focused on the main injury criteria: HIC, NIJ and MOC. HIC is an acceleration-based criterion. Therefore, before comparing numerical and experimental HIC values, the acceleration signals have been analysed.
HIC values, for all the numerical simulations, have been evaluated with the numerical code implemented in Matlab®, the same used for the experimental data; this code was verified comparing the HIC values of different simulations with the HIC score related to the same simulation, evaluated with LS-DYNA [21].

Skin mesh

Since the acceleration time-history always presented an oscillatory trend, an investigation has been conducted in order to understand which head part caused this oscillation. As expected, the Hybrid III skin was the responsible, as represented in Figure 4.3. In order to reduce this oscillation and to find an acceleration time-history and an acceleration peak value close to the experimental result as much as possible, the skin mesh has been split one, two and three times.

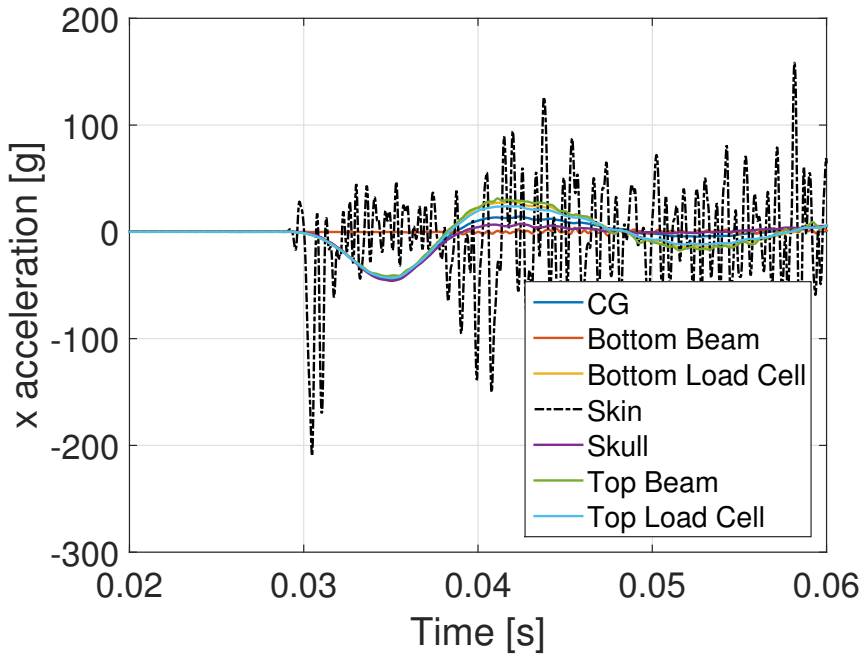

Figure 4.3: x-axis acceleration in different head nodes.

With this modification it was possible to obtain a good correlation between numerical and experimental peak acceleration values and forces. The original mesh was modified increasing the initial number of elements and the final decision was to consider the element split twice.

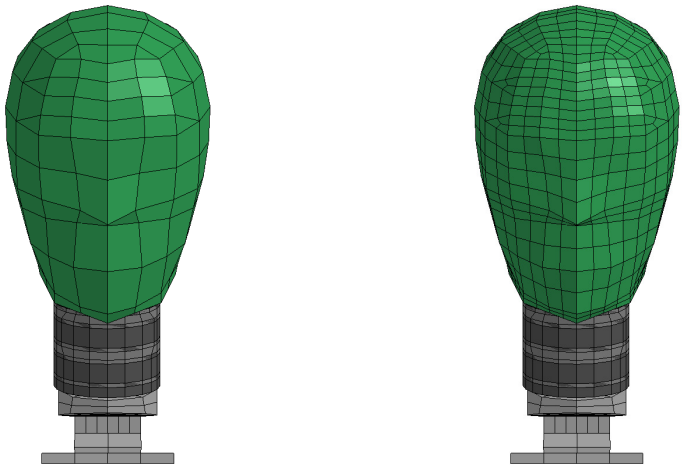

Figure 4.4: View of the Hybrid III head: base model (left), skin mesh split one time (right).

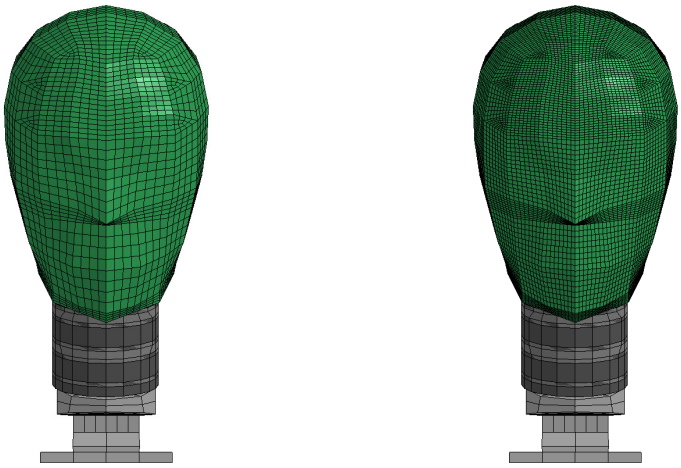

Figure 4.5: View of the Hybrid III head: skin mesh split two (left) and three (right) times.

Number of times the mesh was split	$a_{x_{max}}$ [g]	$F_{x_{max}}$ [N]	HIC_{15}
1	44.97	863.13	37.22
2	31.38	806.58	21.97
3	21.84	776.83	12.30

Table 4.1: Acceleration and force peak values and HIC score in different skin mesh configuration, frontal impact.

As a consequence of the refined mesh, the duration of the simulation increased. On the contrary, the head acceleration peak decrease such as the maximum x-axis force score. As a consequence of acceleration decrease, also the HIC resulted lower as the more the element were split.

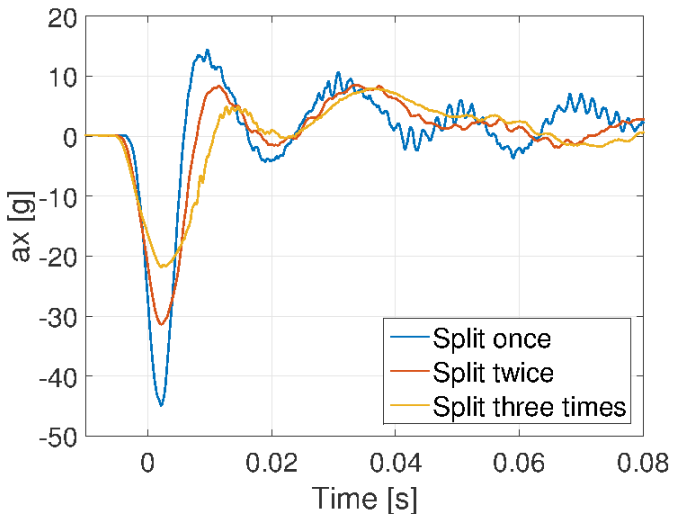

Figure 4.6: x-axis acceleration in different skin mesh configurations.

Neck stiffness

The *head* experimental tests were conducted in two different neck configurations concerning the steal beam inside the neck component as described in the previous Chapter, in Section 3.3. Hence, at the beginning, the numerical analysis focused on neck stiffness and in particular on the inner element of the neck. Every component has been analysed and its parameters tailored to recreate the actual dummy behaviour. The neck of the Hybrid III numerical model used is mainly composed by solid parts. The only part which is not solid is the beam in the inner neck (Figure 4.8); thus, its stiffness has been analysed since considered similar in behaviour as the real one. The analysis of the neck components mainly focused on the material properties: in particular the Young modulus or the Bulk modulus were evaluated and, whether necessary, modified. The correlation between numerical and experimental results has been verified comparing the acceleration signals: HIC is an acceleration-based criterion. Also forces and moments took an important rule in this trade.
Hereby are reported the analysis only for the frontal head tests, as example. Every impact direction has been evaluated and the results compared with the experimental tests. In the following Tables the maximum values of x acceleration and force are presented. Only the horizontal

direction values are reported because in the frontal impact the load direction were the x-axis.

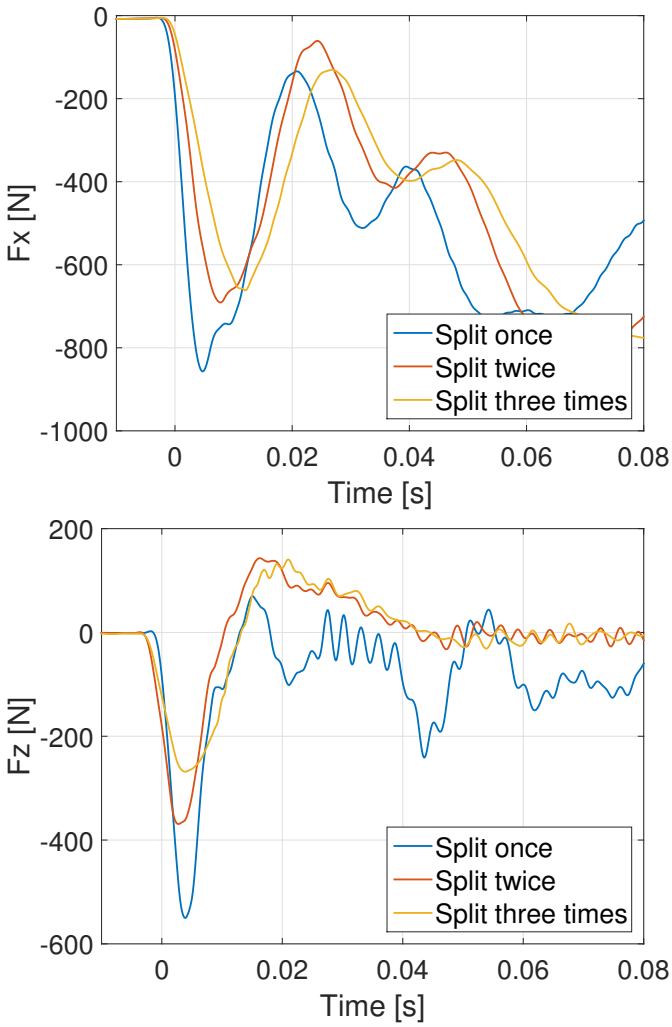

Figure 4.7: x-axis force and z-axis force in different skin mesh configurations.

The sensitivity analysis of the element in the neck has been conducted twice:

- with the standard mesh configuration;
- with the two-times split mesh.

The graphs presented reported the curves only for the final split configuration. Nevertheless the scores of the main interesting values are reported in two Tables, one for the base model sensitivity analysis and

the second for the split mesh configuration. Hence, bearing in mind the peak results obtained in the experimental tests (refer back to Chapter 3 and reported entirely in Appendix B), the improvement achieved with the splitting of the mesh resulted clear.

No split			
E [MPa]	$a_{x_{max}}$ [g]	$F_{x_{max}}$ [N]	HIC_{15}
5000	81.80	1300.0	95.98
1000	81.26	1223.1	93.57
100	80.30	1231.5	91.94
1	82.10	1229.5	94.44

Table 4.2: Simulation results, inner beam sensitivity analysis, skin mesh no split.

Inner beam Despite the geometrical analogy between real ATD's beam in the inner neck and the FEM beam (Figure 4.8), the numerical beam has no relevant role in neck stiffness as the real one. Variations in the inner beam Young modulus turned out to be negligible in the condition analysed.

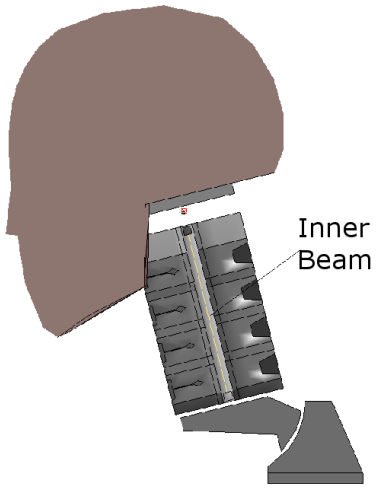

Figure 4.8: Beam element in the inner neck.

Split	
E [MPa]	$a_{x_{max}}$
1e6	40.97
1000	40.95
1	40.97

Table 4.3: Simulation results, inner beam sensitivity analysis, skin mesh split.

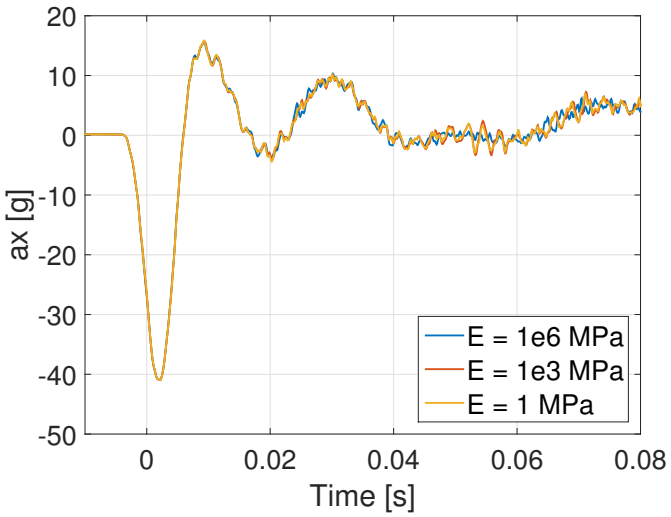

Figure 4.9: x-axis acceleration, sensitivity analysis of inner beam element.

The experimental tests shown that the steel cable which runs through the inner neck influences the neck responses in every impact condition (Appendix B). In the numerical model, an analogous beam was recognised in the inner neck (Figure 4.8). The investigation of its stiffness has been evaluated and the results are presented in Figure 4.9 where the different curves refer to different beam stiffness, as shown in the legend. In Figure 4.9 it is interesting to notice how the beam stiffness did not introduce important variations on the acceleration signal. For this reason, other neck elements have been analysed.

Outer beam Similar to the previous element in geometry but defined as a solid –not a beam as the previous element analysed– in the model was the outer beam shown in Figure 4.10.

No split			
E [MPa]	$a_{x_{max}}$ [g]	$F_{x_{max}}$ [N]	HIC_{15}
6500	85.26	966.24	103.65
650	84.43	843.16	119.76
65	81.02	855.04	99.73
6.5	81.68	779.00	100.72

Table 4.4: Simulation results, outer beam sensitivity analysis, skin mesh no split.

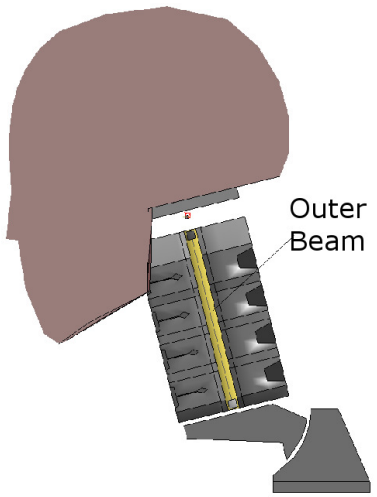

Figure 4.10: Outer beam element in the inner neck.

Split	
E [MPa]	$a_{x_{max}}$ [g]
6.5e5	42.52
6500	42.68
6.5	42.55

Table 4.5: Simulation results, outer beam sensitivity analysis, skin mesh split.

The Young modulus variation lightly influenced both the maximum peak of acceleration and force but no trend has been spotted (Table 4.5).

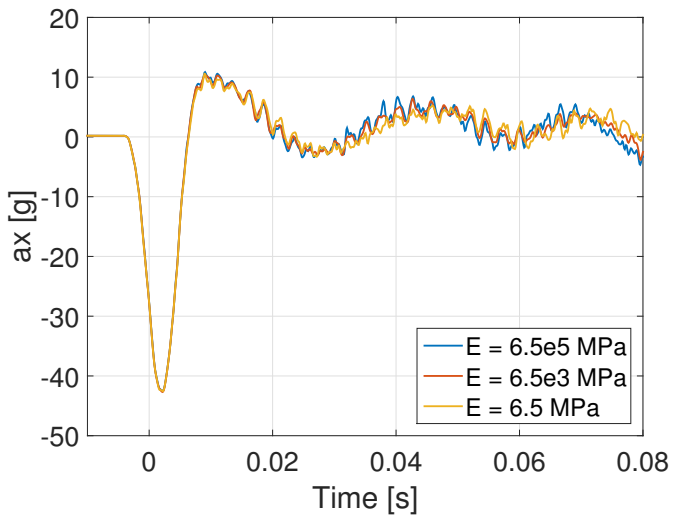

Figure 4.11: x-axis acceleration, sensitivity analysis of outer beam in the inner neck.

Discs Five elements in the neck were analysed simultaneously since their characteristic were the same. Those elements were five discs that can be associated to the five lower cervical vertebrae –the first

and the second upper neck vertebrae are not modelled– or to the five intervertebra discs. Related to their distribution in all the neck heights, the contribution of discs stiffness is quite important.

No split			
E [MPa]	$a_{x_{max}}$ [g]	$F_{x_{max}}$ [N]	HIC_{15}
40000	81.83	1235.40	96.58
7000	80.44	1235.00	95.40
700	80.44	1235.00	95.40
7	81.28	1234.40	94.34

Table 4.6: Simulation results, neck discs sensitivity analysis, skin mesh no split.

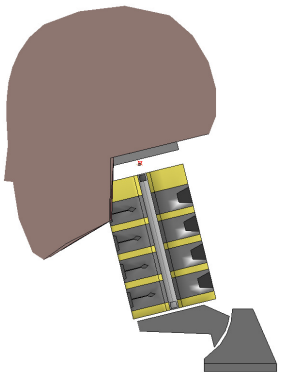

Figure 4.12: Discs in the inner neck (painted in yellow).

Split	
E [MPa]	$a_{x_{max}}$ [g]
7e5	76.32
7	40.92

Table 4.7: Simulation results, neck discs sensitivity analysis, skin mesh split.

The result obtained with discs stiffness variation has been compared with the experimental data and the good results and correlation justified the modification of discs material Young modulus.

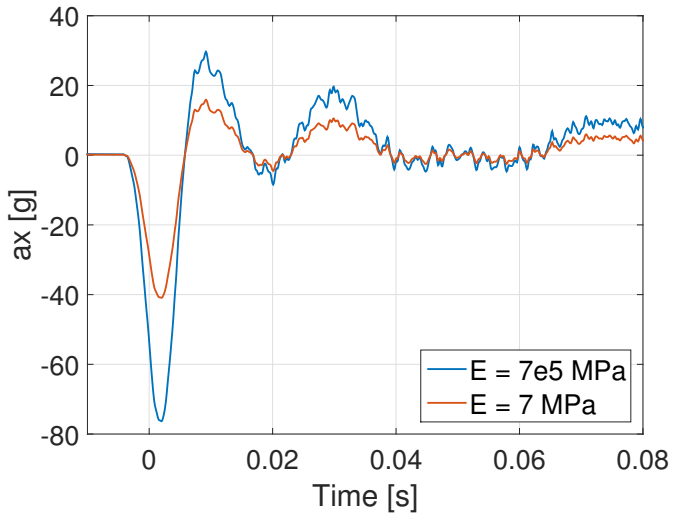

Figure 4.13: x-axis acceleration, sensitivity analysis of the disc parameters.

External structure To complete the neck analysis, two other parts have been studied. Here the results related to the solid structure in the neck (Figure 4.14); this part was added in previous work conducted at LaST on the base of the LSTC dummy model (Figure 2.4).

No split			
B[a][MPa]	$a_{x_{max}}$ [g]	$F_{x_{max}}$ [N]	HIC_{15}
15	80.00	1212.60	94.80
10	82.35	1233.40	94.76
1	81.63	1093.70	94.51

Table 4.8: Simulation results, solid structure inner neck sensitivity analysis, skin mesh no split.

[a]Bulk Modulus

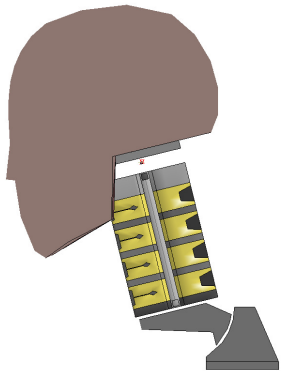

Figure 4.14: Solid structure in the inner neck (painted in yellow).

Split	
B [MPa]	$a_{x_{max}}$ [g]
10	41.02

Table 4.9: Simulation results, solid structure inner neck sensitivity analysis, skin mesh split.

The main difference was recorded thanks to the modification of the mesh, but the variation of the bulk modulus of the neck element do not significantly influenced the acceleration peak nor the force peak values.

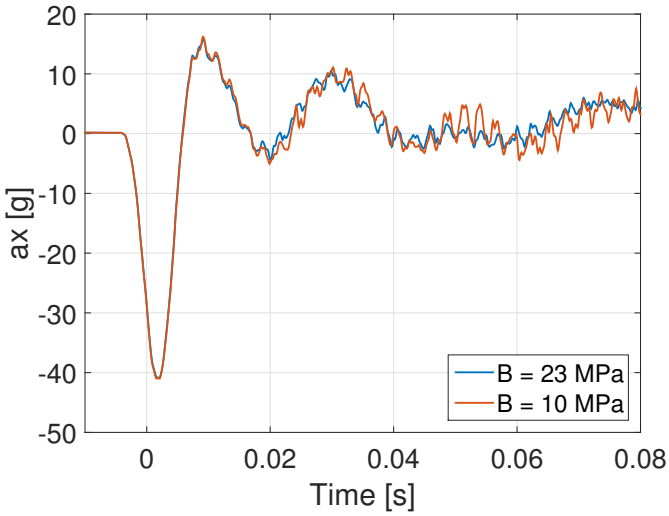

Figure 4.15: x-axis acceleration, solid structure in the neck, sensitivity analysis.

External shell structure There is another structure in the neck which has been considered. It is different from the one previously discussed because it is modelled with shell elements. Its influence has been evaluated at first removing completely the part. The results obtained are shown in Figure 4.16 and reported in Table 4.10. Since its influence is not fundamental in the evaluation of head acceleration and upper neck

forces, the analysis of the shell element didn't go deeper than this.

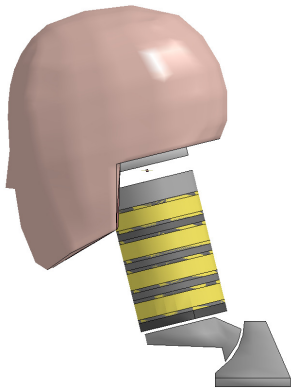

Figure 4.16: Shell structure in the neck.

No split		
$a_{x_{max}}$ [g]	$F_{x_{max}}$ [N]	HIC_{15}
80.6	1300	95.24

Table 4.10: Simulation results, neck shell structure sensitivity analysis, skin mesh split.

The sensitivity analysis conducted on the neck elements resulted lightly significant in forces and accelerations results. The main improvement was caused by the split of the skin mesh.

4.1.2 Drop tests

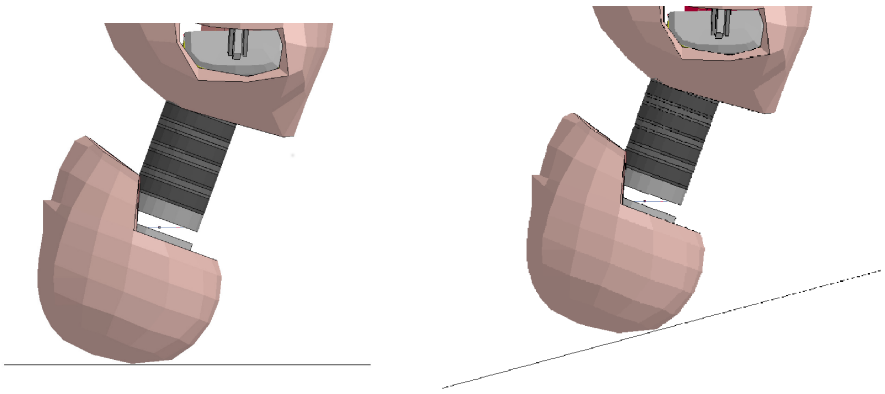

Figure 4.17: Numerical configuration of the 0° drop test (left) and inclined at 15° drop tests (right) with Hybrid III.

The complete 50th percentile Hybrid III ATD FE model was used to reproduce the experimental drop tests for the comparison. The ATD were rotated and no boundary conditions were created: it was free to fall without any external constrain. In order to reproduce the impact

surface, a rigid wall was created above the ATD head and, for the non-horizontal tests, it was rotated about its y-axis. To replace the three different heights, three initial velocity were assigned to the whole dummy body. Hence, its position with respect to the rigid wall remained always the same: 1 mm above the rigid wall. This condition gave the possibility to reduce the time duration of the simulations.
For the drop tests, the terms of comparison between the numerical simulations and the experimental tests were the z-axis measures. A sensitivity analysis has been conducted for the plate definition. A shell element was at first selected and then changed with a rigid wall: the results were very close one another but the computational cost related to the rigid wall was shorter –the same analysis were conducted with THUMS 4.2.3 and for a similar reason the same choice were then selected–. Because of the good results obtained with the Hybrid III head model with the modified skin mesh (elements doubled) in *head tests*, the same configuration has been used for the *drop tests* simulations.

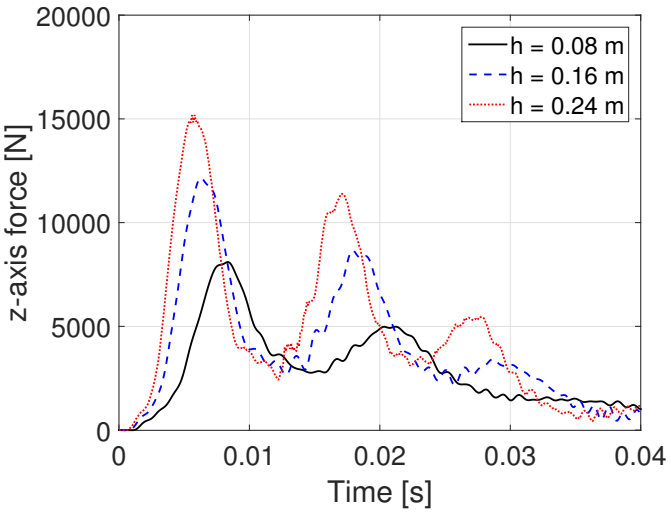

Figure 4.18: z-axis neck force comparison in different heights configuration with Hybrid III.

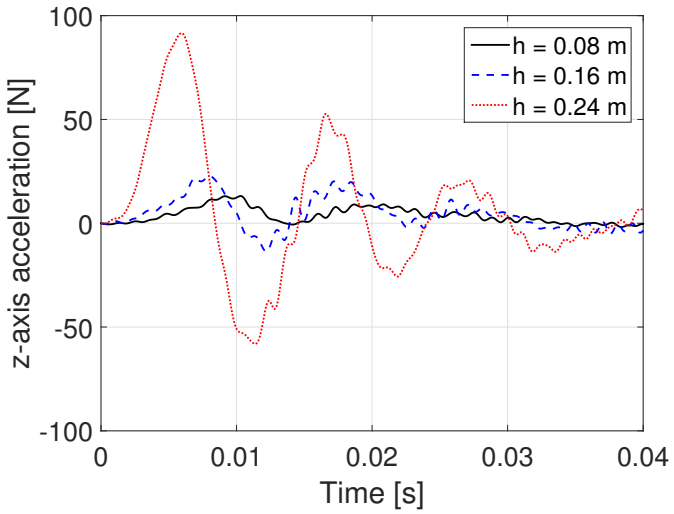

Figure 4.19: z-axis head acceleration comparison in different heights configuration with Hybrid III.

Figures 4.18 and 4.19 display the trend of the axial compressive neck load and head acceleration: they increased with respect to the heights, which means that increased with the impact velocity. It must be noticed that the higher the velocity –the heights to which the ATD was hung up– the earlier the forces reached its maximum value; the same happened for the acceleration. Thus the maximum force score was reached at the same time instant at which the z-axis acceleration reached its maximum value. The data regarding the impact test onto inclined rigid wall are not here exposed but they presented the same results previously obtained for 0°drop test.
The results, as expected, shown that:

- forces in the neck are higher as the heights increased;
- head acceleration increased with the heights;
- maximum peak is reached earlier for higher height.

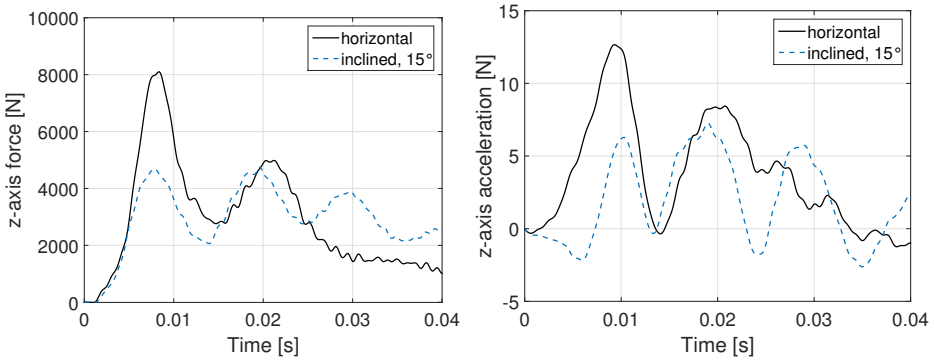

Figure 4.20: z-axis force (left) and head acceleration (right) in 0° and inclined drop.

Figure 4.20 shows the comparison of the two plane orientation analysed; it is easy to read that in horizontal (0°) condition the force and acceleration observed were higher than in inclined configuration. This happened in every height considered, both at 0.08 m, 0.16 m and 0.24 m. Horizontal configuration were heavy than inclined.

4.2 THUMS

THUMS, *Total HUman Model for Safety*, is one of the most detailed FE Model of the human body: high-resolution computer tomography (HRCT) scans were used to accurately represent the geometry and physical properties of the human body and its internal organs. The THUMS has the purpose to predict kinematics, kinetics and internal stresses and strains of a human being. The THUMS head and cervical spine, which this work in particular referred to, had previously been validated against multiple cadaver tests. Its cervical spine has been demonstrated [24, 25] to replicate the force-displacement response, bony damage and ligament damage in simulation of direct axial loading, as well as the torque angle response in torsional failure tests.
The objective of this study is to determine the level of correlation of the classical mechanical parameters –as the linear head acceleration or the NIJ values– with the degree of injury that can be recorded with the human body model considered. It must be noticed that in the accident database, only the severity of the injury is notified, using the injury criteria. Some authors [26, 27] tried to correlate the injury criteria scores

with tolerance levels through the AIS code.
One of the reason for the diffuse adoption of injury criteria is the fact that they can be easily recorded on dummies. Related to this, their evaluation on FEM Hybrid III is quite straightforward as well. On the other hand, such parameters have some limits: they are referred to an injury that is localised in specific areas, such as the head CG, the upper neck or the lower neck, that is where the instrumentations are mounted on the real dummy. It induces that, for example, the physical response of the neck to an impact, as the intra-cervical movement, is not considered.
This is not a limit for THUMS, that has human-like behaviour and that can become a convincing substitute of the Hybrid III in crash analysis simulations whether a valid and available correlation between the classical injury criteria and its responses in different scenarios exists.
The most important head and neck injury criteria base their formulation on linear accelerations and forces (and moments). Due to this, their time-history curves are selected as term of comparison.
In particular, the main purpose of the first part of the analyses described in this chapter is the comparison between different solutions for the evaluation of linear accelerations and forces in THUMS in order to understand if it could be possible to create a sort of instrumentation for this FE human being model. As a model of human being and not a dummy model, THUMS has nothing similar to an accelerometer or a load cell mounted on it. In addition, no direct comparison of THUMS results with Hybrid III FEM data would be possible, as those are, by definition, two models of different structure. For a first row validation of the THUMS simulations, tests with Post Mortem Human Subject (PMHS) were used, when available [4, 8, 28]. Beside this qualitative validation, different data of easy calculation from basic physics law has been checked: kinetic energy, internal energy, total energy and external work were collected and analysed to always confirm the simulation scenario.

4.2.1 Simulations set up

The same tests were conducted both with the FEM of Hybrid III and THUMS, on the base of the experimental tests set up previously described. As done in Chapter 3, also the simulation tests were divided in two main categories: the *head* tests and the *drop* tests; in the following sections how those test configurations were recreated for THUMS is described. All the simulations was conducted using the THUMS AM50 Pedestrian model, academic version 4.02 with fracture. In order to maintain consistency, all the THUMS simulations were run using the LS-DYNA non-linear explicit finite element solver version 971-R8.0 with single precision. For the comparison and the analysis of the results, all the filtered data were then processed using a code specifically written in Matlab®R2014b.

The reference system for the evaluation of the values of interest was subjected to analysis. In the Hybrid III dummy, an accelerometer was mounted in the neighbourhood of the head CG; hence the accelerations are evaluated with respect to the coordinate system centred in the head CG (Figure 4.21). The upper neck load cell measured the forces, thus they were recorded in the load cell reference system and can be transported to the CG coordinate system, once the load cell model and characteristics are known. In FEM Hybrid III the reference systems were analogous to the dummy's. In THUMS the scenario has been partially recreated: a coordinate system centred in the head CG has been created. This coordinate system was orthogonal, with the x-axis directed from posterior to anterior, the y-axis oriented laterally and directed from left to right, and the z-axis oriented in the direction of the column from superior to inferior (Figure 4.21).

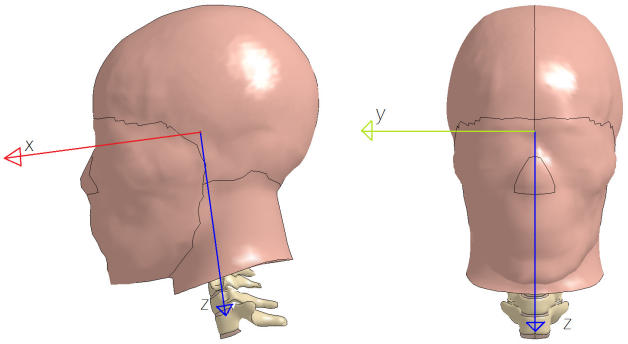

Figure 4.21: Coordinate system.

This CG coordinate system was used for both the acceleration and the forces evaluation. In addition to this, five local coordinate systems were created at five different neck levels. Due to the absence of a load cell element and a reference system related to the instrument, in THUMS the neck forces have been measured with respect to the two coordinate systems –the CG coordinate system and the neck level coordinate system– in order to be able to select the most comparable scenario to Hybrid III instrumentation.

4.2.2 Head tests

As for the experimental and numerical analysis conducted with Hybrid III, also with THUMS numerical activity the *head test* category can be subdivided in three different subsections in relation to the direction of the impactor: frontal, lateral and upper tests. Those impact locations and directions were selected in order to reproduce the experimental set up. The three different impact direction scenario were reproduced for THUMS using Ls Prepost. Some parameters such as the head-impact contact characteristics, the accelerometer position, the rigid body which the accelerometer refers to and the cross sections used for the determination of the forces were selected after specifically sensitivity studies.

Head-neck model

In order to reproduce the head impact configuration, THUMS has been reduced to its head and neck components. No modification were intro-

duced on THUMS if not necessary.
The neck of the Hybrid III dummy is supposed to reproduce the cervical vertebrae (C1-C7); to recreate the same configuration in THUMS simulation, the vertebral column were truncated immediately after the first thoracic vertebra T1, which has been left to reproduce the boundary condition. The reduced head and neck model is composed by 297730 elements, 203526 nodes and has a mass of 6.06375 kg. The Centre of Gravity of the reduced model has been identified using LsPrepost and a node has been created at its coordinate. This node has been used for accelerations evaluations, as explained in the following section. 90000001 is the identification number used for the CG node.
The head model has been the main interests of this activity. The model includes the skin, skull, mandible, eyeballs, teeth, meninges, cerebrum, cerebellum, brainstem, CSF etc. as shown in Figure 4.22. The *meninges* part has three layers: dura mater, arachnoid and pia mater. The *brain* parts includes the white matter and the gray matter. The inferior part of the head model is attached to the neck model through the occipital condyle.

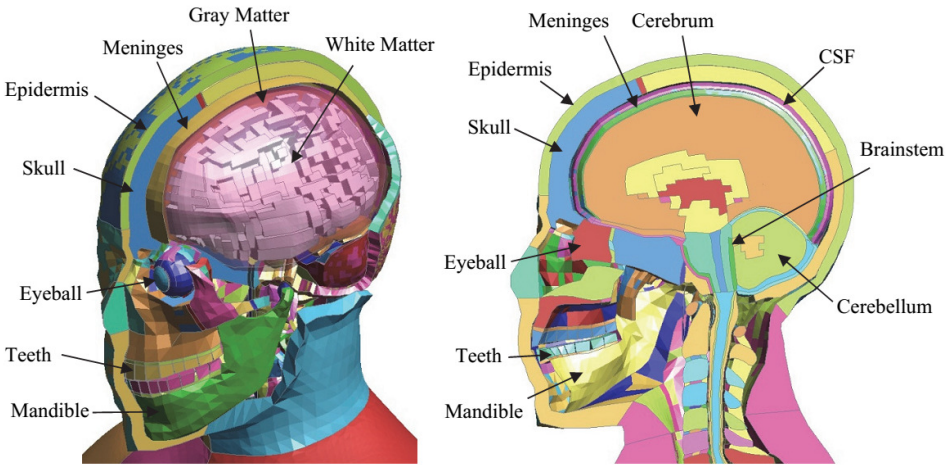

Figure 4.22: Head model [2].

General head test set up

In the experimental head tests configurations, the Hybrid III dummy neck was constrained to the ground at its base. Since the Hybrid III dummy neck corresponds to the cervical vertebrae (C1-C7), the aluminium rigid block at the base of the neck can be compared to the first thoracic vertebra –that actually doesn't exist in Hybrid III dummy nor Hybrid III FEM–. In order to reproduce this boundary condition, the first thoracic vertebra (T1) of THUMS was rigidly constrained and every element below it was ignored. To better simulate the configuration of the experimental tests also the tendons and the flesh were constrained. However, since Hybrid III has no elements that simulate tendons nor muscles and skin, four different BC configurations have been compared to understand their influence on acceleration and force evaluations:

- T1, tendons and neck flesh constrained;
- T1 and tendons constrained;
- T1 and neck flesh constrained;
- only T1 constrained.

The x-and z-axis accelerations in the head CG, the axial forces in the top and bottom cartilage set and the x- and z-axis contact forces are depicted in Figure 4.23 –accelerations– and Figure 4.24 –forces– for the frontal impact.

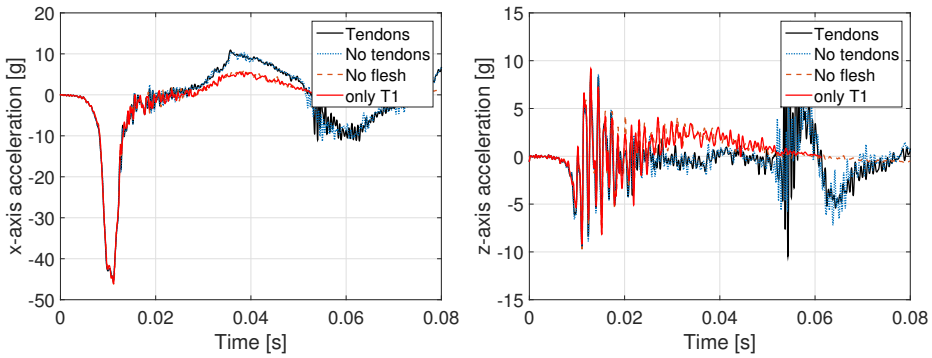

Figure 4.23: x-axis (left) and z-axis (right) acceleration in different BC configurations; frontal impact.

The difference between accelerometer measures (Figure 4.23) became relevant after 0.05 s. It can be related to the second impact between the pendulum and the head. It resulted a lower impact than the first one; the impact happened only if the flesh were constrained, thus it was not registered in BC configuration with only T1 constrained and with no flesh boundary condition (red and dashed curves in Figure 4.23). The second impact was clearly visible in the simulation visualisation as reported in Figure 4.26.

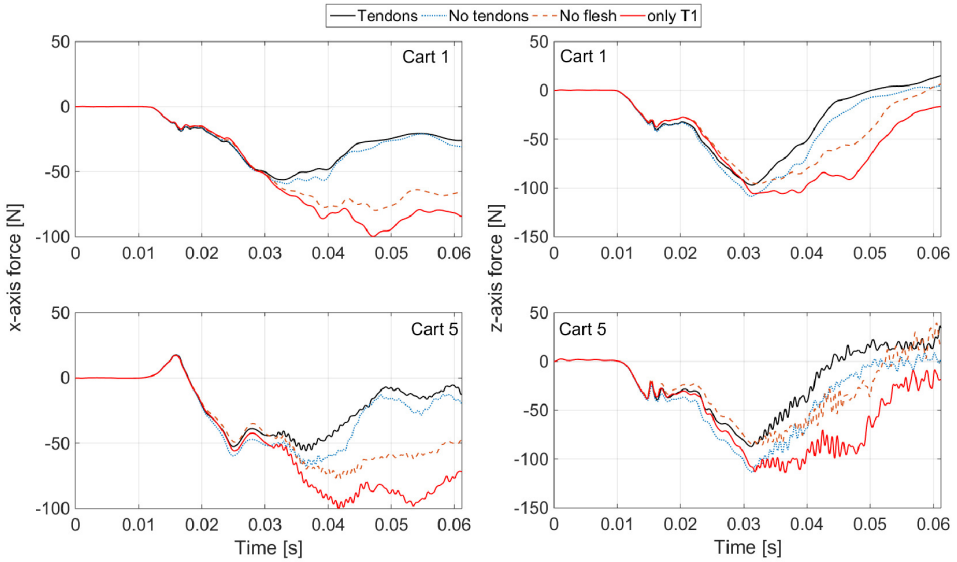

Figure 4.24: axial forces: comparison between different boundary condition configurations; frontal impact.

The importance of flesh BC was clear also with the animation visualisation in LS-DYNA. Since the complete head-neck component was placed in a gravitational field, it underwent the gravitational force from the beginning and without any support at its base, the head and neck flesh started to fall down. Moreover, after the impact, the absence of flesh BC left the head translate in the x-axis direction.

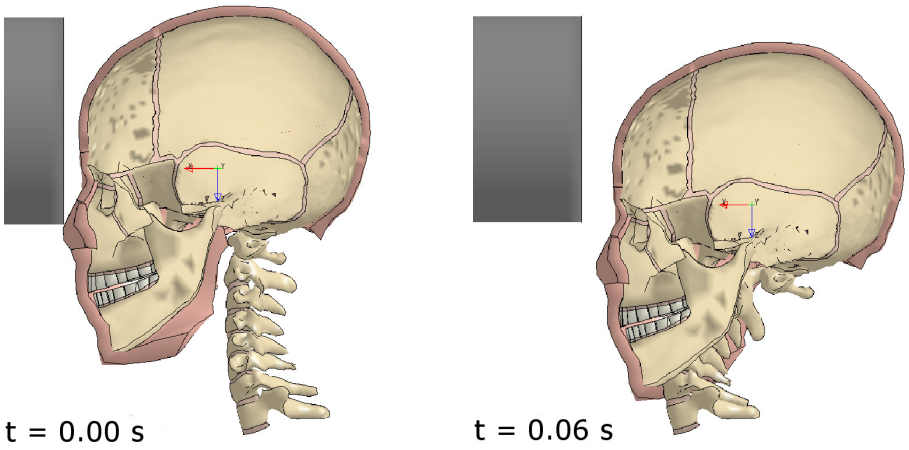

(a) Before-impact configuration. *(b) Post-impact configuration.*

Figure 4.25: Simulation visualisation of no flesh BC; frontal impact.

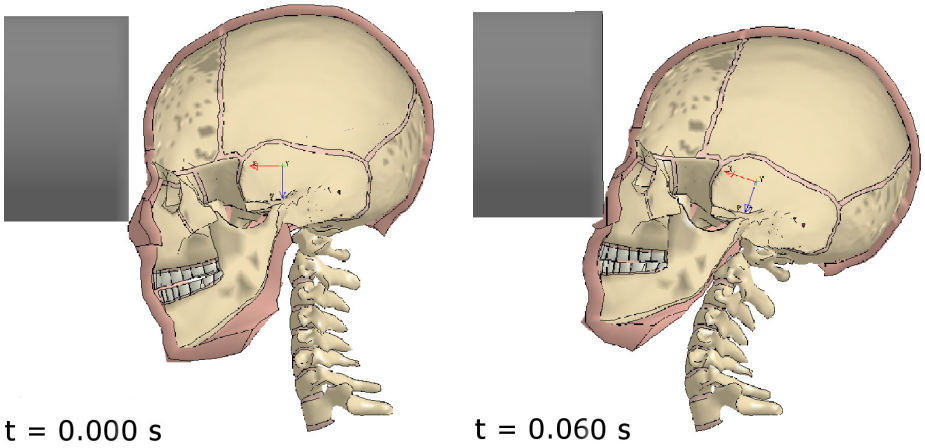

(a) Before-impact configuration. *(b) Post-impact configuration.*

Figure 4.26: Simulation visualisation of complete BC; frontal impact.

Further investigations were conducted on the presence-absence of the tendons, which influence was not immediately clear by visualisation. Therefore, the x- and z-axis forces in different neck levels were compared. In Figure 4.27, 4.28 and 4.29 the axial forces in some neck levels considered are depicted.

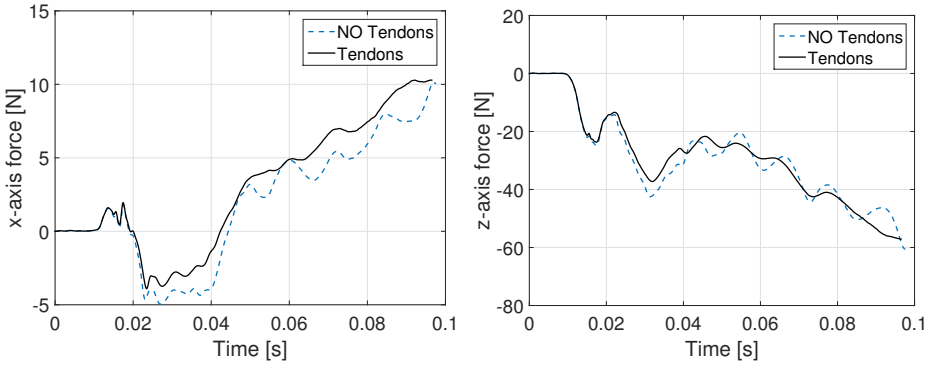

(a) Vertebra C3.

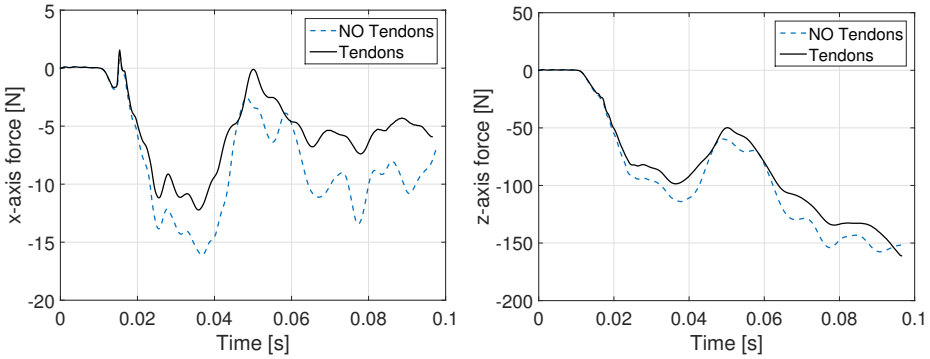

(b) Vertebra C7.

Figure 4.27: Comparison of C3 (a) and C7 (b) axial forces in frontal impact with tendons and without tendons.

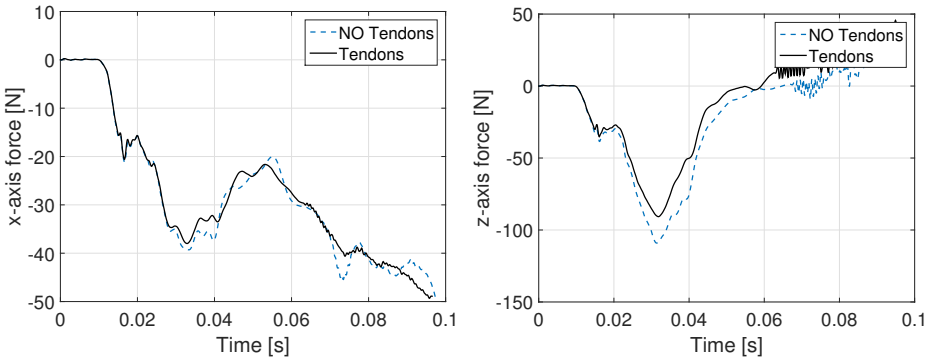

(a) Top cartilage.

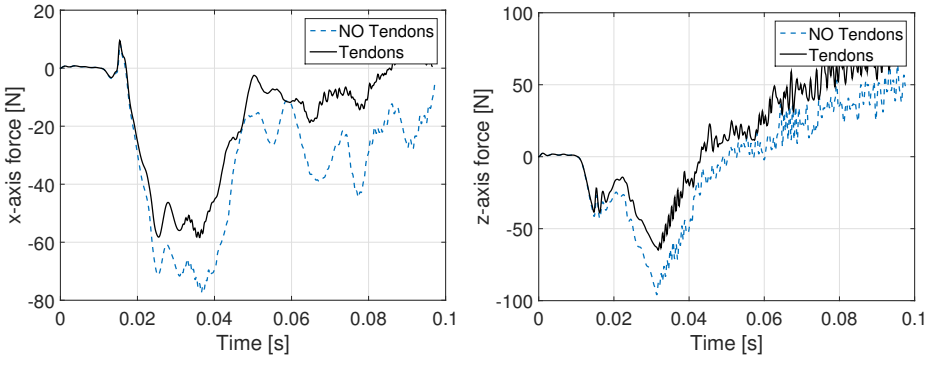

(b) Bottom cartilage.

Figure 4.28: Comparison of top (a) and bottom (b) cartilage axial forces in frontal impact with tendons and without tendons; frontal impact.

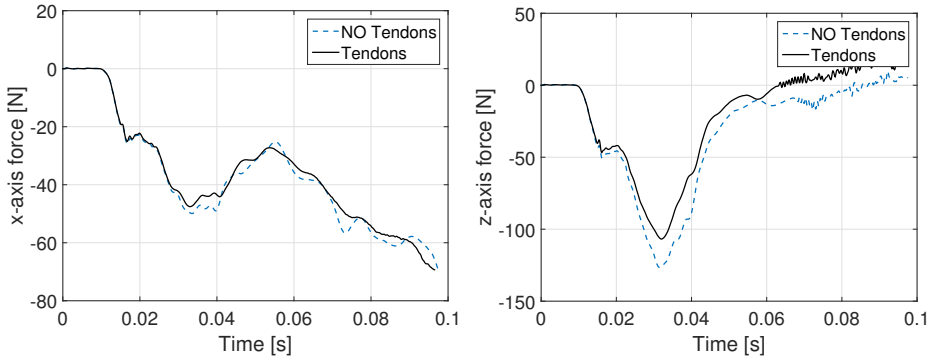

(a) Top plane.

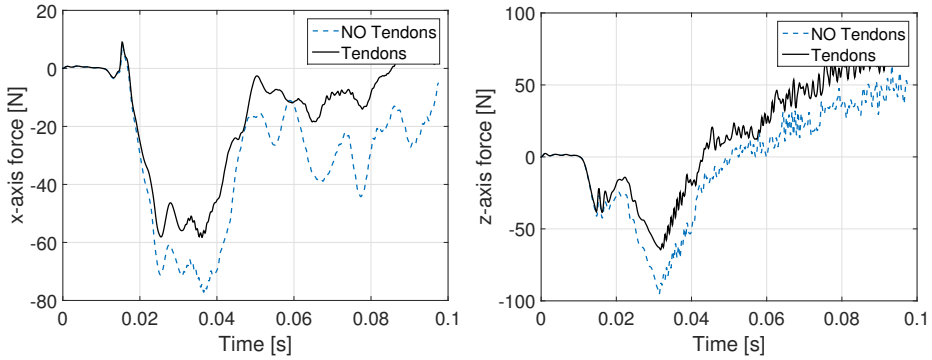

(b) Bottom plane.

Figure 4.29: Comparison of top (a) and bottom (b) plane axial forces in frontal impact in BCs with tendons and without tendons; frontal impact.

In every neck level the presence of the tendons became important 0.02 seconds after the impact; this introduced differences in the neck peak forces which resulted lower with the tendons rigidly constrained. The major differences of tendons presence-absence were evaluated in the planes forces. This is related to the fact that the tendons were selected as active parts in the cross sections plane definition. Constrained tendons and flesh have been chosen as BC (Figure 4.30). Even if the acceleration evaluation is not strongly influenced by the tendons BC (Figure 4.23), the evaluation of the forces in the neck made the difference relevant. In addition, this boundary configuration has been selected also because it has been considered as the most comparable with the experimental tests set up.

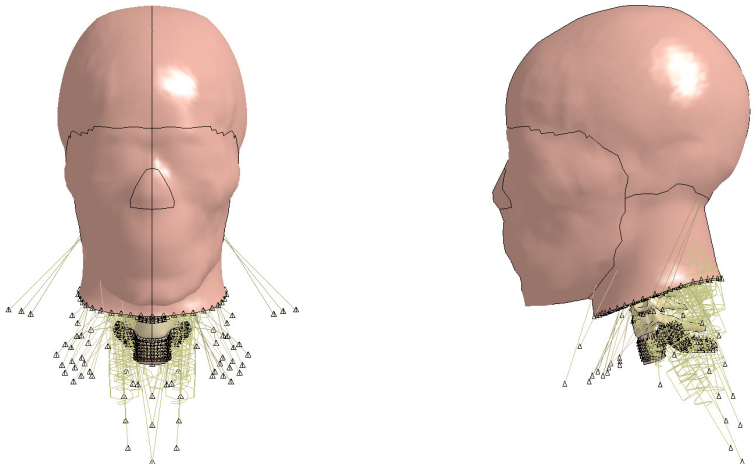

Figure 4.30: Head and neck model, with the constrained nodes highlighted.

The contact used for every impact test was the *automatic surface to surface*, with shell elements created on both the head and the cylinder surface. Segment-based penalty formulation has been used (*Soft*=2 in the contact card); this is a powerful algorithm which is based on segment-segment approach instead of a node-segment such as in the traditional contact algorithm. The head of THUMS was the most coarsely meshed surface in comparison with the cylinder, thus it has been chosen as the master surface. For maintaining the coherence with Hybrid III simulations, the same cylinder model has been used with no changes in boundary and initial conditions. For the same reason, the three different configurations of frontal, lateral and upper impact were obtained rotating the THUMS head and neck model, as done also in the experimental set up. In addition, the THUMS head has been positioned with always the same distance from the cylinder, which initial velocity was 1.428 m/s in all the test.
The sensitivity analysis has been conducted with the same criteria in all the three impact directions in order to investigate the influences of each modification in different scenarios.

Cadaver head tests

Since the THUMS is a surrogate of a human being, the comparison with cadaver tests has been considered to validate the work performed and the measures obtained. In order to not misread the cadaver data used,

a simple one-way analysis of variance (ANOVA, ANalysis Of VAriace) was conducted in Matlab®: considering the data from Loyd et al.[4], reported in table 4.11, 4.12 and 4.13, the influence of the head mass and the impact velocity[1] on the acceleration peak, the impact force peak and the HIC value has been analysed (p^2<0.05 means high influence). This has been considered necessary due to the important difference between the mass of THUMS head and neck (6.064 kg) with respect to the cadaver head (3.26 kg,*mean*) and the impact cylinder velocity (1.428 m/s) with respect to the initial impact velocity of the cadaver tests (2.06, m/s *mean*). It has been found that the mass has little influence on the evaluation of all the values of interests[3]. On the other hand, the velocity has a major influence on the values and on the base of these results, a linear regression with the velocity as unique independent variant has been used to initially predict the values of peak impact force and HIC with the known initial conditions. Once the force has been estimated, the peak head acceleration was calculated on the base of the Newton's second Law (Equation 4.1).

[1] impact initial velocity, evaluated thanks to the known heights of impact as $\sqrt{2gh}$

[2] p represents the *p-values* which is defined as the probability of obtaining a results equal or *more extreme* than the actually observed data

[3] one-way ANOVA results:

- acceleration peak: *p=0.8* for frontal impact, *p=0.75* for lateral impact, *p=0.9617* for upper impact;
- impact force peak: *p=0.73* for frontal impact, *p=0.58* for lateral impact, *p= 0.8978* for upper impact;
- HIC value: *p=0.889* for frontal impact, *p = 0.59* for lateral impact, *p = 0.967* for upper impact.

Frontal impact				
Head mass [kg]	Impact velocity [m/s]	Impact force peak [N]	Acceleration peak [g]	HIC
3.16	1.698	4339.94	140.0	221
	2.426	6289.82	202.9	581
3.27	1.698	3778.87	117.8	185
	2.426	5517.54	172.0	505
3.21	1.698	2812.07	89.3	87
	2.438	4440.11	141.0	267
3.08	1.709	2888.54	95.6	108
	2.438	5181.84	171.5	368
3.41	1.704	3813.54	114.0	156
	2.422	5747.07	171.8	402
3.45	1.726	4291.48	126.8	166
	2.409	7432.25	219.6	543
THUMS[4]				
6.064	1.428	2857.30	47.99	44.027

Table 4.11: PMHS frontal head impact: mass, impact velocity, impact force, peak acceleration, HIC [4].

Lateral impact				
Head mass [kg]	Impact velocity [m/s]	Impact force peak [N]	acceleration peak [g]	HIC
3.16	1.704	3437.85	110.9	130
	2.409	5542.73	178.8	434
	2.446	4742.94	153.0	333
3.27	1.733	3759.63	117.2	149
	1.704	3053.89	95.2	102
	2.409	4898.42	152.7	321
	2.426	4327.42	134.9	192
3.21	1.733	3149.01	100.0	112
	1.738	3306.46	105.0	104
	2.438	4345.63	138.0	232
	2.413	3463.92	110.0	192
3.08	1.704	2800.92	92.7	74
	1.732	2834.15	93.8	95
	2.438	4574.52	151.4	223
	2.413	4332.82	143.4	253
3.41	1.692	3422.15	102.3	113
	1.721	3903.86	116.7	149
	2.434	4930.84	147.4	306
	2.426	6777.39	199.0	465
3.45	1.704	4453.94	131.6	153
	1.73258	2369.12	70.0	68
	2.422	5090.22	150.4	260
	2.4261	6308.62	186.4	371
THUMS[5]				
6.064	1.428	2663.80	44.75	41.913

Table 4.12: PMHS lateral head impact: mass, impact velocity, impact force, peak acceleration, HIC [4].

Upper impact				
Head mass [kg]	Impact velocity [m/s]	Impact force peak [N]	acceleration peak [g]	HIC
3.16	1.7155	4494.94	145.0	227
	2.4261	7365.51	237.6	716
3.27	1.7438	4606.5	143.6	255
	2.4261	6572.92	204.9	579
3.21	1.704	4660.53	148.0	222
	2.4098	6549.94	208	494
3.08	1.73258	4006.48	132.6	182
	2.4261	5604.85	185.5	400
3.41	1.7097	4482.58	134.0	185
	2.4261	6656.97	199	465
3.45	1.7097	5259.43	155.4	237
	2.422	8210.67	242.6	615
THUMS[6]				
6.064	1.428	3665.4	61.57	82.55

Table 4.13: PMHS upper head impact: mass, impact velocity, impact force, peak acceleration, HIC [4].

Acceleration

The HIC and peak linear accelerations values are the most commonly reported head injury measures in crash testing generally. This is likely due to the historical nature of the measures as well as their ease of calculation.
The Hybrid III, both dummy and FEM, has an accelerometer in the head's centre of gravity. This makes the evaluation of head linear acceleration and, as a consequence, of HIC very easy in every crash scenario. In order to measure the linear head acceleration in a similar position and to have comparable data, the head CG of THUMS has been associated to an accelerometer. A sensitivity analysis related to the position of the accelerometer and its associated rigid part has been conducted. Hereby the results and the final choice adopted are briefly presented. The procedure has been repeated in all the three impact directions considered. Also for the following *drop* test 4.2.3 the path conducted has been the same.

The analysis conducted were focused on two main aspects:

- selection of node;
- selection of the rigid part to which associate the accelerometer.

Once the head CG of THUMS has been identified, the nearest existent node in the sagittal plane of the head (node ID 88178224) has been chosen and its linear acceleration time-history has been saved. It must be noticed that the node belonged to a rigid part. The second node selected for the collection of the head linear acceleration was the CG itself. Some modifications have been conducted on THUMS in order to evaluate the CG time-history values. On the base of the definition of a seatbelt accelerometer in the LS-DYNA manual, three nodes have been created in order to define the local coordinate system to which the velocities and accelerations of the CG node will be referred in the output:

- node 1: node ID 90000001 in the CG;
- node 2: node ID 90000002; local x-axis run from node 1 to node 2;
- node 3: node ID 90000003; local z-axis was perpendicular to the plane containing nodes 1, 2 and 3.

The three nodes must be all part of the same rigid body. In order to complete the definition of the seatbelt accelerometer for the evaluation of the acceleration in the CG, the three nodes were unified in one node set and constrained to a unique rigid part. The choice for the most suitable rigid part was aspect of investigation. The main reason related to this investigation was the quasi-complete absence of rigid part in the sagittal plane or in the neighbourhood of the CG. Three different rigid part were selected:

- Rigid part named Cover (Figure 4.32). It is the unique rigid part in the sagittal plane in the head of THUMS. This is the same part to which belongs the node previously selected –88178224–;
- part 250 (Figure 4.33), created by the union of two existent parts –88000247 and 88000251– which were respectively on the left and

on the right side of the sagittal plane; the part was made rigid for the purpose;

- part 500 (Figure 4.33), created selecting 12 elements in the occipital bones.

node ID	x	y	z
90000001	831.88	0.108	-34.963
88178224	863.221	0.095	-74.504

Table 4.14: Nodes coordinates in the global reference system.

Frontal test

In frontal impact tests, the highest acceleration component was registered in x direction and so it has been selected as parameter for the comparison of the results. The first investigation compared the axial acceleration measured thanks to the accelerometer related to the new node 90000001 in correspondence of the CG and the evaluation of the raw nodal acceleration. Both of this nodes referred to the same rigid part 88000217, named Cover in the THUMS. The time-history of the x-acceleration is depicted in Figure 4.31.

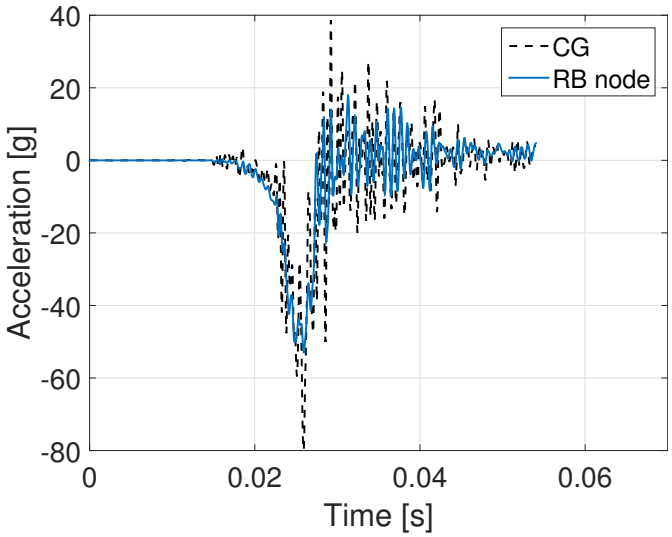

Figure 4.31: x-axis acceleration evaluated in the CG and in the cover central node; frontal impact.

By definition, a seatbelt element accelerometer has to be fixed to a rigid part. Since only one rigid part in THUMS was near the head CG in the sagittal plane of the head, two different rigid parts were created to compare the results and to understand the relation between the accelerometer measurement and the position of the rigid part picked. The first rigid part selected was the *cover*, positioned at the base of the head (Figure 4.32).

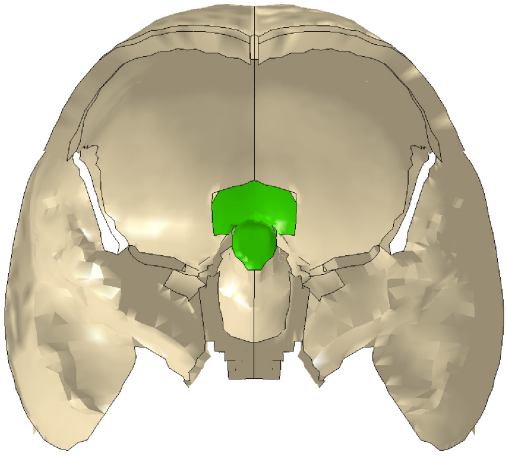

Figure 4.32: Part 88000217, cover.

Two symmetric parts in the neighbourhood of the CG were selected and transformed in one rigid (part named 250 in the following, depicted in Figure 4.33). Since they were very close to the CG and they had little dimension (a change in their material should not influence remarkably the head movements), it has been opted for such an approach.
Moreover, twelve elements on the base of the occipital bone, six from the right and six from the left, were chosen and transformed in a unique rigid part, named 500. This configuration can be considered as the most comparable with the Hybrid III, in which the rigid part which the head accelerometer was referred to, was a unique part with the skull.

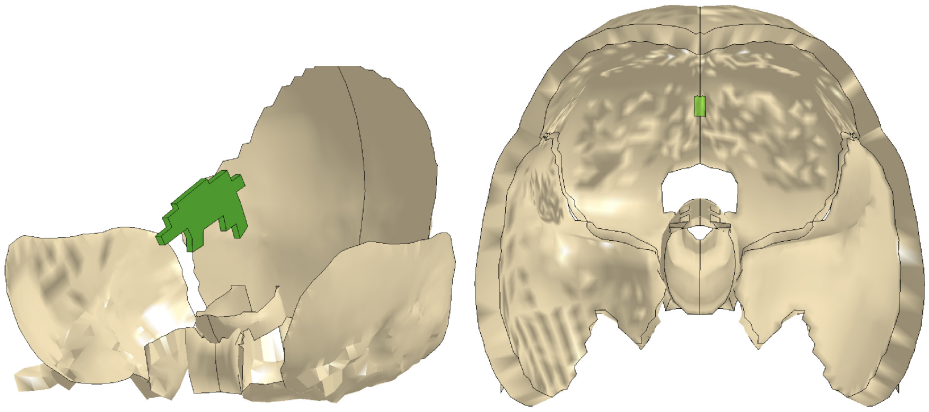

Figure 4.33: Part 250 (left) and part 500 (right).

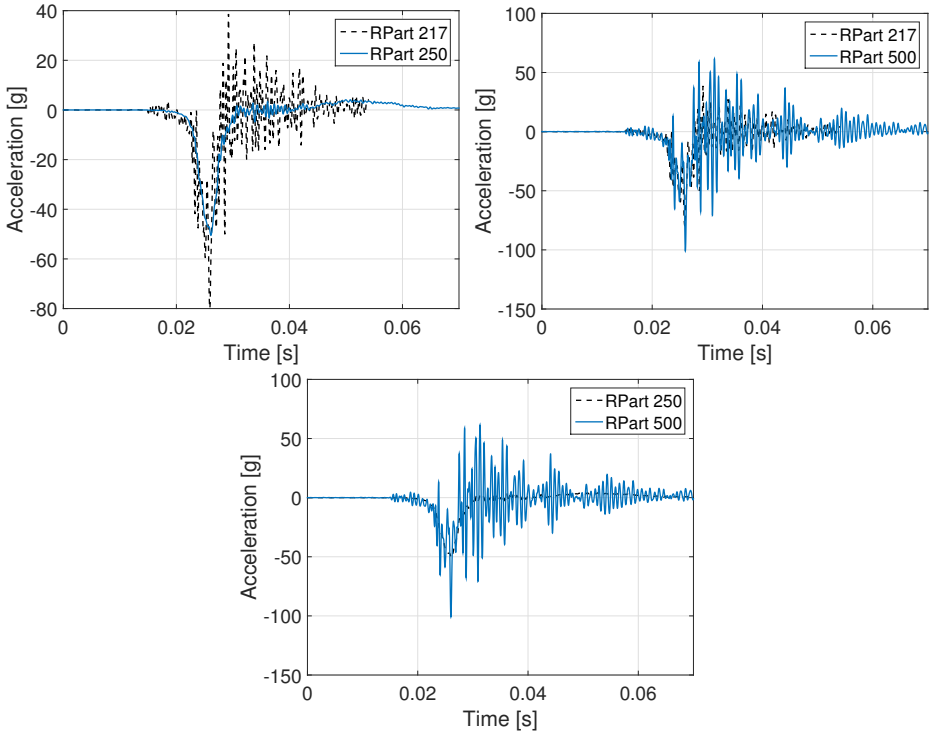

Figure 4.34: x-axis accelerations in CG, considering different rigid parts; frontal impact.

In order to select the best rigid part for the accelerometer definition, the x-axis accelerations related to each of them have been compared (Figure 4.34). Part 217 and part 500 show noisy acceleration signals compared to the signal of part 250. In this frontal impact condition the

rigid part 250 can be considered as the preferable for the accelerometer definition.
A brief investigation has been conducted also on the parameters that influenced the most the contact definition between the cylinder and the THUMS head. The graph in Figure 4.35 depicts the acceleration in the primitive contact definition compared with the final contact solution. The coefficient of friction has been augmented to better represent the real contact situation (friction coefficient = 0.9).

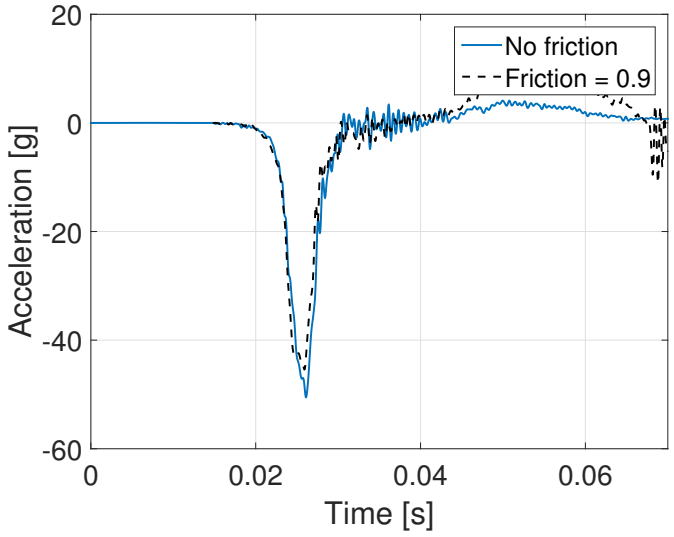

Figure 4.35: x-axis acceleration: comparison between two friction conditions; frontal impact.

Lateral test

As for the frontal tests, also for the lateral test the most suitable position for the measurement of the linear head acceleration has been searched. *y-axis* acceleration has been selected as term of comparison since the most important variation happened in the *y* direction (reference is the local head coordinate system, 4.21). The procedure followed has been the same as in frontal test, thus the main purpose of the work was the investigation of a global criteria for the evaluation of linear acceleration.
Hereby the graphs related to the analyses are presented with a brief description as comment.

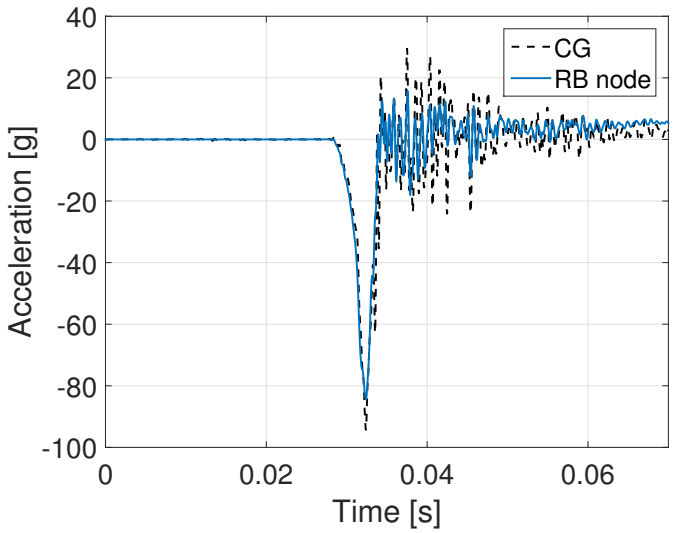

Figure 4.36: y-axis acceleration evaluated in the CG and in the central cover node; lateral impact.

The same analysis conducted for the frontal tests were recreated in lateral impact configuration. Figure 4.37 confirm the expectation: as in frontal impact, the rigid part which the accelerometer is related to that present the lowest noise time-history signal, was the 250.

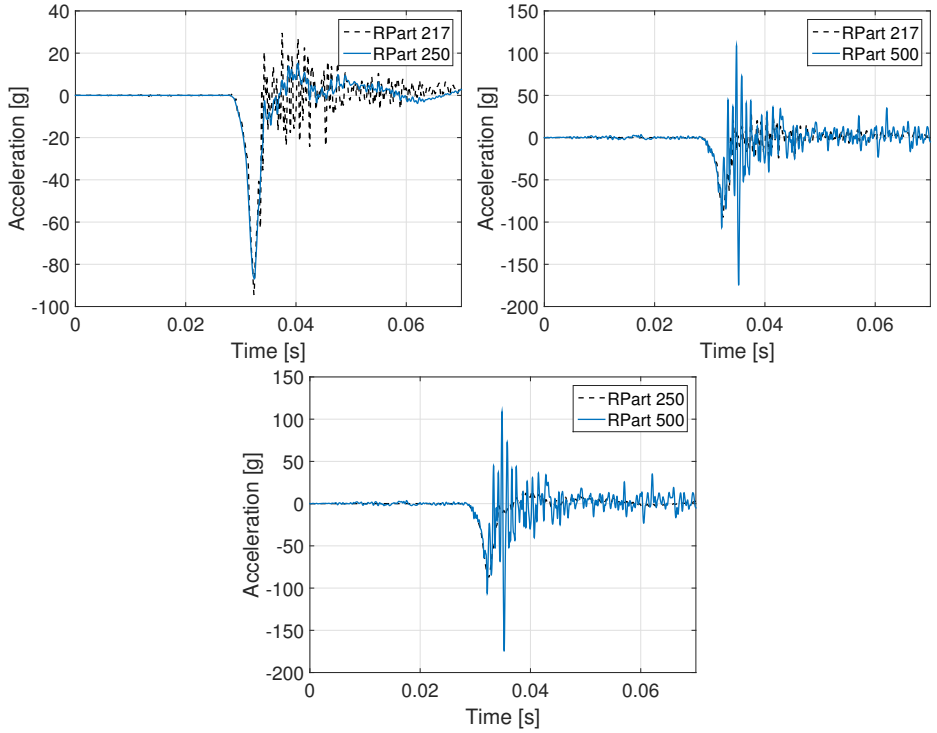

Figure 4.37: y-axis accelerations in CG, considering different rigid parts; lateral impact.

Upper test

At last, also for the upper impact tests, the same procedure has been followed. This repetitiveness has been necessary for the scope of this work: not only for the comparison with the experimental tests previously described, but also for the search of the best instrumentation-like in THUMS. The analysis in this scenario converted on the *z-axis* linear acceleration.

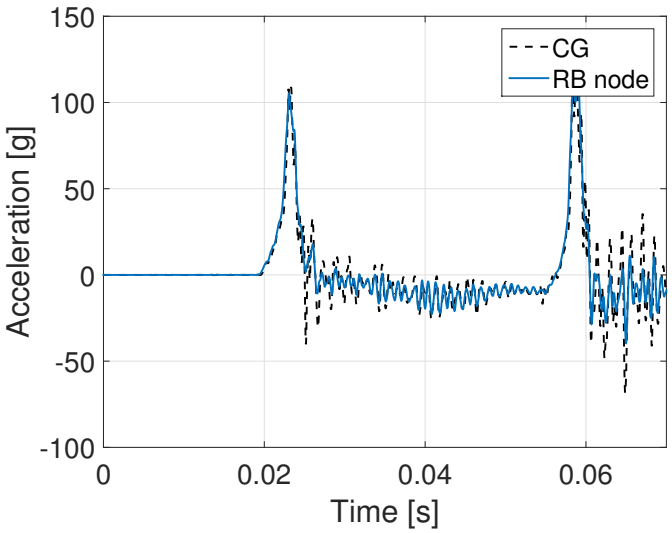

Figure 4.38: z-axis acceleration evaluated in the CG and in the central cover node; upper impact.

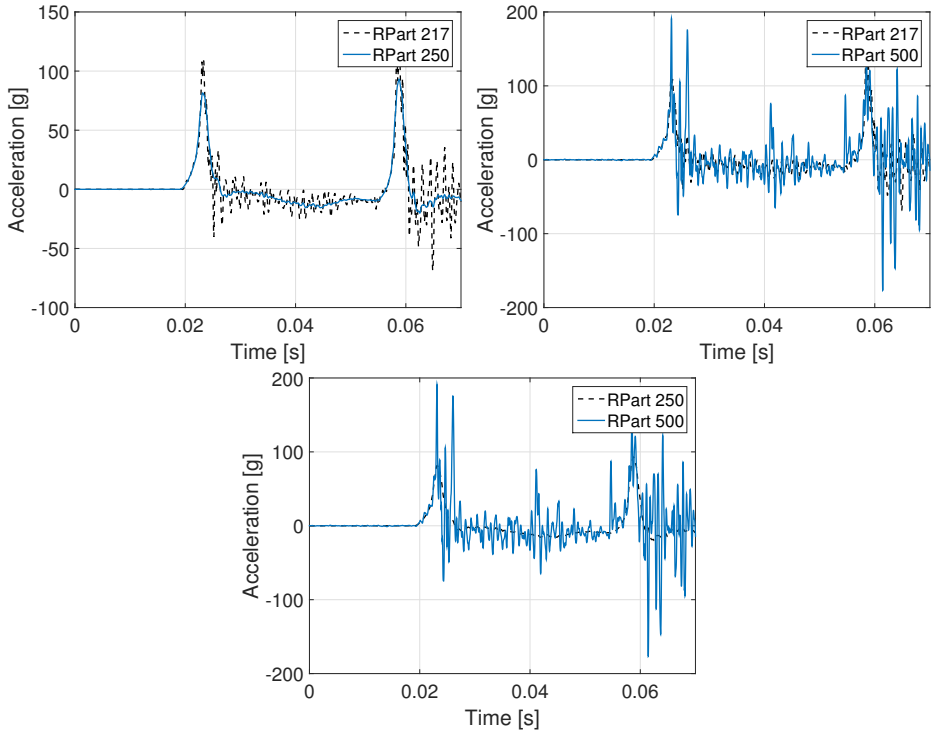

Figure 4.39: z-axis accelerations in CG, considering different rigid parts; upper impact.

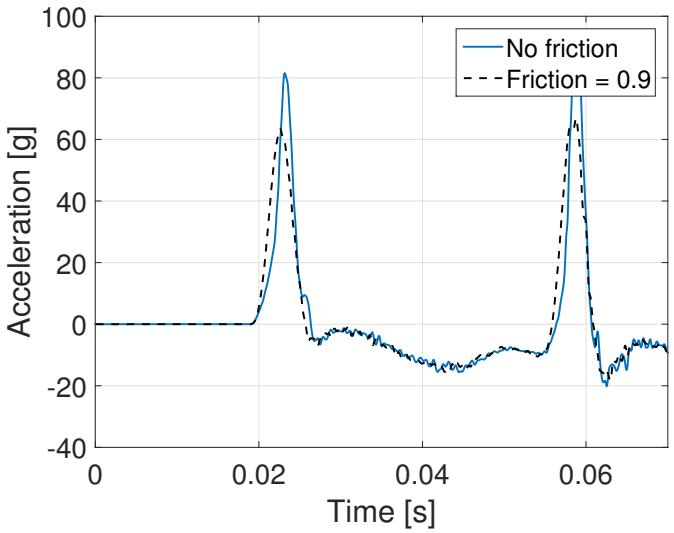

Figure 4.40: z-axis acceleration: comparison between two friction conditions; upper impact.

The rigid part 250 has been finally selected for the definition of the accelerometer. Also the upper test simulations (Figure 4.39) confirmed that part 217 and part 500 gave too noisy time-history signals.
This analysis has been conducted adopting the same class filter for every signals (CFC 1000, Appendix A).

Forces and moments

While the criteria for the determination of the occurrence of fatalities in the head are based on the acceleration, the evaluation of forces stands on the background of neck injuries.
Neck injury risk is evaluated primarily on the basis of NIJ, neck tension force, and neck compression force. The NIJ is a linear combination of neck axial force and the bending moment about a lateral axis passing through the head's occipital condyle (1). Furthermore, in addition to NIJ, neck axial force itself is compared with cut-off values (described in the paragraph 1.3). Due to this, the research for a method of evaluating the neck forces has been considered in this work.

Methodology

The forces at each cervical level of the neck were captured using two different techniques, both based on the definition of cross section in LS-DYNA. This technique was validated for the analysis of neck response of the Global Human Body Models Consortium (GHBMC) during a simulated rotary-wing aircraft impact [29]. Three different cross sections were created at each vertebral level of the cervical spine (except for the top neck level, as explained) to calculate the force contributions from different anatomical components of the neck. In particular, the three cross section categories can be classified as:

- Vertebrae cross sections: defined with the *set* option; the elements which the cross section cuts are on each vertebra. Thus, seven vertebra-cross section are defined, from C1 to C7, plus one for the upper C2; those were used to capture forces contributions from bones;
- cartilages cross sections: defined as well with the *set* option; they were related to the elements representing the intervertebral discs between the vertebrae, from C2-C3 to C6-C7. Five IVD cross sections were defined as no disc exists between the two top vertebrae;
- planes cross sections: created using the definition of *cross section planes*; five planes were defined at the same five level of the IVD to understand the contributions from ligaments, muscles and soft tissue at each level of the cervical spine. The *plane* option in the cross section definition yielded the advantage of the automatic generation of the set of element through which the forces are evaluated. For every plane, the designation of the correspondent part set must be assigned, in order to not evaluate extra forces coming from undesired part. If no part is assigned to the plane, LS-DYNA will include automatically all the parts of the model and all their elements that lie on the plane concur at the forces computation.

The definition of the cross section yielded the possibility to straightly evaluate forces and moments with only light modification to THUMS,

such as the addition of new set of elements. In the cross sections definition, only deformable elements to one side of the interface were selected.
Particular attention was given to the influence of tendons as previously explained (Section 4.2.2).
The first two cervical vertebrae, C1 (Atlas) and C2 (Axis), depicted from the THUMS neck in Figure 4.41, are geometrically atypical. Due to this, two different cross sections were defined for the C2 vertebra, one for the *dens* (bottom-right in Figure 4.41), the protuberance of C2, where it joins the skull, and one for its body. No Intervertebral Disc (IVD) exists between these two vertebrae.

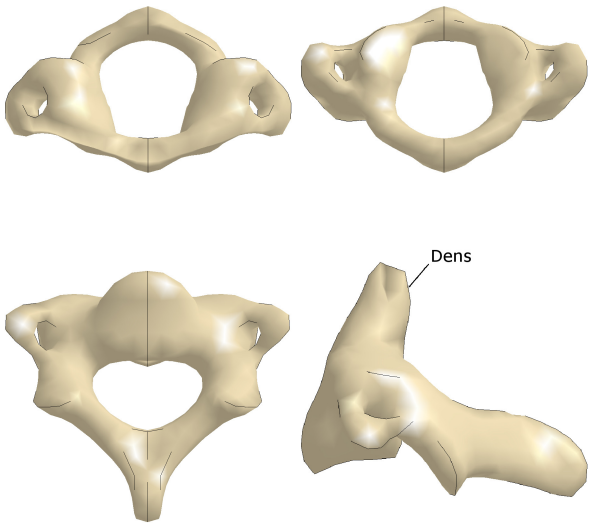

Figure 4.41: The atypical C1 and C2 cervical vertebrae.

The remaining cervical vertebrae, C3-C7, are similar to one another in structure (Figure 4.42) and contain intervertebral discs between each adjacent vertebral body.

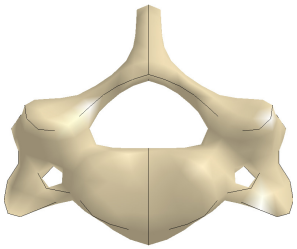

Figure 4.42: Superior view of a typical cervical vertebra.

The IVDs' elements have been used for the definition of the five cartilages cross sections. Both the vertebrae and the cartilages cross sections are depicted in Figure 4.43.

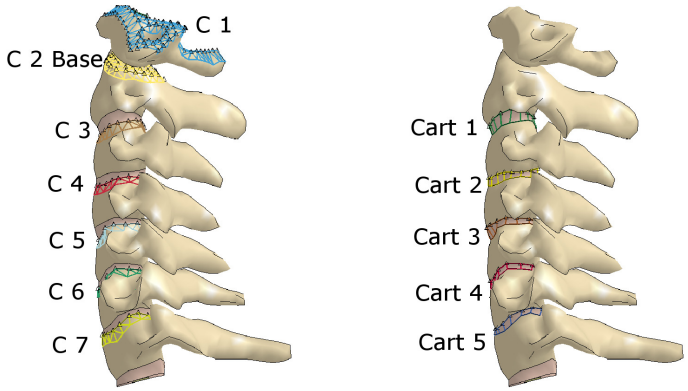

Figure 4.43: Cross sections in the vertebrae (left) and in the IVDs (right).

The plane definition was subjected to variation during the analysis. A radius was set and a circular cut plane was created; its centre was defined selecting the node in the centre of the nucleus polposus of the IVD (Figure 4.44). From the results of the same simulation with only different radius values, the computational cost of the plane was observed to be relevant. The higher the radius the slower the simulation[7]. The principal approach to the plane definition was related to the interesting in the evaluation of every neck part contribution to the forces, such as flesh, tendons, muscles.

[7] R = 20 simulation arrived at the end time; R = 80 simulation was interrupted because of wall-time.

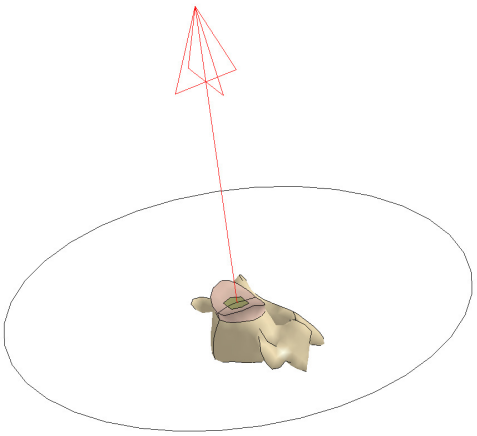

Figure 4.44: Cross section plane.

According to the results reported by Ono et al. [30] activation of he neck muscles is considered to occur within a range from 70 ms to 140 ms after the impact: since this study focused on frontal, lateral and upper impact scenarios with shorter phenomenological time duration, muscle activation would not be necessary. In the simulations the passive muscle responses were simulated. The same cross section were used for the collection of moments. For the purpose of those dissertation, only the moments about x-axis and y-axis were taken into account (described in Section 4.2.2). The forces and the moments were evaluated in two different coordinate systems:

- the local head coordinate system, the same used for the accelerations (Figure 4.21);

- the local neck coordinate system, different for each level considered: seven references system were created as seven were the vertebrae.

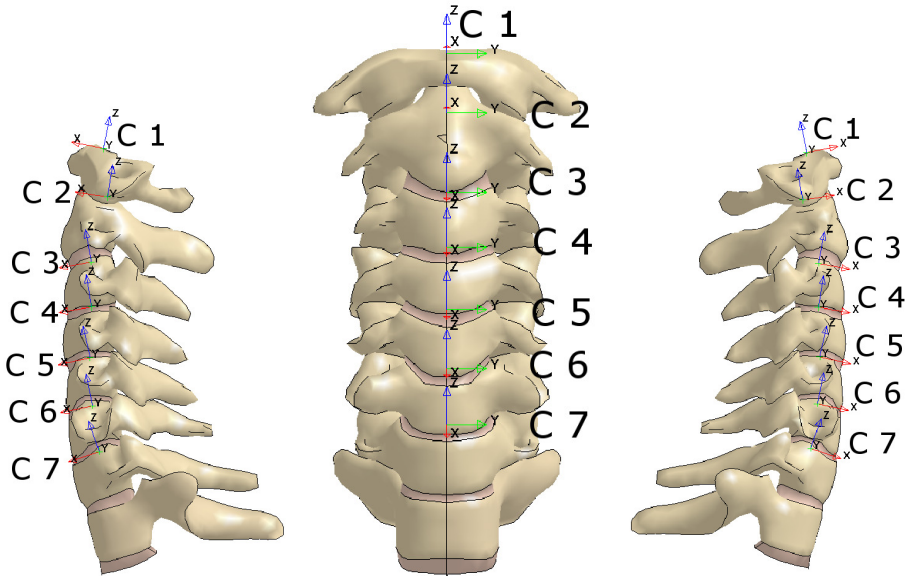

Figure 4.45: Local coordinate system defined for every vertebra.

In Figure 4.47 the forces in the two reference systems are depicted. The main differences are registered in x-axis direction: the head coordinate system has the x-axis in horizontal direction while the local neck system has different orientation for each x-axis at different neck levels.

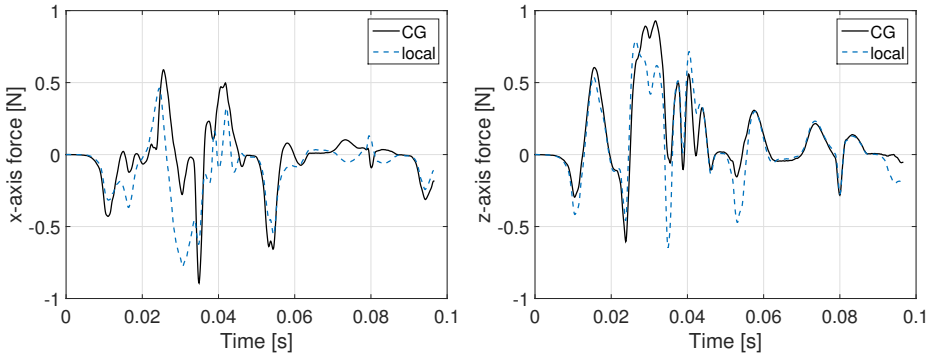

(a) Vertebra C1.

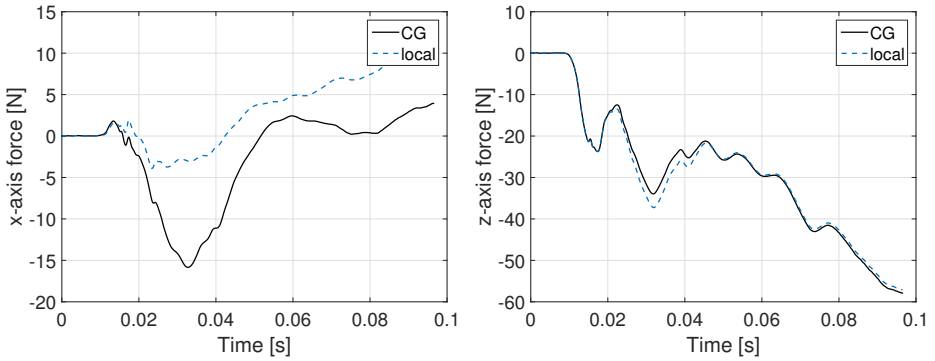

(b) Vertebra C3.

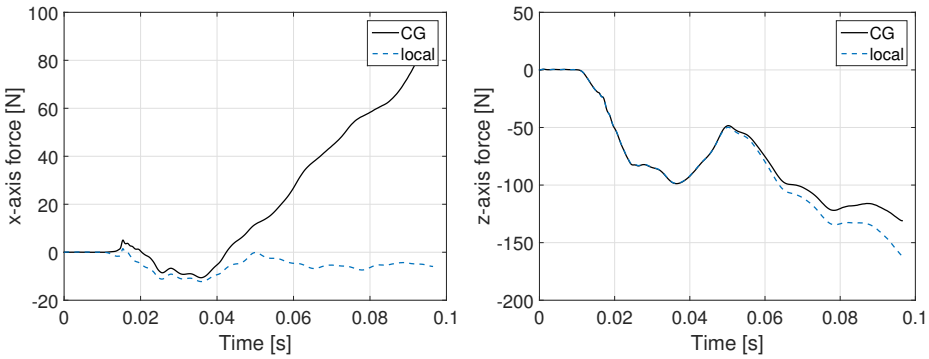

(c) Vertebra C7.

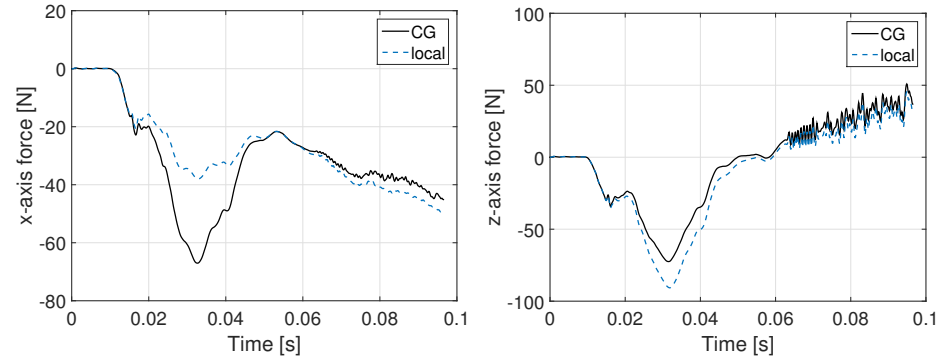

(a) Cartilage 1.

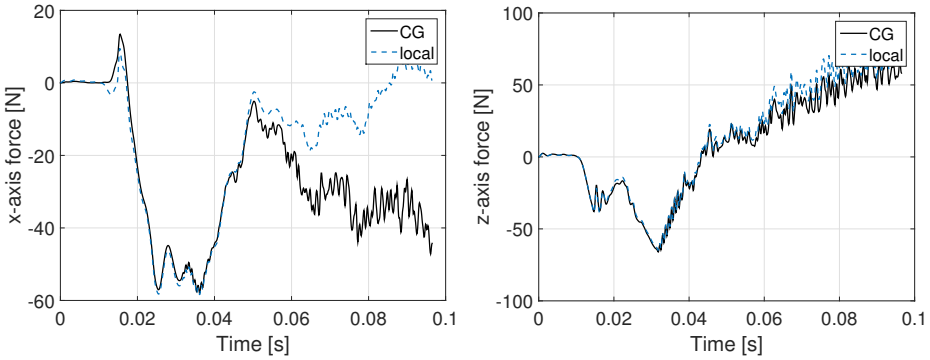

(b) Cartilage 5.

Figure 4.47: Comparison of axial forces in vertebrae (a, b, c) and IVD (d, e) in head local system and vertebrae local system.

Frontal test

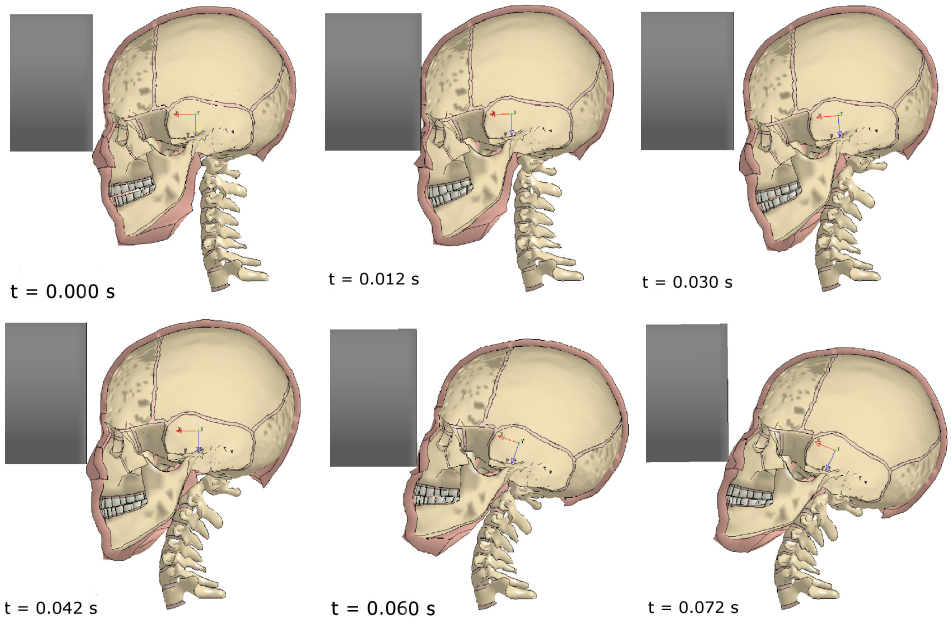

Figure 4.48: Simulation visualisation of frontal impact configuration.

The axial forces evaluated in the vertebrae for the frontal impact test are depicted in Figure 4.49.
The x-force registered in all the neck components were lower than the axial z-forces. The lower cervical vertebrae tended to experience greater axial forces both in x and z direction than the upper vertebrae. The first two vertebrae had particular behaviour. Both in x and z-direction they experienced a quasi-null force. This could be explained looking at the neck movement: the first two vertebrae rotate the most with respect to the vertical initial position than the other cervical vertebrae which initial movement was a compression.
The movement of the head –in particular the nodding movement– took place predominantly at the *atlanto-occipital* joint between the atlas (C1) and the occipital bone; the atlas rotate upon the pivot of the axis (C2). The forces in both x- and z-axis direction experienced by those topmost vertebrae were the lowest. The intensity of vertebrae forces increase as the level decrease (from top to bottom), as depicted in Figure 4.49. The bottom vertebra C7 experienced the highest force.

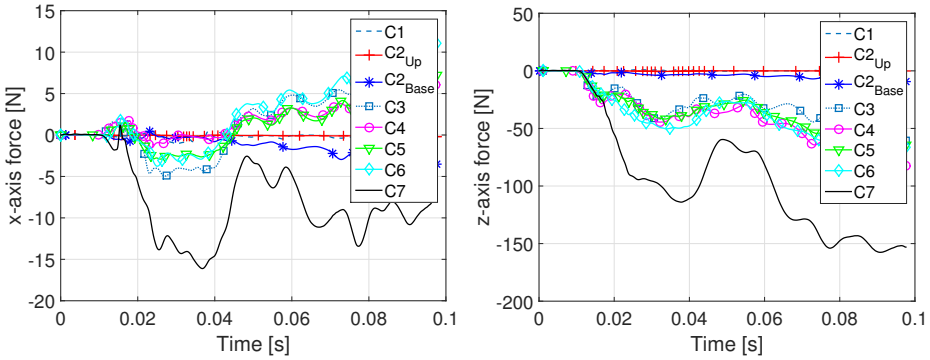

Figure 4.49: Vertebrae axis forces; frontal impact.

The combined analyses of the x- and z-axis axial force shown different periods of positive shear and compression followed by periods of negative shear and tension. The change in load direction can be related with head rotation. Prior to onset of head flexion rotation, all levels underwent axial compression with peaks level occurring approximately at the same time. Maximum compression was noticeable larger for C3-C7 levels than for C1 and C2 levels. The forces registered in the IVD cross sections (Figure 4.50) presented a similar trend to the vertebrae: the lower the neck level –upper neck position–, the lower the axial force.

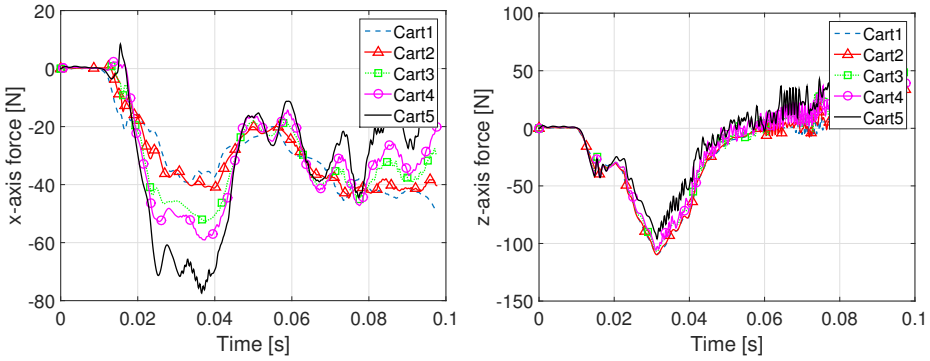

Figure 4.50: IVD axis forces; frontal impact.

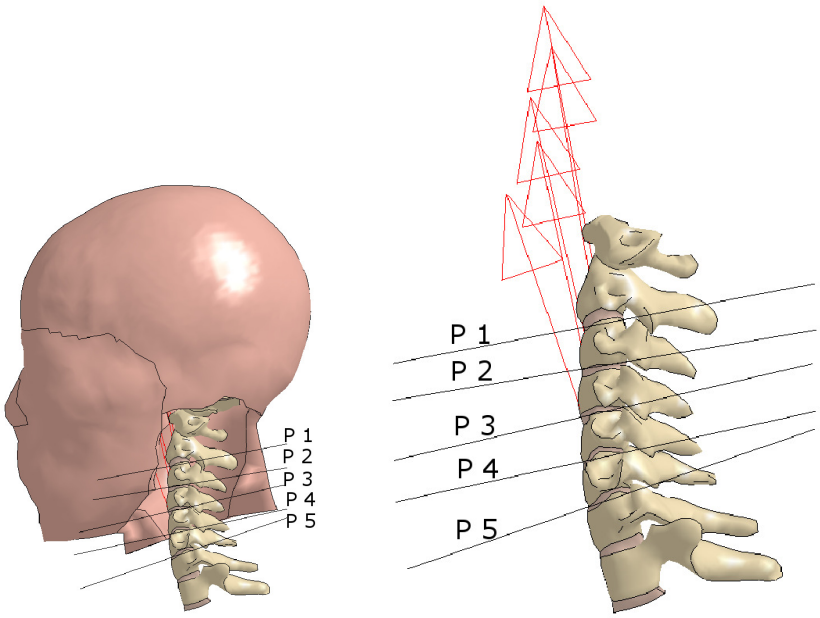

Figure 4.51: Planes used for the forces evaluation.

The forces trend in the various neck levels was similar in vertebrae, IVDs and planes cross sections: the forces increase such as the level increase (from top neck to bottom). Only the fifth plane cross section shows an opposite trend both in x- and z-axis. This is related to the absence of flesh in the part of the cervical column where the fifth plane was defined (Figure 4.51). Thus, the forces experienced by this plane are exactly the same as the forces registered by the fifth cartilage (Figure 4.56, 4.65 and 4.74).

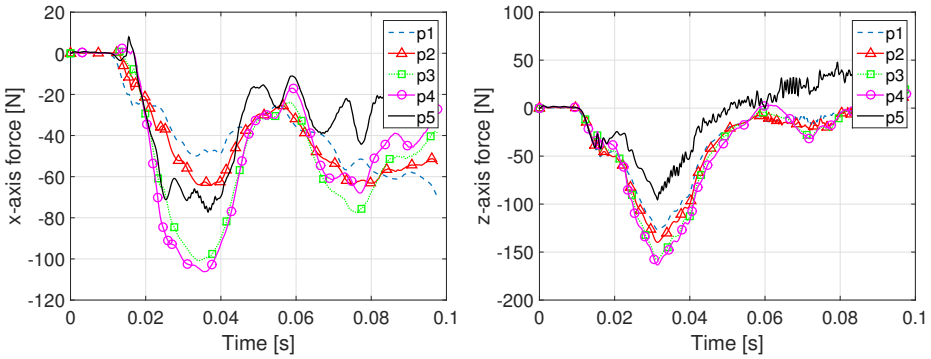

Figure 4.52: Planes axis forces; frontal impact.

Both in x and z direction the plane cross sections recorded the highest forces with respect to vertebrae and IVDs. In plane definition not only the bones or the IVD are selected –as done by the user for the cross section definition– but also the flesh and tendons that surround the cervical column contribute to the force evaluation.
From the evaluation of vertebrae, IVD and plane forces is possible to consider the phenomena concluded within about 40 ms. This consideration is in linear with the cadaver test from literature [4, 6, 28]
In addition to the evaluation of forces directly on THUMS and its neck component, the contact force between the impactor and the head has been recorded during the simulation. This gave the possibility to confirm the relation between head acceleration and forces measured, considering Newton II Law:

$$F = ma \tag{4.1}$$

Once the head acceleration is known –the head and neck total mass is automatically registered in LsPrepost– it has been possible to calculate the axial force between the head and the pendulum. Actually the contact force has been used as a criteria to select the most reliable method for the head acceleration measure – as previously described in this Chapter (4.2.2)– due to the fact that the head mass and the force score do not depend on a user defined node or accelerometer.

m = 6.064 kg;

$\mathbf{a}_x$ = 46.83 g = 459.402 m/s^2;

F = 2785.8 N.

In Figure 4.53 the confirmation of the result obtained is depicted.

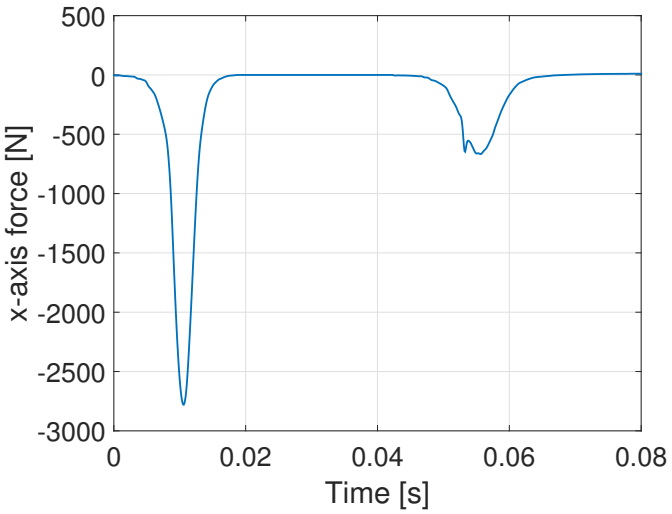

Figure 4.53: Contact axis forces; frontal impact.

Eventually, the vertebrae, IVDs and planes forces have been compared and analysed simultaneously in all the neck levels –vertebrae C1 and C2 were not considered in the analysis because they registered too low forces and because of the absence of correspondence IVDs and planes in those upper neck levels–. In every neck level the cross section defined on the vertebrae registered lower forces than the equivalent cross section in the neck; as a consequence, also in the plane the forces were higher than in the vertebrae. This is related to the material of the IVD (Figure 4.54):

- Mat Fu-Chang foam for the outer part of the intervertebral discs;

- Mat Isotropic elastic-plastic for the nucleus pulposus.

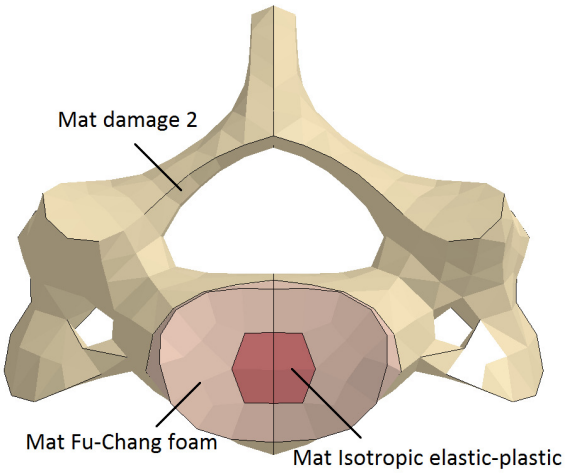

Figure 4.54: Materials of IVDs and vertebrae.

In Figure 4.55 and Figure 4.56 the comparison of the three cross sections are reported for the upper and the lower neck levels; it must be noticed the exception in the last graph of Figure 4.56: the C7 vertebra experienced a higher force than the correspondent plane and cartilage. This is related to its proximity to the constraint in T1.

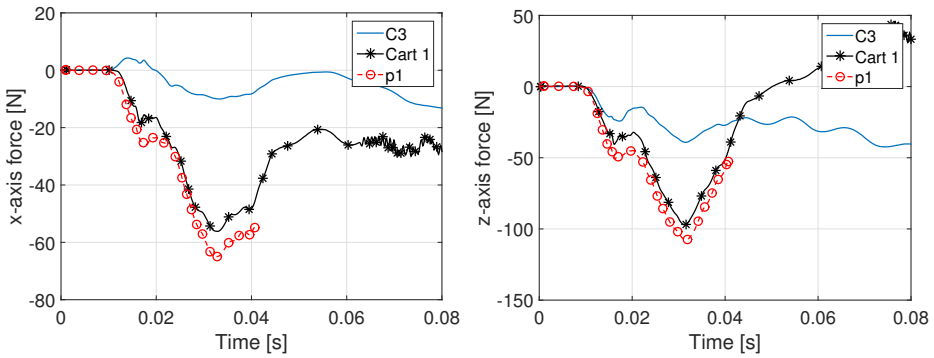

Figure 4.55: Axis force in C3 and in cartilage and plane at the correspondent position; frontal impact.

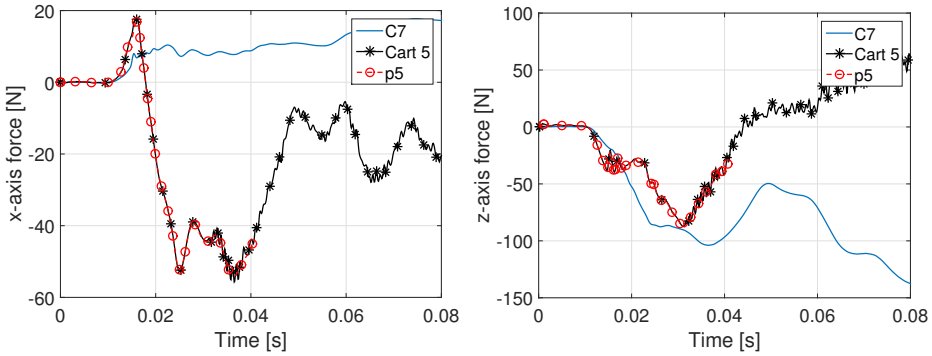

Figure 4.56: Axis force in C7 and in cartilage and plane at the correspondent position; frontal impact.

The forces registered in THUMS neck were lower than the contact one because of the inertia of the head and some dissipation due to the presence of lots of elements. Strong differences are visible going through the neck level from top to bottom.
It must be noticed that those behaviour of THUMS were not registered in Hybrid III: data from Sances et al. [31] reported that the Hybrid III system transmitted about 70-75% of applied force from the head or upper neck to lower neck area. In contrast the cadaver studies shown that about 20-30% of the applied force was transmitted from the head to the lower neck. Thus, the real human behaviour is more represented by THUMS than Hybrid III, as expected.

Moments

Following the analysis of forces, the moments evaluation is presented for the same impact condition. No depth analysis were computed because the same cross section created for the evaluation of forces have been used. The measurement of moments has been considered important at the unique final objective of the NIJ calculation.

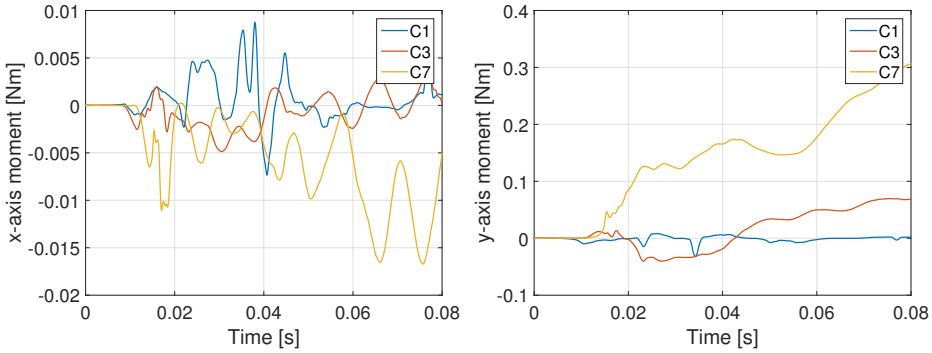

Figure 4.57: Moments about x and y axis in vertebrae; frontal impact.

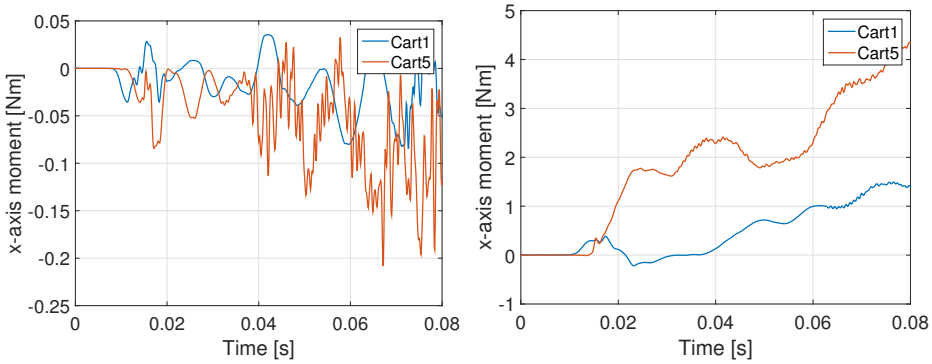

Figure 4.58: Moments about x and y axis in cartilages; frontal impact.

At this point, is possible to evaluate the NIJ for the frontal impact, as well as the MOC: the calculation has been done in two different neck position, considering the top and the bottom IVD peak forces and moments.

Lateral test

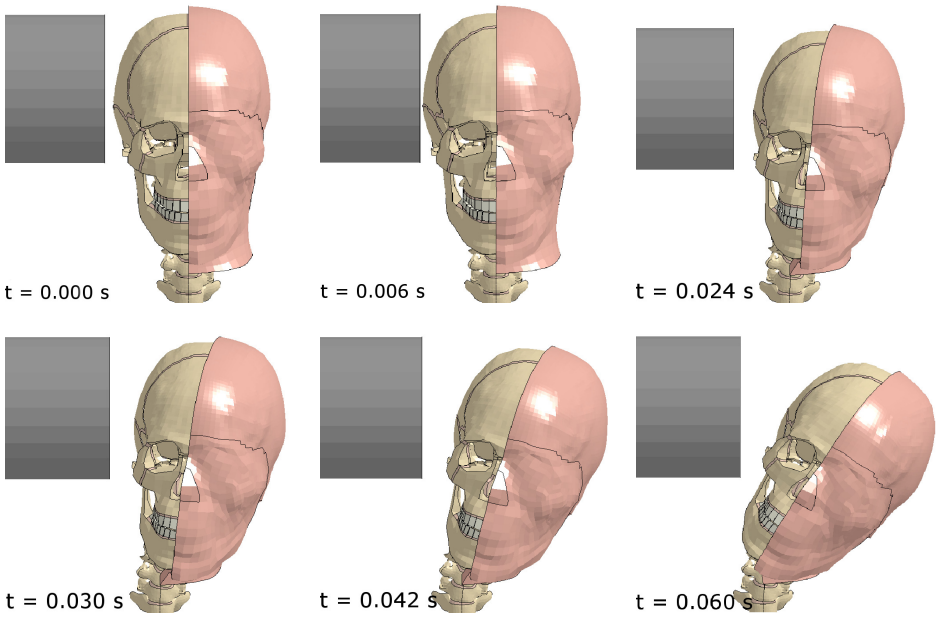

Figure 4.59: Simulation visualisation of lateral impact configuration.

The lateral tests have been conducted considering the y-direction as the main one, both for the previous acceleration analysis (Section 4.2.2) and for the hereby described evaluation of forces. In addition, also the z-axis forces has been analysed. The purpose of z-axis interest is related to the fact that in the head-cervical spine axial compression predominated over flexion because of its anatomical nature. The mechanical responses of the cervical column shown that in axial direction it experienced greater forces than in the off-axis (x and y) directions, even if the impact direction was not the axial one.

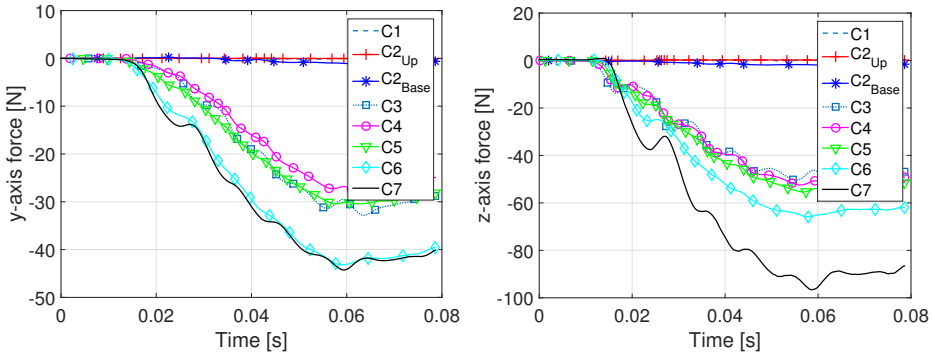

Figure 4.60: Vertebrae axis forces; lateral impact.

The same results obtained in frontal impact are here reported for the vertebrae forces evaluation (Figure 4.60) in lateral impact: as in frontal tests, the lower the neck level, the higher the forces, with vertebra C7 with the higher contribute both in the impactor direction and in the axial neck direction.

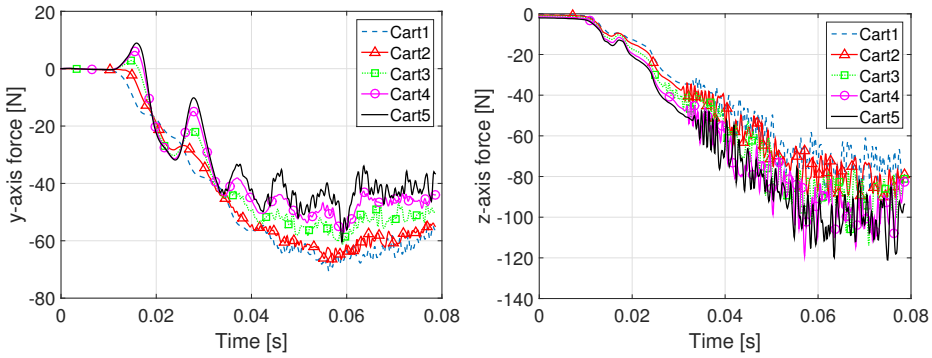

Figure 4.61: IVDs axis forces; lateral impact.

The forces time-history related to the IVDs cross sections presented an oscillatory trend related to the combined compression-tension action to which the IVDs are exposed during the lateral impact. The LS-DYNA simulation visualisation allowed to identify the IVDs behaviour: half the elements resulted compressed during the phenomena and half the elements were stretch.
This is related to the crucial role of IVDs in the spine as shock absorbers. Infact, the IVDs main function, in addition to their basic function to separate the vertebrae from each other, is to distribute pressure in all directions within each IVD under compressive loads (in particular this is

the nucleus pulposus role).

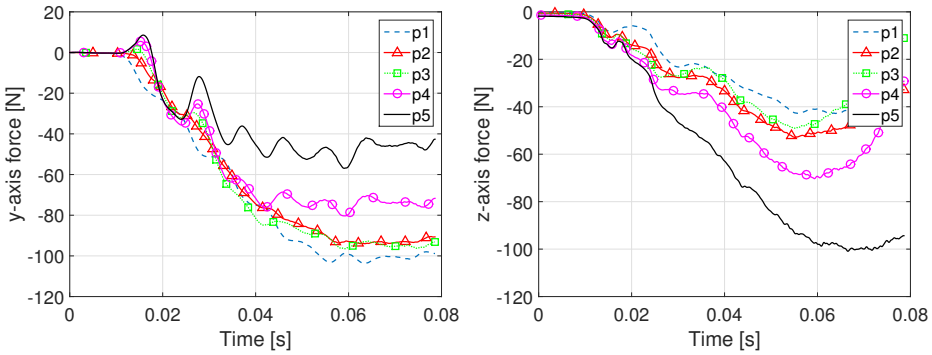

Figure 4.62: Planes axis forces; lateral impact.

The results obtained applying the Newton II Law (Equation 4.1) in the lateral head impact presented an error about 26%:

m = 6.064 kg;

$\mathbf{a}_y$ = 66.695 g = 654.2 m/s^2;

F = 3967 N.

The lateral contact force experienced in the simulation is depicted in Figure 4.63 where the maximum y-axis force registered is 3137.3 N.

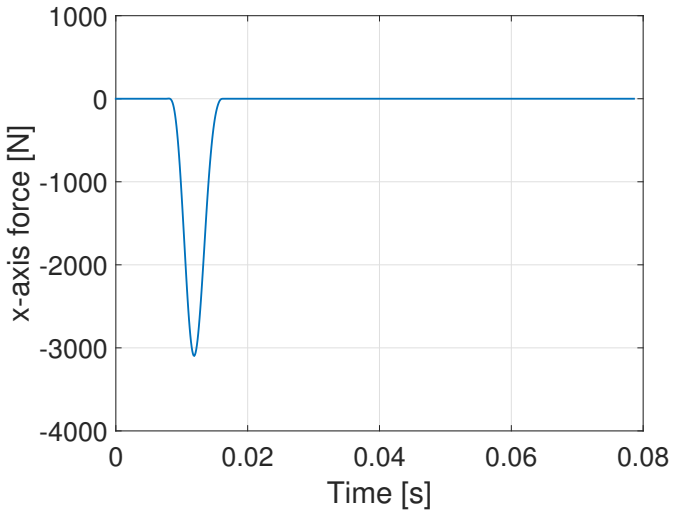

Figure 4.63: Contact x-axis forces; lateral impact.

As in the frontal impact, also for the lateral configuration the different cross sections results have been compared and analysed in order to evaluate the most reliable between the three and to finally select only one of them for the final forces evaluation. As expected, in the upper neck levels the plane experienced the highest y-axis forces compared to vertebrae cross sections and IVDs': the plane cross sections are composed by the same element as IVDs cross section with the addition of flesh and muscles and tendons. Therefore, in the lower neck levels, where the flesh are no more present, the cartilages cross sections and the planes cross sections forces measures were quite identical (Figure 4.65).

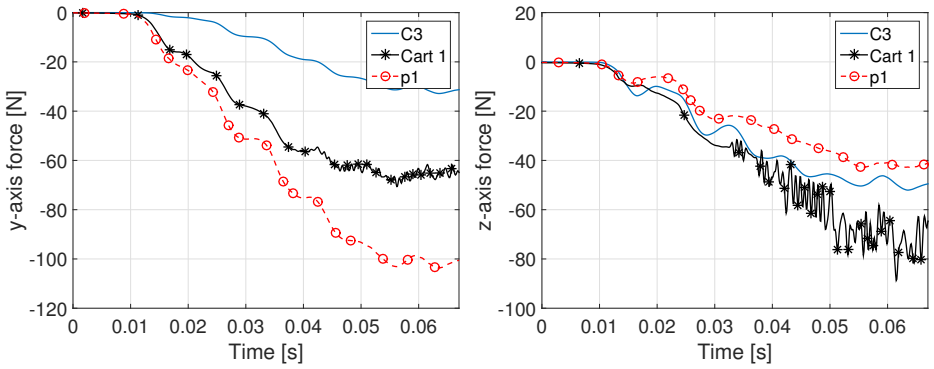

Figure 4.64: Axis force in C3 and in cartilage and plane at the correspondent position; lateral impact.

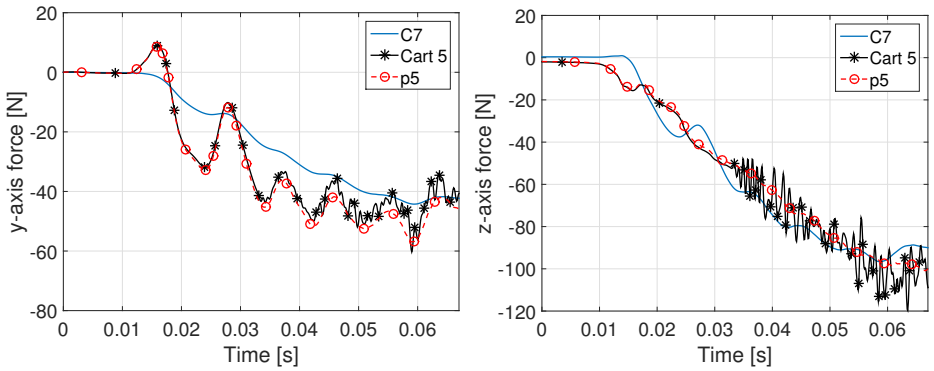

Figure 4.65: Axis force in C7 and in cartilage and plane at the correspondent position; lateral impact.

Moments

In lateral impact test the head rotate the most about the x axis (considering the head coordinate system, Figure 4.21); the IVDs cross sections experienced highest moments than the correspondent vertebrae cross sections, for the same reasons previously explained.

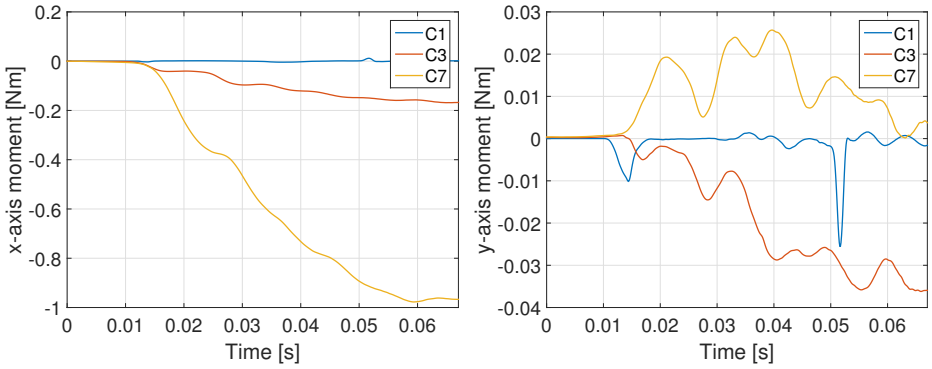

Figure 4.66: Moments about x and y axis in vertebrae; lateral impact.

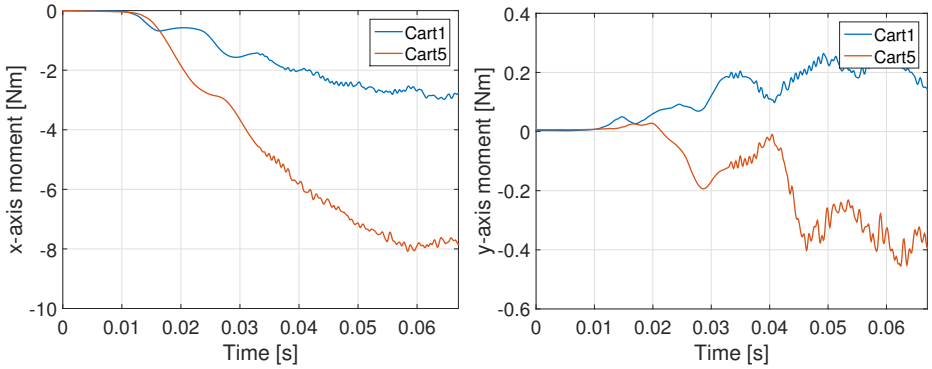

Figure 4.67: Moments about x and y axis in the IVDs; lateral impact.

Upper test

Lots of cadaver tests were conducted with the head in a configuration similar to the upper tests analysed in this work [28]. This gave the possibility to critically read the data obtained.

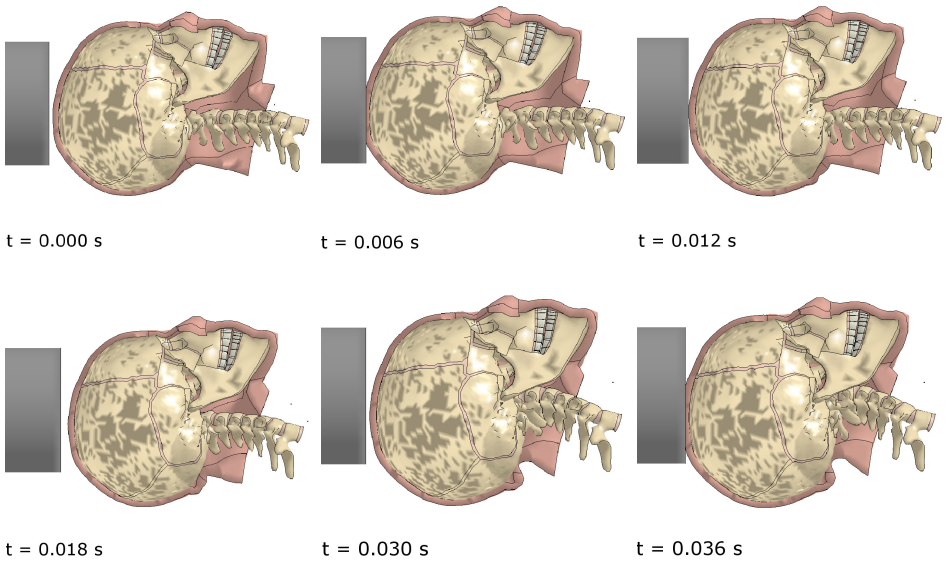

Figure 4.68: Simulation visualisation of upper impact configuration.

For the upper impact tests the z-axis force represent both the impact direction and the cervical column axial forces. On the base of that, only forces in z direction are reported. However, forces in all the three directions were registered. In x-axis direction (the reference coordinate system is centred in the head CG 4.21) the forces were elevated. This is related to the way in which the head was constrained: it underwent not only to the impact forces but also to the gravity field. Different neck levels experienced different x-axis forces in every cross sections considered;

As in every head test conducted, also in upper impact test the Atlas (C1) and Axis (C2) encountered quasi-null forces. Then, the lower in the neck the vertebra, the higher the first peak z-axis force value.

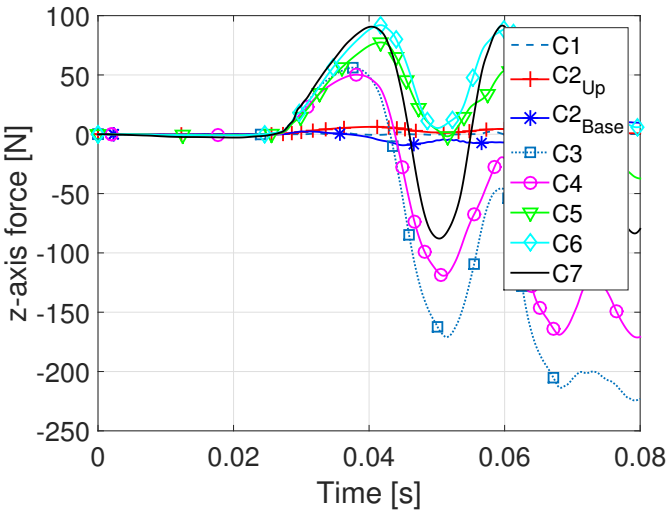

Figure 4.69: Vertebrae axis forces; upper impact.

z-axis forces in the IVDs were very similar one another as in the plane cross section definition. There were no significant differences between the different neck levels.

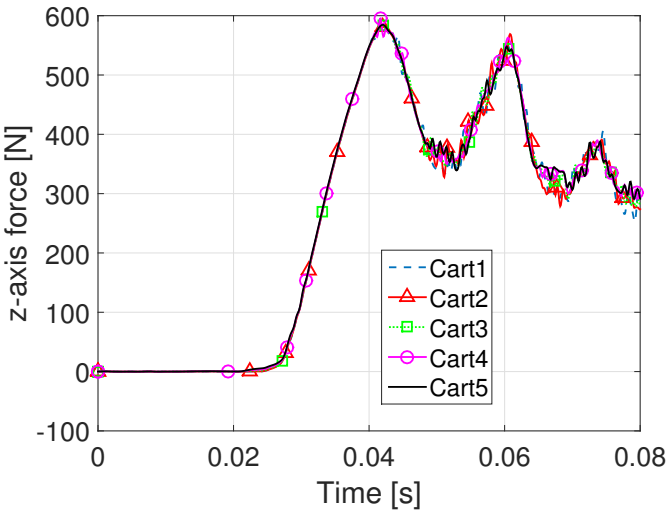

Figure 4.70: IVDs axis forces; upper impact.

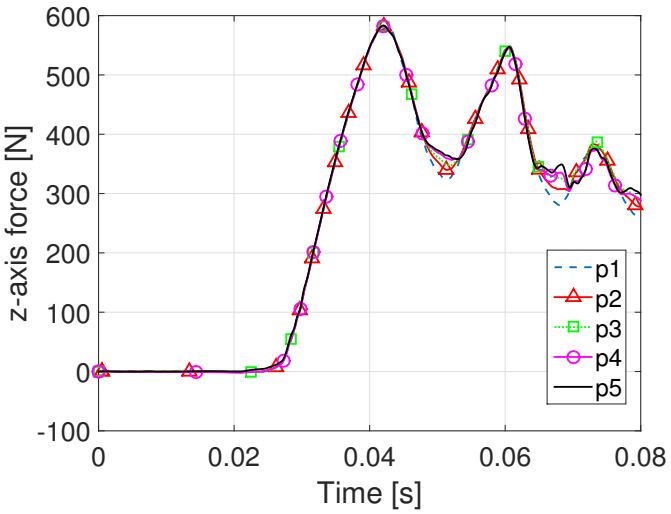

Figure 4.71: Planes axis forces; upper impact.

The calculation of z-axis forces through the Newton II Law gave also in upper test a 24 % error with respect to the LS-DYNA simulation results:

m = 6.064 kg;

$\mathbf{a}_z$ = 66.88 g = 656 m/s^2;

F = 3978 N.

In the graph related to the contact force experienced by the pendulum and the head in contacts (Figure 4.72), the maximum peak is 24% higher than the result obtained applying the Newton II Law.

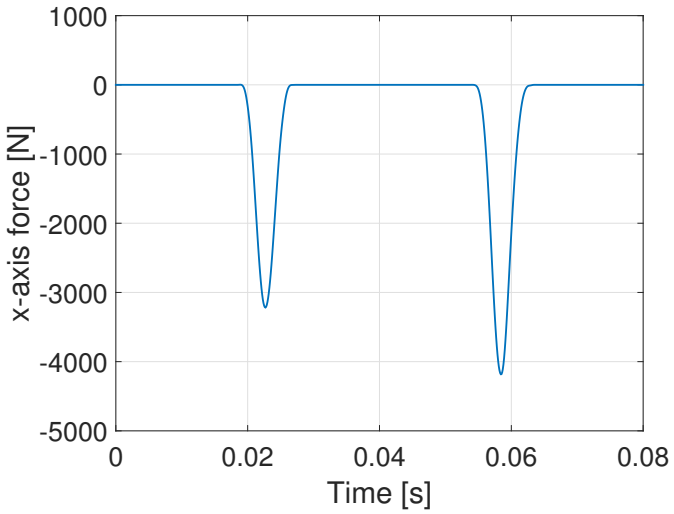

Figure 4.72: Contact axis forces; upper impact.

In this configuration IVDs and planes cross sections experienced the same contact force; the following Figures 4.73 and 4.74 present the comparison between the forces measured with the three cross section definition. Once again the higher forces are experienced by the plane cross section, and in this case also by the cartilages cross section.

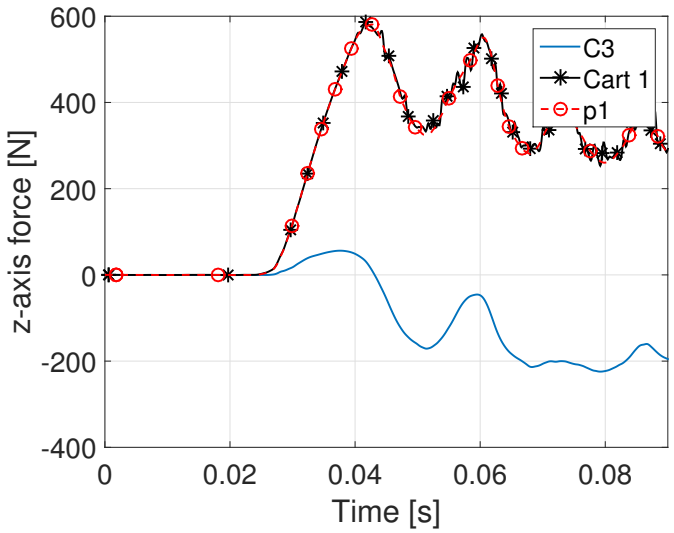

Figure 4.73: Axis forces in C3 and in cartilage and plane at the correspondent position; upper impact.

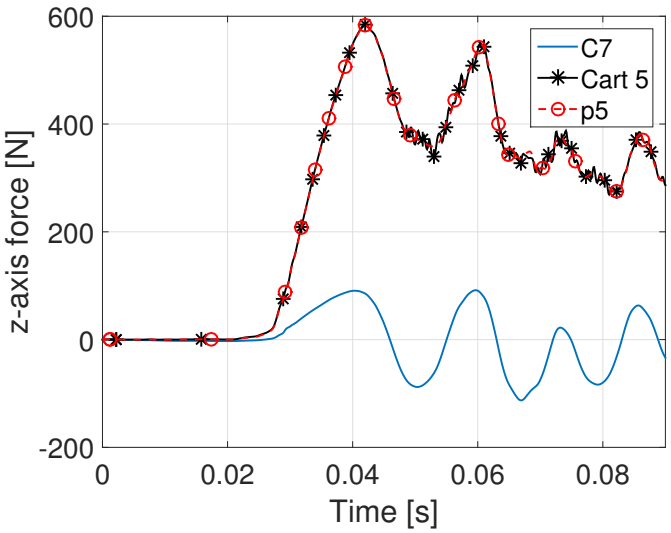

Figure 4.74: Axis force in C7 and in cartilage and plane at the correspondent position; upper impact.

Moments

The evaluation of moments in upper impact has been conducted considering the y and x direction as in the two previously analysed impact direction tests. It must be noticed that in every head impact tests the moment maximum values were always far from the critical values presented in Section 1.3

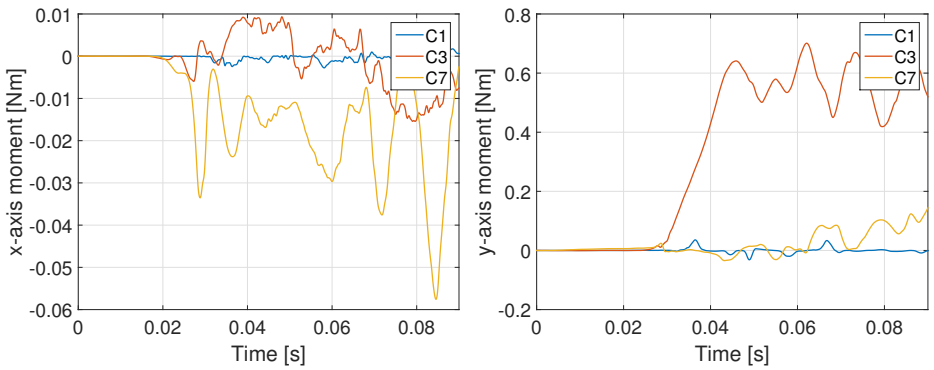

Figure 4.75: Moments about x and y axis in the vertebrae; upper impact.

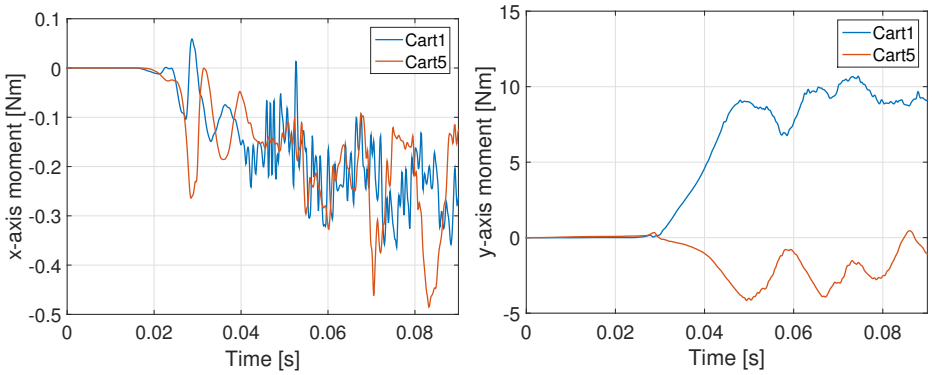

Figure 4.76: Moments about x and y axis in IVDs; upper impact.

4.2.3 Drop tests

The *drop* tests have been conducted as well using the current 4.02 Academic version of THUMS. For those simulations, the complete model has been used and no boundary conditions nor contacts have been introduced.
THUMS has a total mass of 77.14 kg –this data was recorded in LsPrepost– with 1975422 elements. Thus the simulations took long time. This has been validated with a simple test simulation with only the THUMS rotated upside down and the rigid wall under its head –no cross sections, no new set of element for the cross section definition–.
Two main set up have been studied:

- drop impact against rigid wall;
- drop impact against shell element.

For both of them, a brief sensitivity analysis has been conducted in order to found a simulation condition as similar as possible to the experimental one. In order to maintain consistency to the head tests results, the accelerations measurements were conducted in the same node: the head CG, where the accelerometer has been created. The same rigid part (part 250) has been used for the definition of the accelerometer. The neck forces were evaluated using the Secforce database, such as in the head test. Similar conclusions were deducted: for the evaluation of forces in the neck, the cross sections in the IVDs are more reliable.
Three different drop configurations were analysed with LS-DYNA as in the experimental tests with respect to the angular inclinations of the plane of impact: 0°and 15°. For each one of this plane configuration, three different initial velocity were assigned to the complete THUMS to simulate the three different heights of the experimental tests. For the same reason, in the two inclined test simulations, three different orientation of THUMS with respect to its z-axis have been analysed. No big difference were registered, as found in the experimental tests.

Cadaver drop tests

The data reported in Table 4.15 are referred to studies conducted on fresh intact unembalmed human male cadavers free from bone disease

and cancer. Ages of the cadavers ranged from 54 to 82 years (mean age: 69), their heights ranged from 169 to 183 cm (mean: 177 cm); the cadaver weights ranged from 61 to 91 kg (mean: 72 kg). The THUMS characteristics are similar to the mean values of the PMHS used, thus those data were selected as terms of comparison. In six specimens the midsagittal portion of the C5 or C6 vertebral body was surgically removed and a Model 9251A force gauge (Kistler Instrument Corp., Amherst, NY) implanted into the space and fixed. Thus, the force along the axis of the spine was measured (Table 4.15). The HIC was measured thanks to a Model 7267A triaxial accelerometer (Endevco, San Juan Capistrano, CA) attached to the parietal region of the skull with screws.

Mass [kg]	Impact velocity [m/s]	Impact force peak [N]				Head acc. peak [g]
		x-axis	y-axis	z-axis	neck axial [a]	
64	4.225	1200	525	4500	1100	-
66	4.225	-	888	3000	-	-
61	4.225	-	-	6405	-	-
67	4.8522	900	800	5555	-	-
83	4.8522	1333	1444	5871	-	-
82	5.425	1330	1330	7110	2600	-
64	5.425	800	533	7120	-	-
61	5.425	2044	1888	14660	-	-
83	5.425	-	-	14329	-	-
81	5.425	-	-	-	1824	430
79	4.8522	-	-	9786	-	340
73	4.8522	-	-	11560	1112	400
91	4.8522	-	-	12840	-	267
57	4.8522	-	-	12440	1780	-

Table 4.15: Results of drop impact with PMHS [5, 6].

[a] Neck axial force in the cervical force transducer

Rigid wall or shell

In order to compare the results obtained with the plane of impact simulated as rigid wall or as shell, the 0° , 80 mm height scenario has been considered. In this condition, different parameter related to the rigid wall or the shell have been studied[8]:

- impact against rigid wall, with three different *friction coefficient*: 0, 0.9 and 1;
- impact against shell:

FS[a]	FD[b]	Soft
0[c]	0	0
0.9	0.9	0
0	0	2[d]
0.9	0.9	2

Table 4.16: Contact parameters between the head and the shell

[a] Static coefficient of friction
[b] Dynamic coefficient of friction
[c] Even if the friction coefficient as null has no physical meaning, it is here reported for the sake of completeness.
[d] segment-based contact

The *soft* parameter can be useful in contact definition whether the material constants of the elements which make up the surfaces in contact have a wide variation in the elastic bulk moduli [23]. In the soft constraint option, the interface stiffness is based on the nodal mass and the global time step size. This method of computing the interface stiffness will typically give much higher stiffness value than would be obtained by using the bulk modulus; therefore this method is the preferred approach when soft foam materials interact with metals: in the present configuration the head of THUMS, covered by shell element of mat fabric, hit a solid surface; thus it has been considered the parameter Soft = 2 since it is for general shell and solid element contact.
The z-axis forces in the same neck levels are compared both for the

[8] the parameters analysed are related to the contact between the head and the plane surface

rigid wall (Figure 4.77) and for the shell (Figure 4.79) in the different configurations analysed –three heights in 0° drop impact, three heights and orientations in inclined drop impact–.

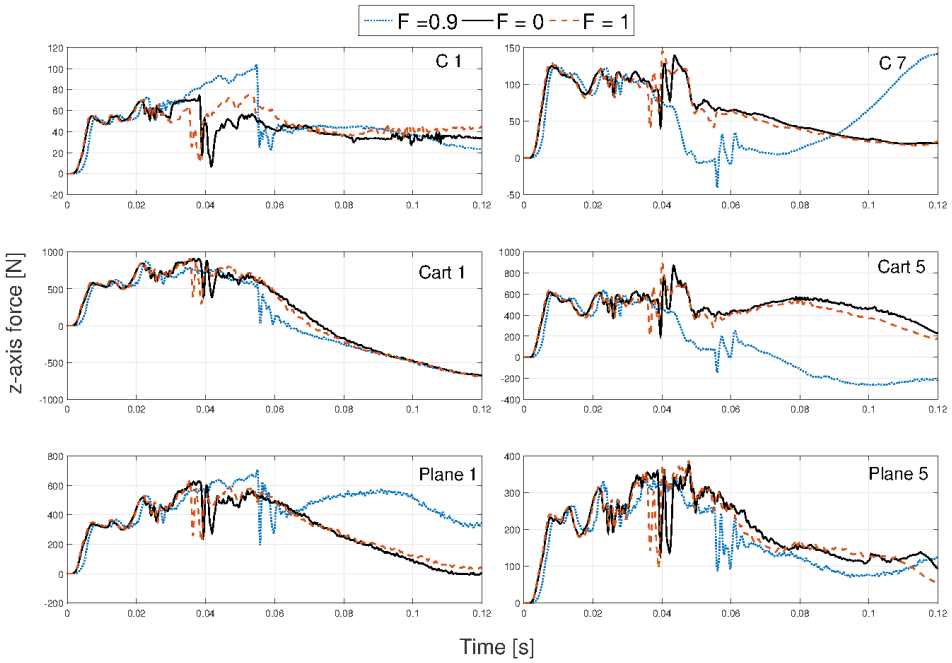

Figure 4.77: z-axis force in different neck level, sensitivity analysis with different friction coefficient conditions (F in the graphs) against rigid wall.

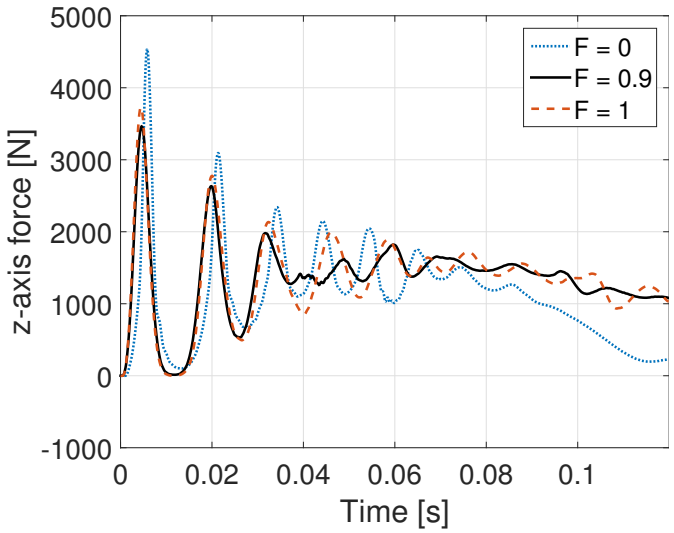

Figure 4.78: z-axis force on the rigid wall.

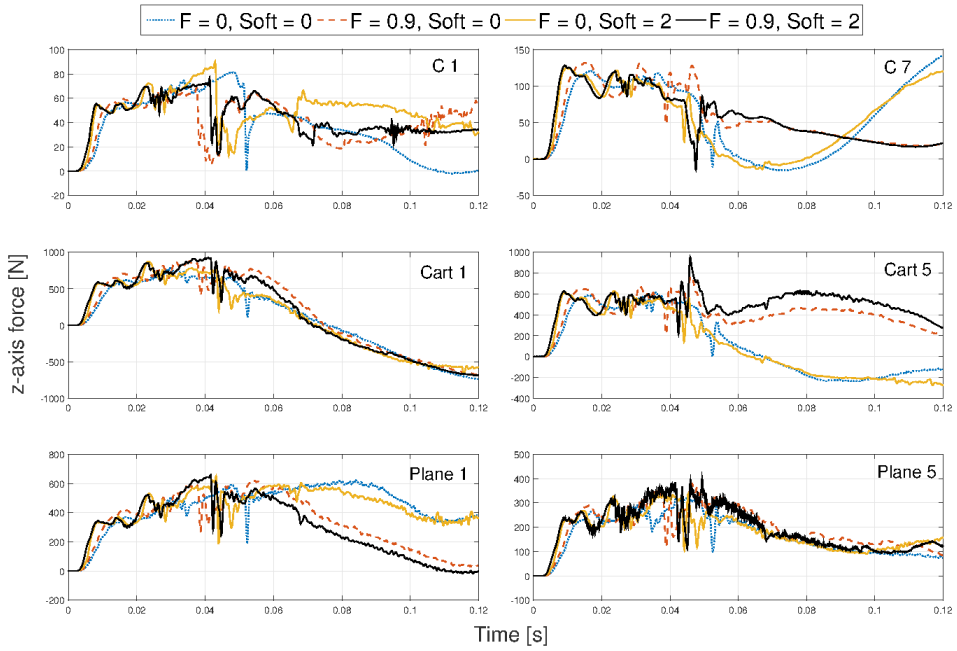

Figure 4.79: z-axis force in different neck level, sensitivity analysis of shell.

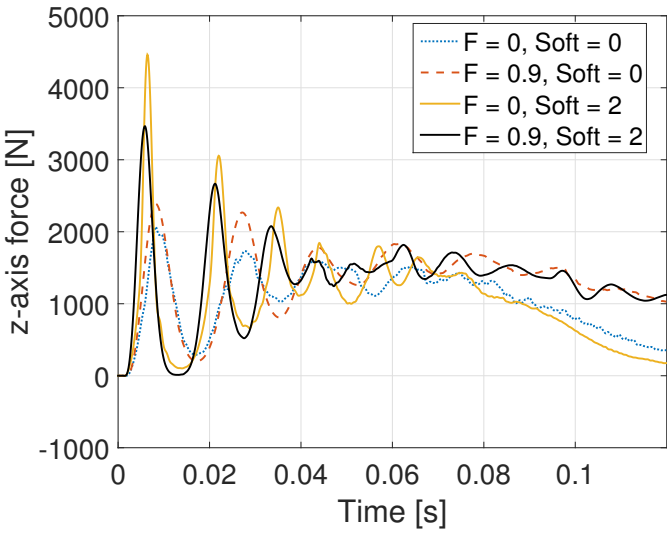

Figure 4.80: z-axis force on the shell.

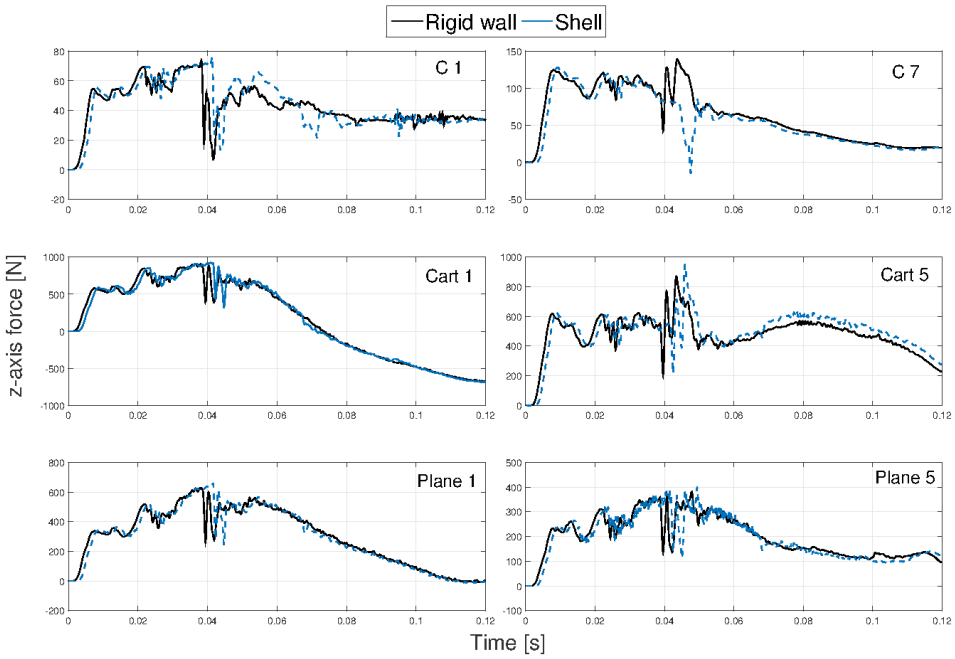

Figure 4.81: z-axis force in different neck level, comparison between shell and rigid wall.

The rigid wall has been chosen as impact plane, as no big differences have been registered (Figure 4.81 and Figure 4.82), but the computational cost of the rigid wall resulted preferable.

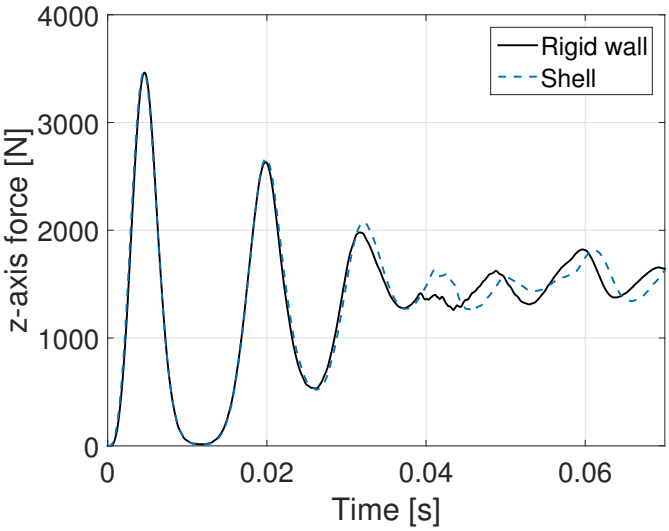

Figure 4.82: z-axis force comparison: rigid wall and shell.

0° drop

The first series of drop test were conducted onto a rigid horizontal surface. It was recreated in the numerical environment as s rigid wall, defined in a separate file with respect to the THUMS model. Hence, the impact surface were always the same for every scenarios.
Following the experimental procedure, the numerical drop simulation with THUMS has been conducted in three different heights.

0° drop, height: 0.08 m

In order to explain the selection of only IVDs cross section for the evaluation of neck forces and moments, the trend of the forces measured in the vertebrae, in the IVDs (Figure 4.83) and in the plane cross sections (Figure 4.84) are here presented for the 0°drop at 0.08 m heigh. In every test scenario the trend resulted similar.

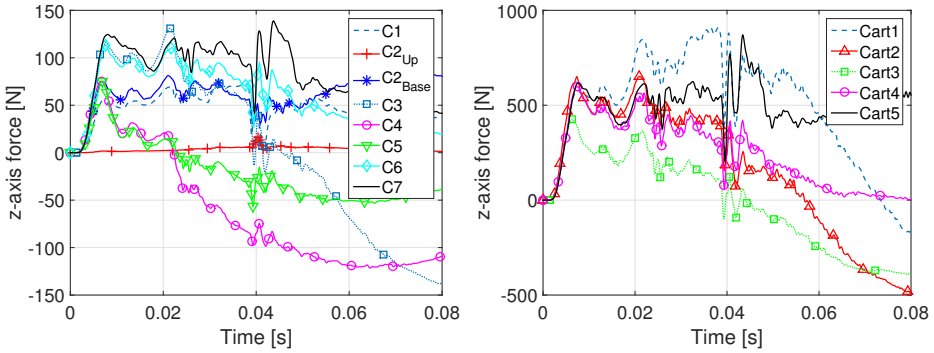

Figure 4.83: z-axis force in vertebrae cross sections (left) and in IVDs cross sections (right), 0° drop test, 0.08 m.

As for the *head tests*, also in the *drop tests*, the C7 vertebra shown the highest force in relation to the other vertebrae.
As highlighted also in the head tests, the upper vertebrae (Atlas in particular, C2) recorded quasi-null forces both in x-direction and in axial z direction. The same procedure used in *head tests* has been followed also for the evaluation of forces in *drop tests* and five planes have been created in the neck at the correspondence of the five IVDs of interest (the five in the cervical spine, from C1 to C7).

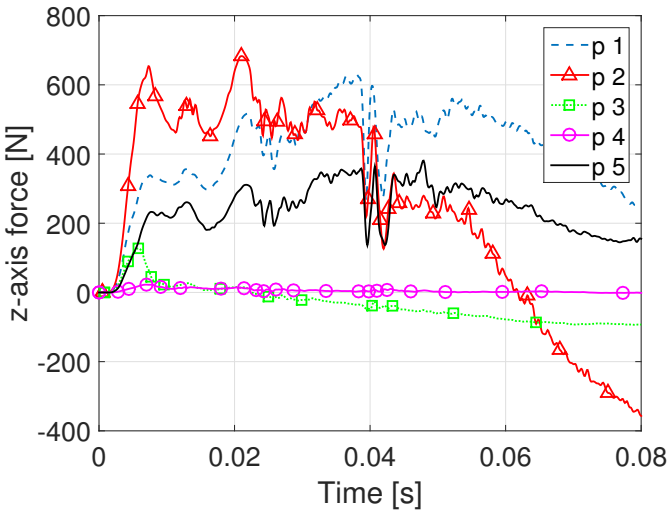

Figure 4.84: z-axis force in all the planes, 0° drop, 0.08 m.

Comparing the results depicted in Figure 4.83 and Figure 4.84 can be highlighted an important results:

- IVDs and planes cross sections measured quite the same axis forces: the difference consisted in the presence of neck surround as flesh, tendons, ligaments, spinal cord and other elements that contribute to the forces in the plane section definition; this confirm the result previously observed in head tests;

- no regular trend can be found going through the neck level;

- the same cross section underwent both compression and tension but in different element; the resultant is a summation of both the contributions

Coherently with the head tests analysis, the contact force has been registered. However, the complete THUMS cannot be considered a rigid body as done –with approximation errors– for the head: Newton II Law cannot be applied in order to verify the peak value of the contact force.

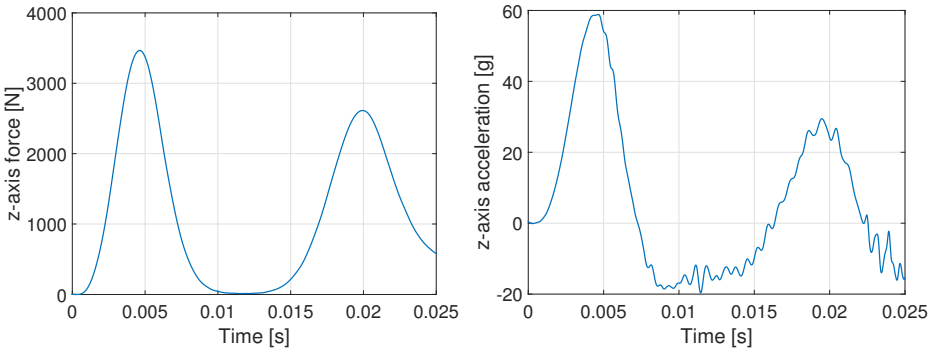

Figure 4.85: z-axis force on the rigid wall and z-axis head acceleration, 0° drop, 0.08 m.

0° drop, height: 0.16 m

In the numerical simulation the heights were reproduced bestowing different initial velocity to the whole THUMS which was free to fall with no external constrain. In the present drop height scenario, where THUMS was hang up to 0.16 m, the same conclusion reported for 0.08 m drop heigh can be confirmed:

- Vertebra C7 shown the highest z-axis force than the other vertebrae cross sections;
- planes and IVDs cross sections registered similar forces but more elements are considered in the planes, so the forces are larger than in the IVDs;
- vertebrae forces were small compared to the IVDs and planes.

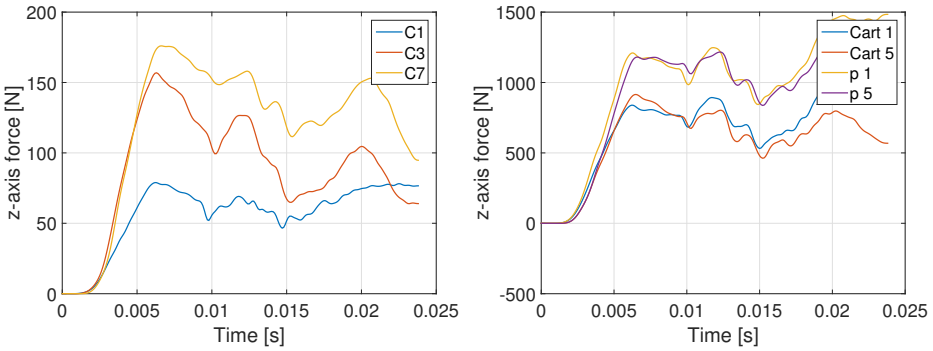

Figure 4.86: z-axis force in the vertebrae (left), IVDs and planes (right), 0° drop, 0.16 m.

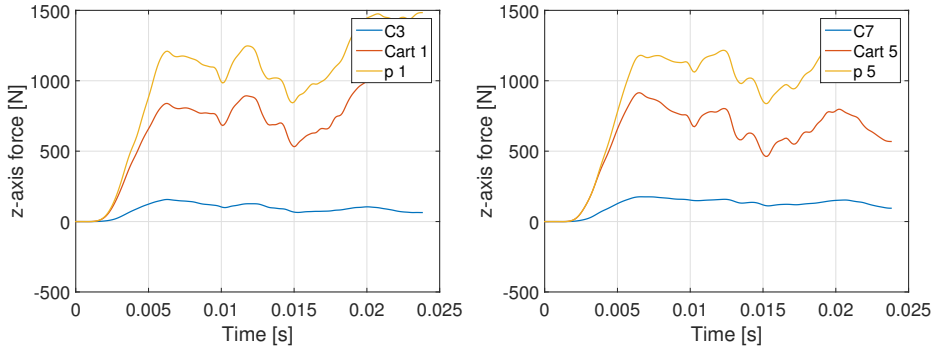

Figure 4.87: z-axis force comparison in vertebrae IVDs and planes, 0° drop, 0.16 m.

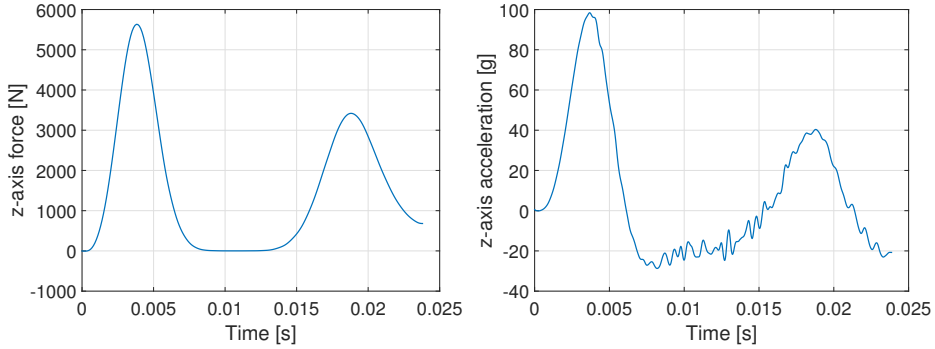

Figure 4.88: z-axis force on the rigid wall (left) and head acceleration (right), 0° drop, 0.16 m.

0° drop, height: 0.24 m

The THUMS were positioned at 1 mm from the horizontal rigid wall and the initial velocity of 2.1654 m/s was assigned to the whole THUMS. The numerical simulation of drop test conducted at height of 0.24 m recorded analogous results with respect to the lower heights:

- Vertebra C7 registered higher z-axis forces than the other vertebrae in the neck;
- plane cross sections recorded the highest force values;
- plane cross section forces were comparable to the IDVs forces but the presence of a reduced number of elements in the IDV cross sections made them registered lower forces.

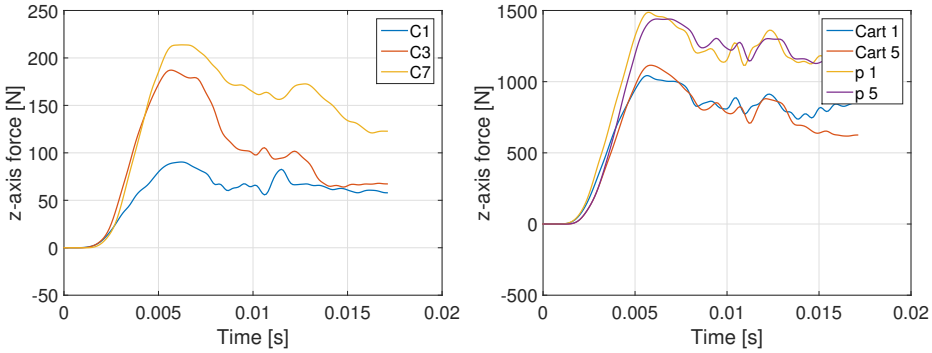

Figure 4.89: z-axis force in the vertebrae (left), IVDs and planes (right), 0° drop, 0.24 m.

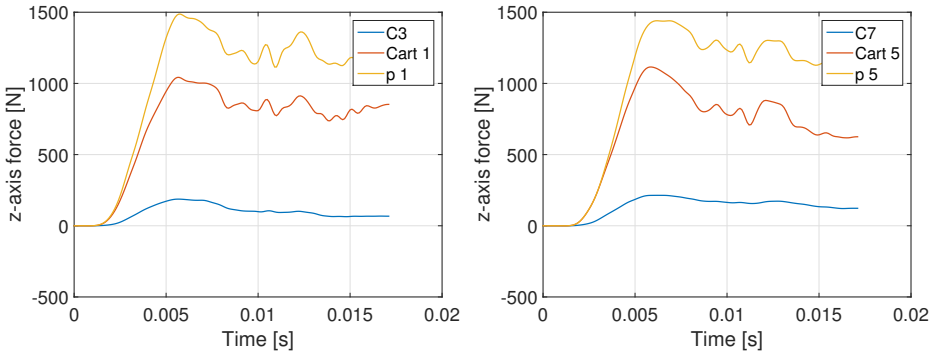

Figure 4.90: z-axis force comparison in vertebrae IVDs and planes, 0° , 0.24 m.

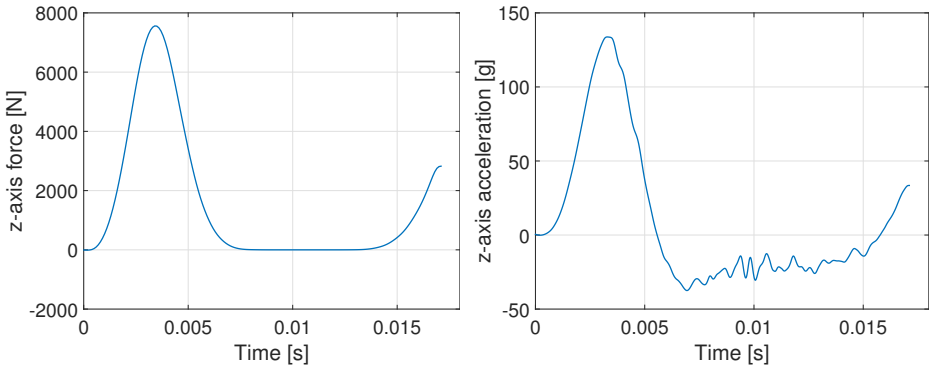

Figure 4.91: z-axis force on the rigid wall (left) and head acceleration (right), 0° , 0.24 m.

To understand the influence of heights in forces evaluation, the C7 vertebra forces and the IVD z-axis force at the correspondence neck

level have been compared in the three heights configuration (Figure 4.92). The results obtained are in accordance with literature [31, 4]: peak z impact forces and accelerations increased with the drop height.

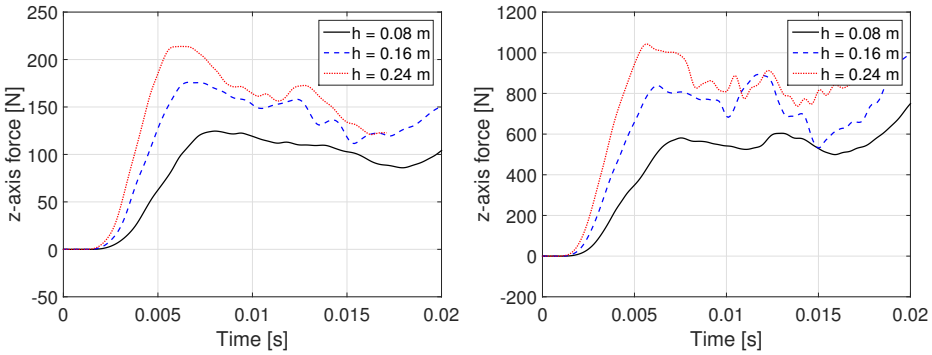

Figure 4.92: z-axis force comparison in vertebra C7 (left) and IVD Cart 5 (right) in different heights configuration.

As well, also the z-axis acceleration are higher as higher the drop heights (Figure 4.93).

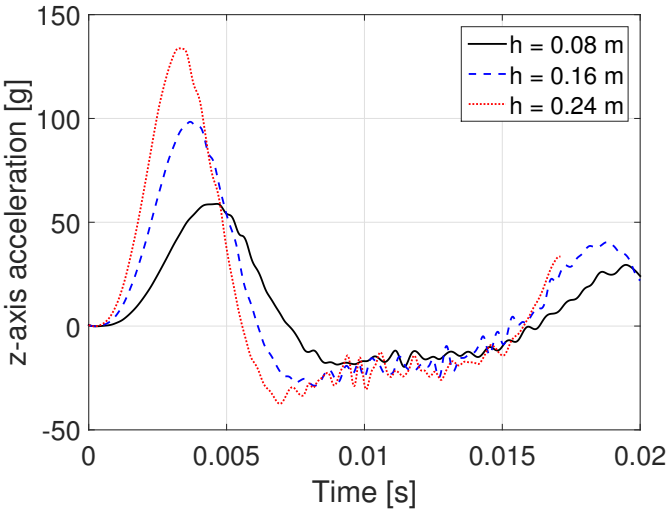

Figure 4.93: z-axis head acceleration comparison in different heights configurations.

15° drop

THUMS were suspended head down and dropped above a rigid wall defined in a separate card with respect to the Human model. The creation of a dedicated card for the plate allowed the use of the same

rigid wall in every orientation condition: include transform and the angle definition made the plate orientate with the desired inclination. The test conducted with the inclined plate confirmed what registered with the drop tests in the 0°plane configuration:

- The lower the neck level, the higher the z-axis forces in vertebrae cross sections;
- plane cross section presented highest forces;
- IDVs and planes experienced similar forces.

In the following sections are presented the z-axis forces in the three different kind of neck cross sections, the head acceleration measured in the head CG node specifically created, and the z-axis contact force registered on the plate above the THUMS.

15° drop, height 0.08 m

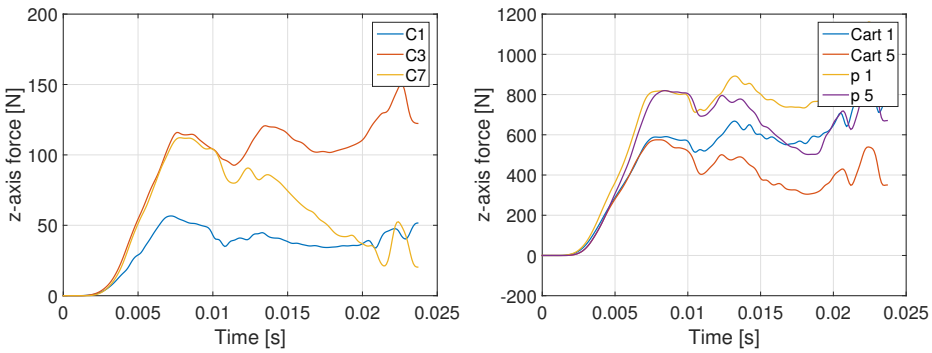

Figure 4.94: z-axis force in the vertebrae (left), IVDs and planes (right), 15° , 0.08 m.

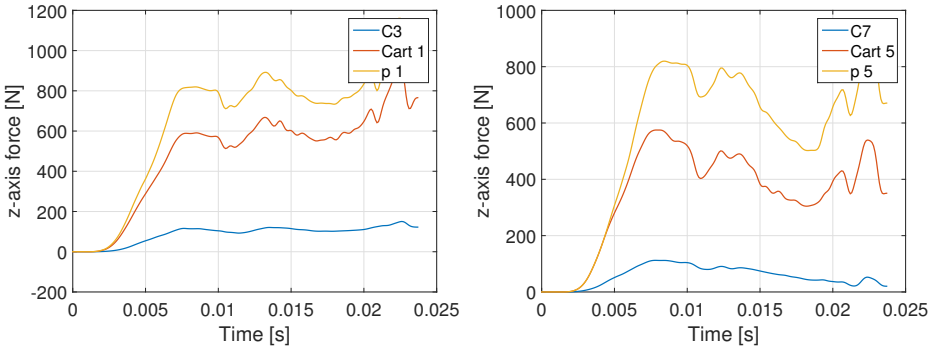

Figure 4.95: z-axis force comparison in vertebrae IVDs and planes, 15°, 0.08 m.

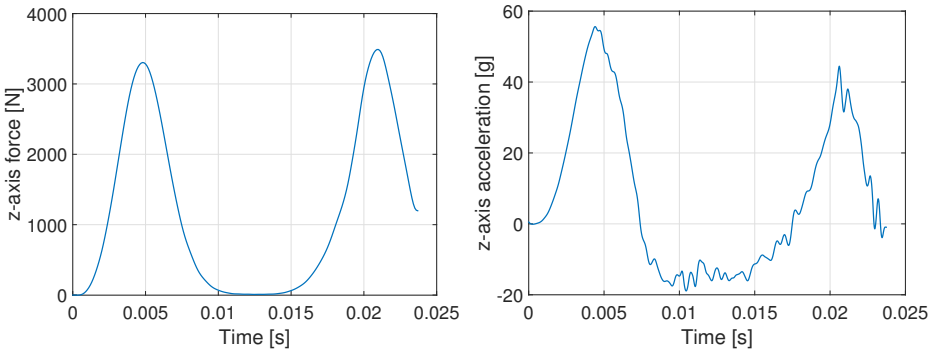

Figure 4.96: z-axis force on the rigid wall (letf) and head acceleration (right), 15°, 0.08 m.

15° drop, height 0.16 m

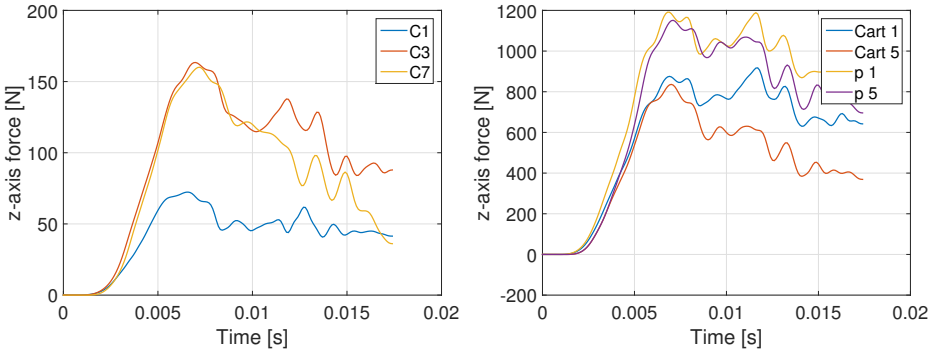

Figure 4.97: z-axis force in the vertebrae (left), IVDs and planes (right), 15°, 0.16 m.

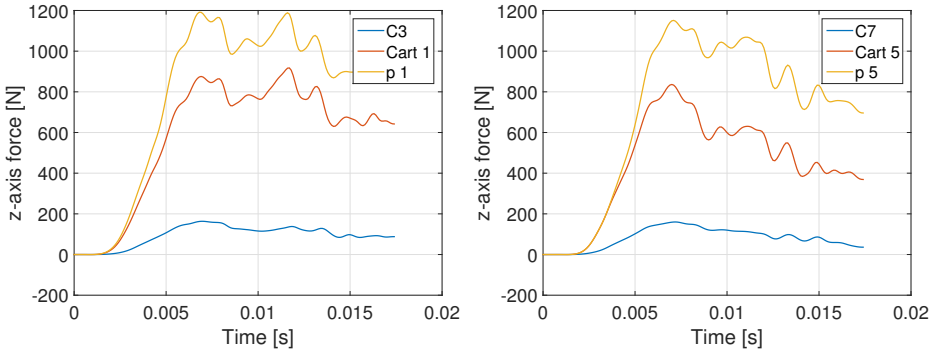

Figure 4.98: z-axis force comparison in vertebrae IVDs and planes, 15°, 0.16 m.

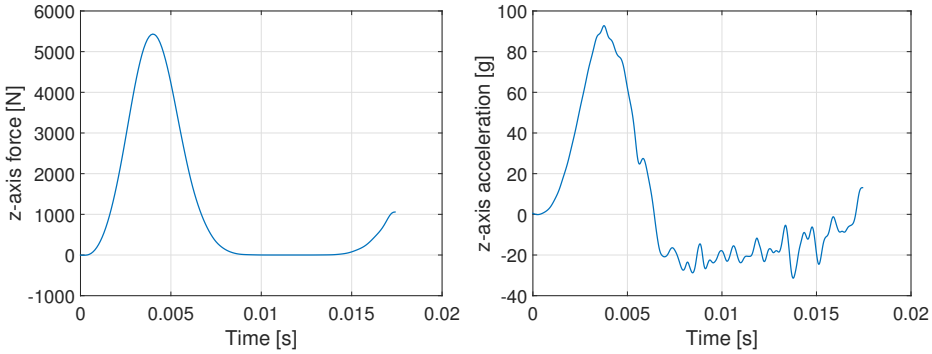

Figure 4.99: z-axis force on the rigid wall (left) and head acceleration (right), 15°, 0.16 m.

15° drop, height 0.24 m

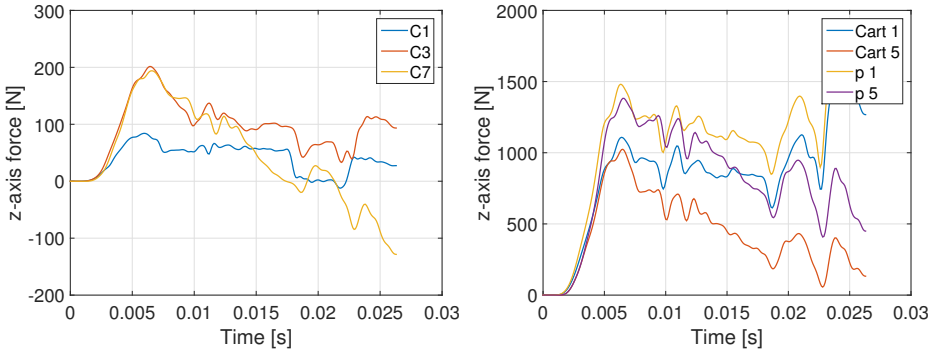

Figure 4.100: z-axis force in the vertebrae (left), IVDs and planes (right), 15°, 0.24 m.

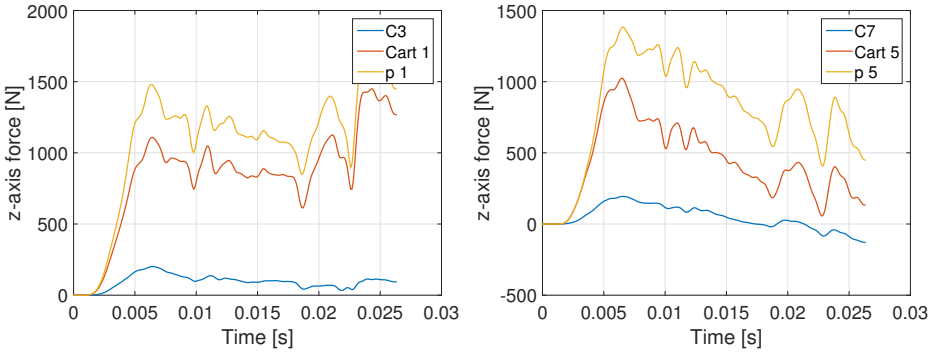

Figure 4.101: z-axis force comparison in vertebrae IVDs and planes 15°, 0.24 m.

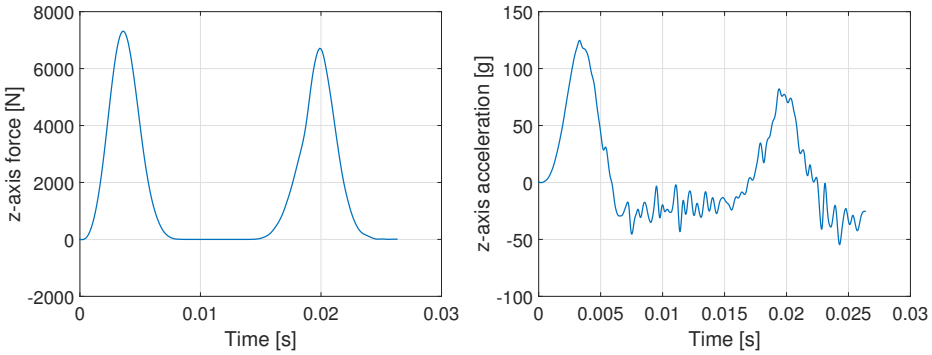

Figure 4.102: z-axis force on the rigid wall (left) and head acceleration (right), 15°, 0.24 m.

4.2.4 Brain injury visualization

The previous analysis were focused on the individualisation of a valid technique for the evaluation of measurements such as linear acceleration and axial forces. Once those values have been registered following the technique described, it has been considered necessary to establish a relationship between them –the kinematic parameters– with physical injury metrics, such as CSDM (cumulative strain damage measure), brain pressure, MPS (maximum principal strain).

Since the brain injuries constitute a significant portion of injury resulting from car collisions, motorcycle crashes and sports collisions, the development of strategies to prevent or minimize these injuries is very important. In order to obtain a proper assessment of brain injures outcome, a biomechanical study of human concussion that attempts to relate mechanical input to localized tissue deformation and damage is

needed. Recently, the use of finite element head models (FEHM) has suggested some possible injury predictors based on the head response: shear stress/strain response could be the injury indicator for subarachnoid hematoma and diffuse axonal injury (DAI), the Cumulative Strain Damage Measure[9] (CSDM) can be related to strain-induced DAI [27]. The brain parts of THUMS include the *white matter* and the *gray matter*. Incompressive and viscoelastic material is assumed for the brain. A damage material is defined for the skull. The head model of THUMS Version 4.02 AM50 can be used to reproduce brain injury simulations. Some suggested values for brain injury threshold strains and stresses are given from literature [27, 26] and reported in Table 4.17.

ICP[a]	> 235 kPa < 173 kPa	severe or fatal injury minor or no injury
Strain	>0.2	injury
Shear stress	11 to 16.6 kPa	injury
CSDM	55% brain volume experienced a 15% strain level	55% probability of concussion

Table 4.17: Brain injury values.

[a]InterCranial Pressure

The determination of such tolerance levels is complicated and is one of the main difficulties in the research of a relationship between various injury measures (such as HIC, AIS, brain pressure, CSDM) is the determination of tolerance levels. Since measurements of the brain tissue deformations and responses can not be calculated in-vivo, they must be estimated afterwards, often with the assistance of numerical models themselves. The Abbreviated Injury Scale (AIS) was introduced by the Association for the Advancement of Automotive Medicine (AAAM) as an anatomically-based coding system to classify and describe the severity of specific individual injuries. AIS codes range from 0 (no injury) to 6 (fatal injury). Empirically determined relationship between HIC scores and the probability of head injury are widely used in the automotive industry to estimate the risk of injury. Some have compared AIS scores for real life injuries to HIC scores or other indices of injury calculated

[9]an accumulated volume of elements that exceed a pre-determined maximum principal strain

from the reconstruction. HIC and tolerance levels have been explained and tabulated in Table 4.18.

HIC	AIS	Level of brain concussion and head injury
135-519	1	headache or dizziness; light brain injuries, light cervical injuries.
520-899	2	concussion with or without skull fracture; less than 15 minutes unconsciousness, corneal tiny cracks, detachment of retina, face or nose fracture without shifting –linear fracture–.
900-1254	3	concussion with or without skull fracture, more than 15 minutes unconsciousness without severe neurological damages closed and shifted or impressed skull fracture without unconsciousness or other injury indications in skull, loss of vision shifted and/or open face bone fracture with antral or orbital implications, cervical fracture without damage of spinal cord.
1255-1574	4	closed and shifted or impressed skull fracture with severe neurological injuries.
1575-1859	5	concussion with or without skull fracture with haemorrhage in skull and/or critical neurological indications; unconscious grater than 12 hours.
>1860	6	non survivable.

Table 4.18: Levels of consciousness in relation to the head injury criteria.

In order to study the relation between the AIS and the HIC values in THUMS, the head impact tests were reproduced with higher impactor velocity than the previous analysed. Frontal, lateral and upper impacts were reproduced in LS-DYNA with three different impact velocities: 3 m/s, 3.5 m/s and 4 m/s. In relation to the impact direction, the linear accelerations measured in the three directions were different such as HIC scores measured.

Impact direction	Impactor velocity [m/s]	HIC
Frontal	3.0	432.3
	3.5	712.96
	4.0	2050.3
Lateral	3.0	737.58
	3.5	1083.9
	4.0	2376.7
Upper	3.0	650
	3.5	1065
	4.0	1599

Intercranial pressure

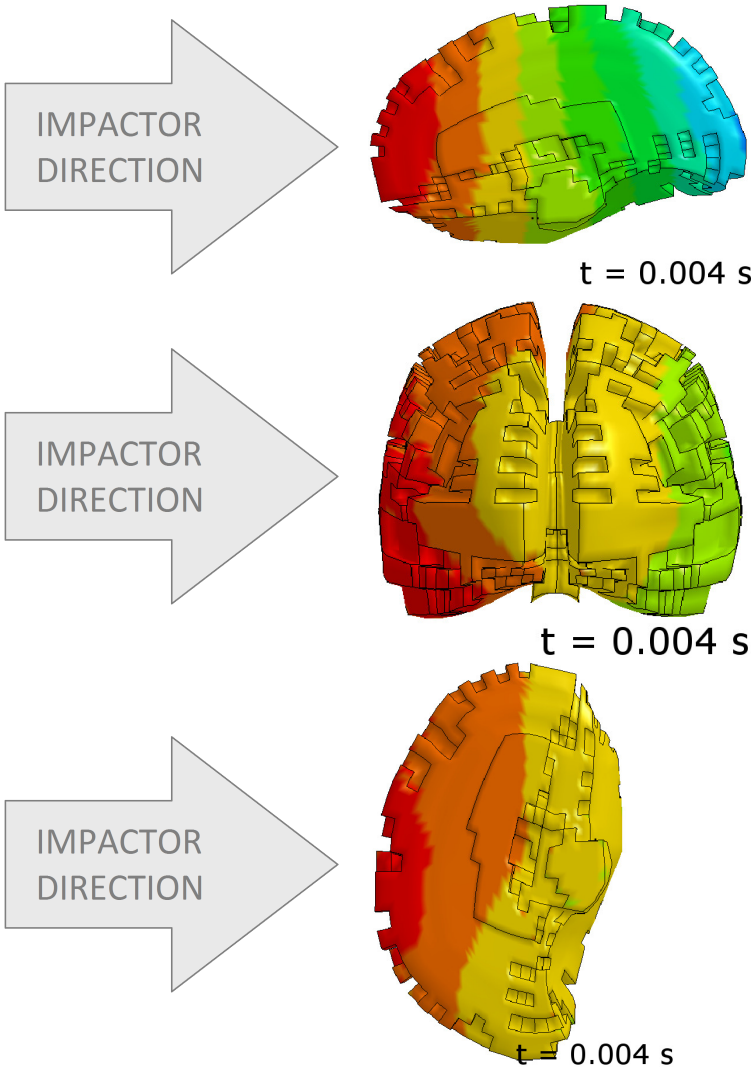

Figure 4.103: Pressure distribution in frontal, lateral and upper impact, v = 4 m/s, t = 0.004 s.

CSDM, Cumulative Strain Damage Measure

CSDM was proposed by Takhounts et al. [32] to establish a kinematically based injury metric to predict DAI (Diffuse Axonal Injuries). CSDM is a cumulative (non decreasing) measure that depends on time; its computation requires the initial brain volume and the actual maximum first principal strain (FPS) of each element of the FE brain model.

Then the CSDM is calculated by adding the volume of the brain that experiences a strain greater than some threshold level of strain (usually 0.1-0.25 [32]). The CSDM metric predicts injury by monitoring the accumulation of strain damage. This is accomplished by calculating the volume fraction of the brain which sometime during the event is experiencing strain levels greater than specified levels. This strain level is based on the maximum principal strain calculated from a strain tensor that is obtained by the integration of the rate of deformation tensor [33]. The CSDM can be computed as:

$$CSDM_t(\epsilon_0) = \frac{\sum_{k=1}^{N} V_k \psi_k^{\epsilon}(t, \epsilon_0)}{\sum_{k=1}^{N} V_k} \leq 1 \tag{4.2}$$

where

N is the total number of element in the part considered;

ψ_k**(t)** is the function given by

$$\psi_k^{\epsilon}(t, \epsilon_0) = maxH(|\epsilon_k(\tau) - \epsilon_0|) \tag{4.3}$$

in which

$\tau \in$[0, t]

H is the Heaviside step function

ϵ_0 is the prescribed threshold level of strain (usually ϵ_0 = 0.1-0.25)

Because of the cumulative character of the function, the CSDM always increases during an impact: from the initial value of 0 it increases as the brain experiences strains. A damaged volume –a volume is considered damaged once it passes the given threshold–, even if the strain in that element reduces at a later time, it is still considered to be damaged.

Brain parts considered: all white and gray matters. Brain material properties: both Mat Kelvin-Maxwell viscoelastic, with a Maxwell formulation. G_0 = 0.006 MPa, G_∞ = 0.0012 MPa, β (decay constant) = 80.

The best way to think about it is that the CSDM is a measurement of the total volume of the brain that exceeded a certain strain level. CSDM has been used for the entire brain but is theorised to be most associated with injury to the corpus callosum.

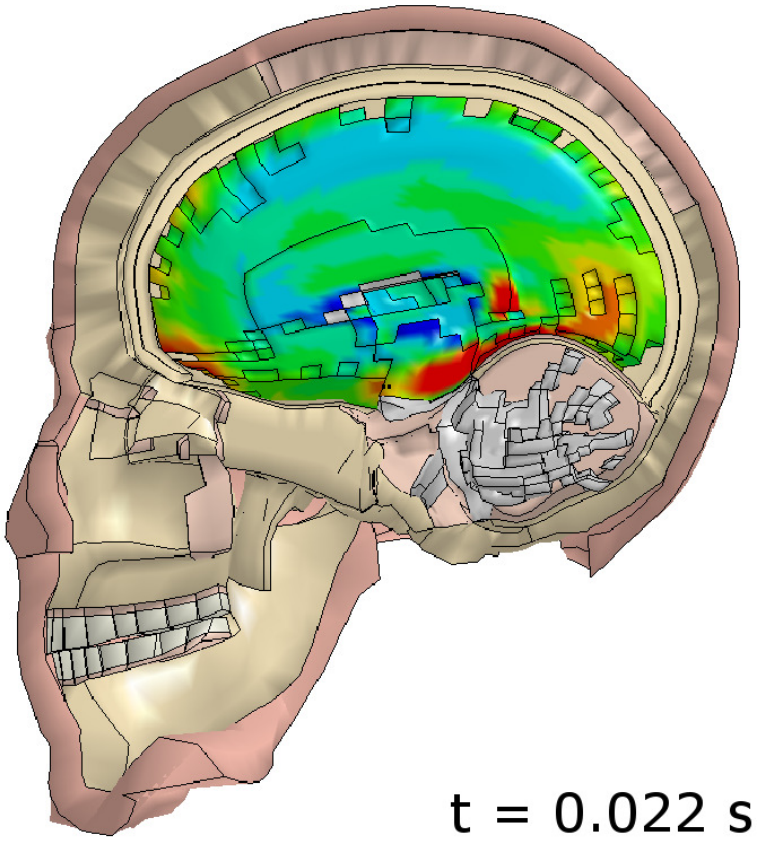

Figure 4.104: CSDM in frontal impact, v = 4 m/s.

Chapter 5

Comparison of the Results

There is an ever increasing need for accurate and detailed finite element models of crash test dummies in the academia, government and industry to furhter advance the performance of the models with respect to their physical counterparts. The numerical models should provide a better biofidelity than the crash test dummies in various impact scenarios. Since the computational models are useless unless it has been proven that they can accurately replicate results from experimental testing, this Chapter describes the comparison between experimental test (deeply analysed in Chapter 3) and numerical simulations.

5.1 Introduction

The comparison between experimental tests and numerical simulations was conducted following an evolving path implemented during the current activity. The following procedure was chosen on the base of the following reasons:

- the experimental data, because of their nature and because of the way in which they are collected through the DAS, were filtered. Consequently the results from the simulations have to be filtered in order to be comparable with the experimental data;
- in numerical simulations the acceleration signals are calculated using an *element seatbelt accelerometer*. This element removes numerical noise reporting more stable data than the raw nodal accelerations [23]. For this reason, the experimental acceleration

data were analysed and in filtered, in order to have a better comparison between numerical and experimental signals. However, the final solution does not take into account any filters applied on numerical data.

5.2 Hybrid III

The experimental ATD and the numerical Hybrid III model are similar in instrumentation: their own head accelerometers and neck load cells have been used in this activity.

5.2.1 Head test

Acceleration comparison

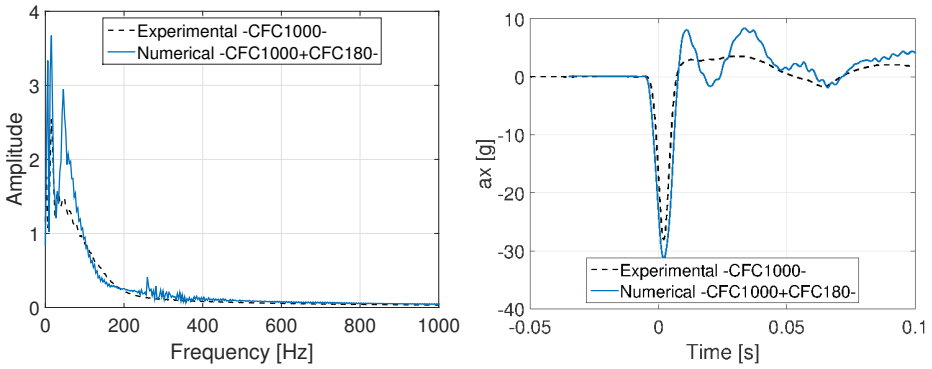

Figure 5.1: Frequency spectrum (left) and time history plot (right) of experimental and numerical Hybrid III head acceleration; frontal impact.

As example, in Figure 5.1 is reported the frequency and time comparison between x-axis acceleration signal of experimental test and numerical analysis in frontal impact test. Frequency spectrum of signals were obtained through a numerical code implemented in Matlab® . The acceleration signals comparison –frequency content of experimental data and frequency content of numerical measures– showed a similar trend in every *head test* (frontal, lateral and upper direction):

- numerical signals presented higher frequency content that were not registered for experimental signals.

Hence, the numerical data were filtered in order to reduce the high frequency contribution and to have more comparable signals.

Force comparison

Not all the analysis conducted is here reported: the final comparison between the experimental force time history and the numerical one is presented in the following section for the frontal impact direction scenario. Must be noticed that the experimental curve was obtained from the measurement of the load cell in the upper neck of the Hybrid III. No other forces were recorded. On the contrary, in numerical simulations, forces were collected in different neck levels. This was important for THUMS analysis but not for Hybrid III since the neck reacted as a single rigid body and no dissipation was experienced. In fact, in numerical simulation with Hybrid III model, the forces were registered only in the upper neck load cell in analogy with real dummy.
Figures 5.2 and 5.3 report the comparison between experimental and numerical axial forces both in x and z directions.

Previous studies [31] demonstrated that the Hybrid III force transmitted to the neck is substantially greater than the failure force measured in the human cadaver and it should be considered when the Hybrid III is used in rollover or vertical drop studies.

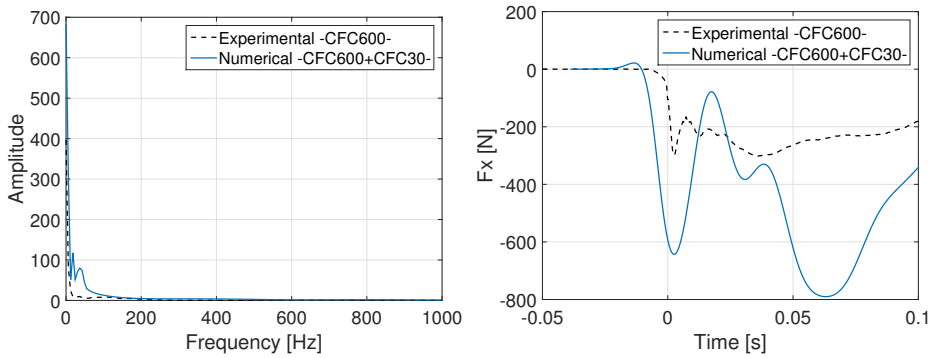

Figure 5.2: Frequency spectrum (left) and time history plot(right) of experimental and numerical Hybrid III x-axis forces; frontal impact.

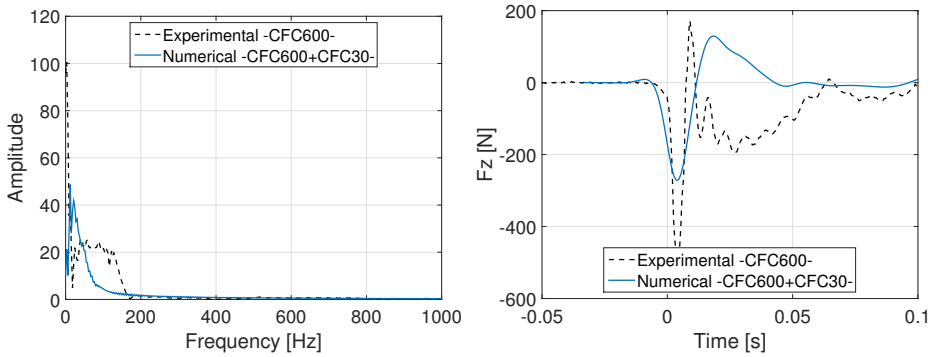

Figure 5.3: Frequency spectrum (left) and time history plot(right) of experimental and numerical Hybrid III z-axis forces; frontal impact.

The filter chosen for the forces numerical signals were the CFC 30 (Appendix A), added to the CFC 1000, applied in accordance to the regulation [14].

5.2.2 Drop test

The frequency analysis has been conducted also for the comparison between numerical drop test and experimental results with Hybrid III. To maintain consistency and in order to find a criteria of filtering the data which would fit the highest number of scenario, the same class of filter has been used –different class of filter has been adopted to the curves on the base of literature data prior the finding of the best solution–.
The filter selection was always the same both for *head tests* and *drop tests*:

- numerical acceleration: CFC 1000 (in accordance to the regulation, SAR J211 [14]) and additional CFC 180;

- numerical forces: CFC 600 (in accordance to the regulation, SAR J211 [14]) and additional CFC 30.

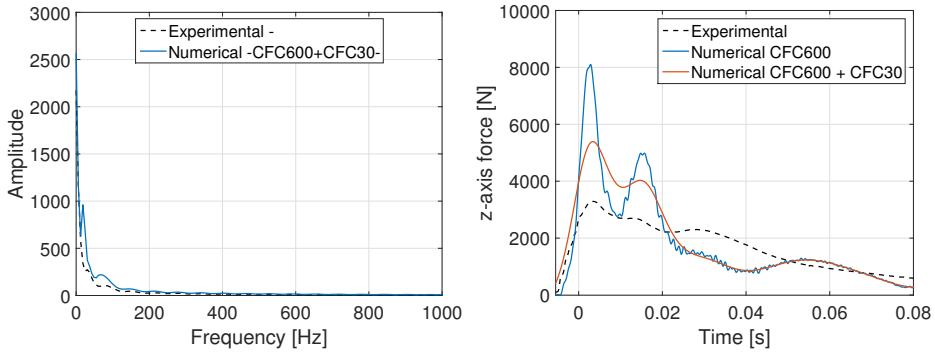

Figure 5.4: Filtered frequency content and time-history of z-axis numerical force in comparison with experimental test; 0° drop, h = 0.08 m.

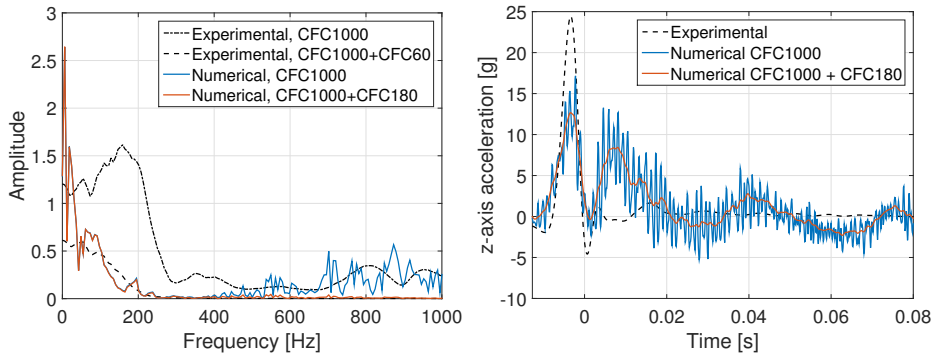

Figure 5.5: Filtered frequency content and time-history of z-axis numerical acceleration in comparison with experimental test; 0° drop, h = 0.08 m.

From the curves reported, it can be noticed that the no filtered signals presented the highest noise level.
The frequency content comparison between the experimental and the numerical *drop tests* is not here exposed but presented a similar trend observed for *head tests*: this made possible the selection of the same class filter for the two test scenarios.

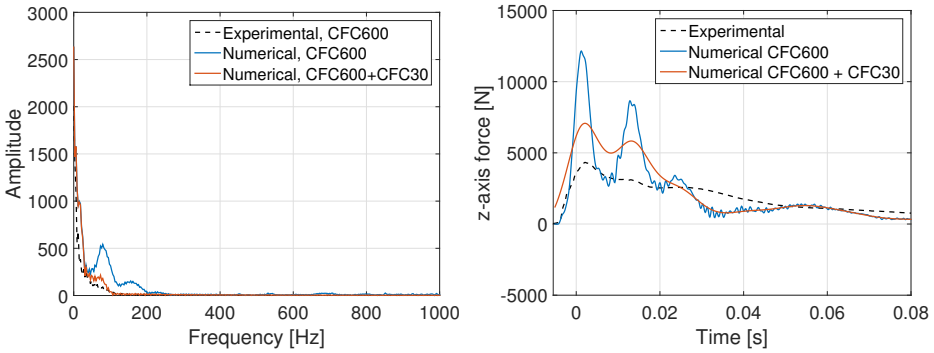

Figure 5.6: Filtered frequency content and time-history z-axis numerical force in comparison with experimental test; 0° drop, h = 0.16 m.

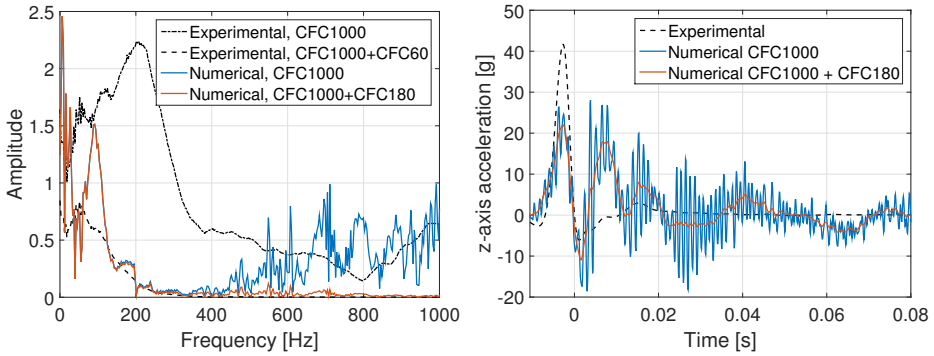

Figure 5.7: Filtered frequency content and time-history z-axis numerical acceleration in comparison with experimental test; 0° drop, h = 0.16 m.

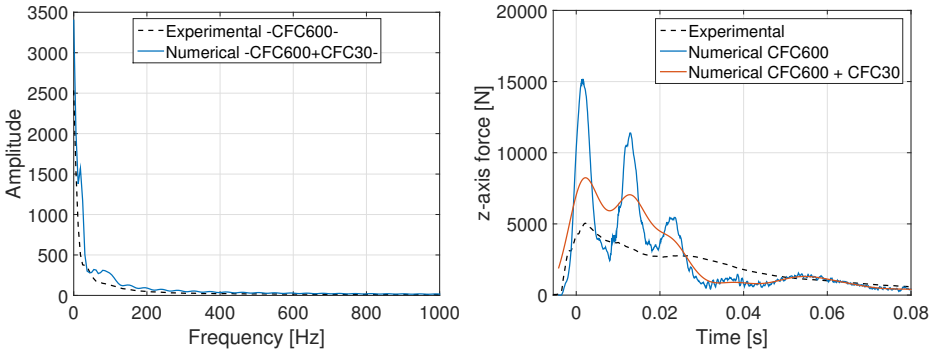

Figure 5.8: Filtered frequency content and time-history z-axis numerical force in comparison with experimental test; 0° drop, h = 0.24 m.

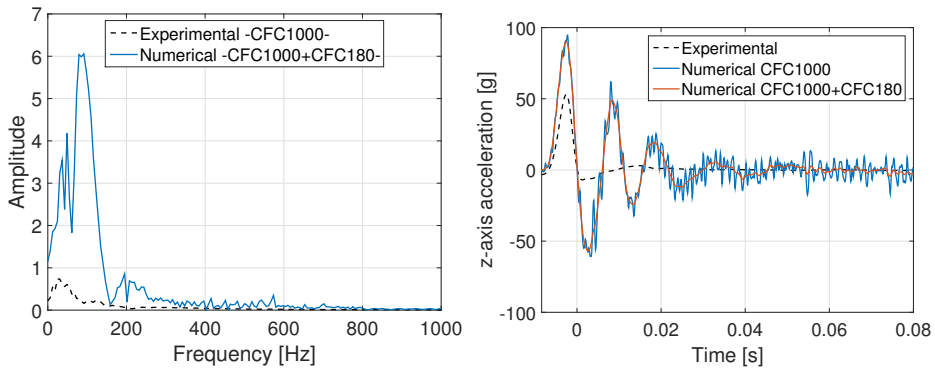

Figure 5.9: Filtered frequency content and time-history z-axis numerical acceleration in comparison with experimental test; 0° drop, h = 0.24 m.

5.3 THUMS

5.3.1 Head test

Acceleration comparison

Tables 5.1, 5.2, 5.3 summarise the values of the peak linear acceleration and the HIC registered in the *head test* simulations. The experimental data, both with Hybrid III and with PMHS, are reported and used as a term of comparison. The acceleration maximum value evaluated on the node 88178224, which belongs to the cover rigid part, was quite the same in every scenario analysed: this was used as a confirmation of the fact that the introduction of different rigid parts such as the 250 and 500 did not affect the behaviour of the model.
From the results comparison in the table, was clear that the HIC evaluated in the experimental tests with the Hybrid III was the lowest; it was related to the stiffness of the HIII neck.

FRONTAL			
Part ID	Node ID	Max a_x [g]	HIC
88000217	90000001	79.91	60.49
	88178224	52.98	45.62
250	90000001	46.83	30.54
	88178224	53.21	45.55
500	90000001	100.97	273.04
	88178224	53.77	45.99
Experimental test[a]	CG	46.126	19.87
Estimated data from PMHS	CG	47.997	44.02

Table 5.1: Absolute maximum acceleration values and HIC; frontal impact.

[a]Media of the values from the three repeated tests

LATERAL			
Part ID	Node ID	Max a_y [g]	HIC
88000217	90000001	94.34	122.08
	88178224	84.41	75.19
250	90000001	71.56	66.70
	88178224	84.45	74.799
500	90000001	199.81	458.85
	88178224	85.45	74.92
Experimental test	CG	46.74	17.12
Estimated data from PHMS	CG	44.75	41.90

Table 5.2: Absolute maximum acceleration values and HIC; lateral impact.

UPPER			
Part ID	Node ID	Max a_z [g]	HIC
88000217	90000001	132.53	90.06
	88178224	116.49	104.75
250	90000001	59.808	66.88
	88178224	115.66	104.52
500	90000001	211.52	–
	88178224	116.06	103.68
Experimental test	CG	52.28	21.44
Estimated data from PHMS	CG	61.57	82.5

Table 5.3: Absolute maximum acceleration values and HIC; upper impact.

Experimental test comparison

The accelerations time-history were also compared with the experimental data conducted with the Hybrid III dummy model. Part 250 has been chosen after the analysis of the Graphs with the time-history acceleration measured from the element seatbelt accelerometer related to the three different rigid parts analysed. In all the three impact directions (Figure 5.10, 5.12 and 5.14) the acceleration time-history of the CG evaluated with the accelerometer related to the rigid part 250 was the most comparable with the acceleration time-history of the experimental test; this part and the CG have been selected for the acceleration evaluation with THUMS.
The graphs in Figure 5.10, 5.12 and 5.14 are focused on the neighbourhood of the peak.

Frontal

In Figure 5.10 the three accelerometer curves –referred to the three parts in the head considered for the element seatbelt accelerometer definition– are depicted. The Graph is focused on the neighbourhood of the peak.

HIC	30.54
x-axis acceleration peak [g]	46.83

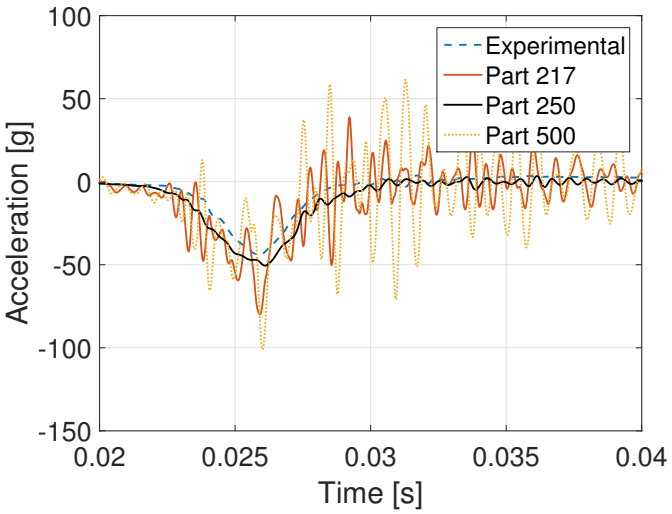

Figure 5.10: x-axis accelerations in CG, considering different rigid parts; comparison with experimental data; frontal impact.

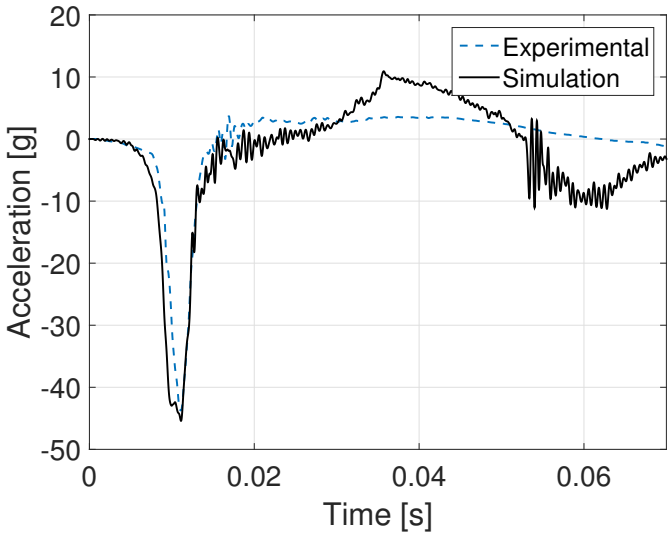

Figure 5.11: x-axis acceleration; comparison between the final simulation configuration and the experimental tests; frontal impact.

Lateral

HIC	71.56
y-axis acceleration peak [g]	66.69

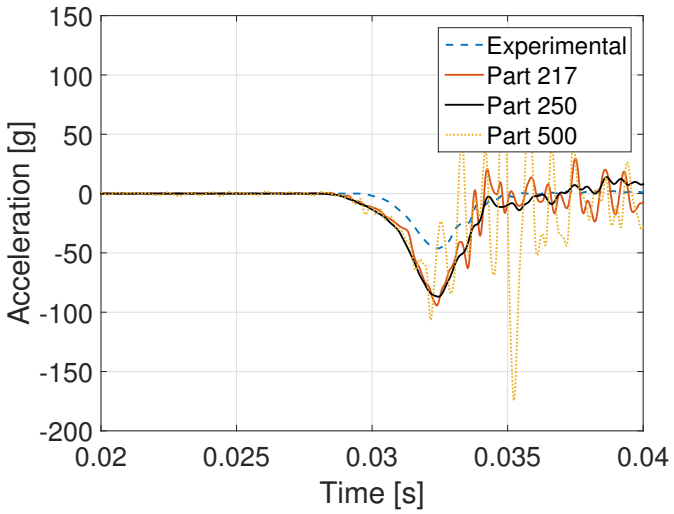

Figure 5.12: y-axis accelerations in CG, considering different rigid parts; lateral impact.

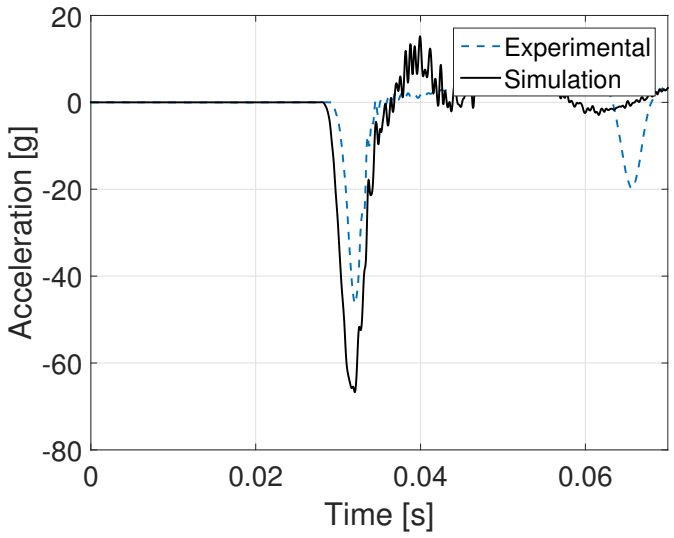

Figure 5.13: y-axis acceleration; comparison between the final simulation configuration and the experimental tests; lateral impact.

Upper

HIC	59.81
z-axis acceleration peak [g]	66.88

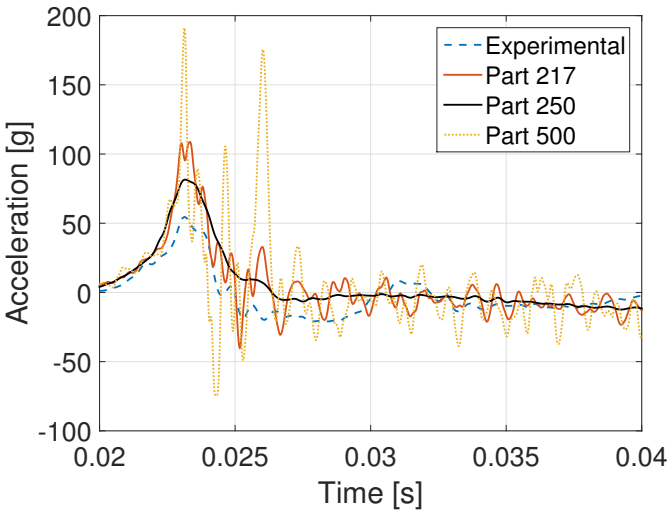

Figure 5.14: z-axis accelerations in CG, considering different rigid parts; upper impact.

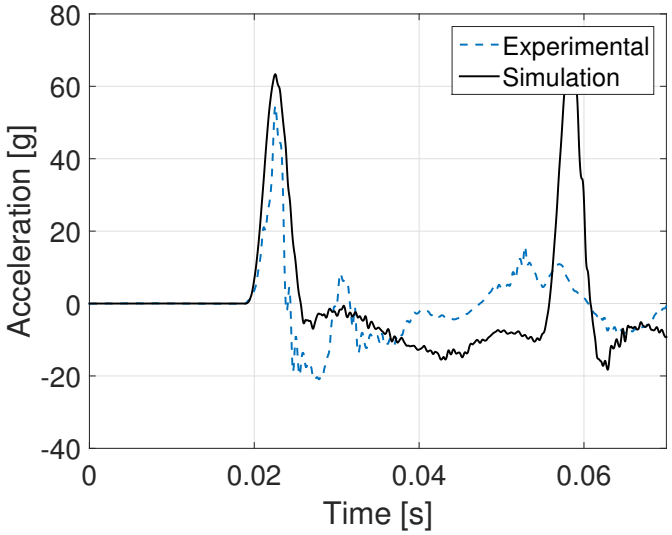

Figure 5.15: z-axis acceleration; comparison between the final simulation configuration and the experimental tests; upper impact.

Forces comparison

Experiments [34, 31] show that, relative to the human neck, the Hybrid III neck is:

- 3 to 5 times stiffer in extension;
- 3 to 4 times stiffer in flexion;

- 5 to 6 stiffer in lateral bending.

In the following sections are presented the forces registered in THUMS neck –IDV forces– and the experimental forces coming from the Hybrid III upper neck load cell. It must be noticed that a scale factor of 4.5 has been used for the final forces comparison.

Frontal

The comparison between experimental and numerical forces has been conducted considering the IDVs cross sections modelled in THUMS neck. In Figure 5.16 both the upper and the bottom IDV cross section force are reported and compared with the experimental x-axis and z-axis forces.

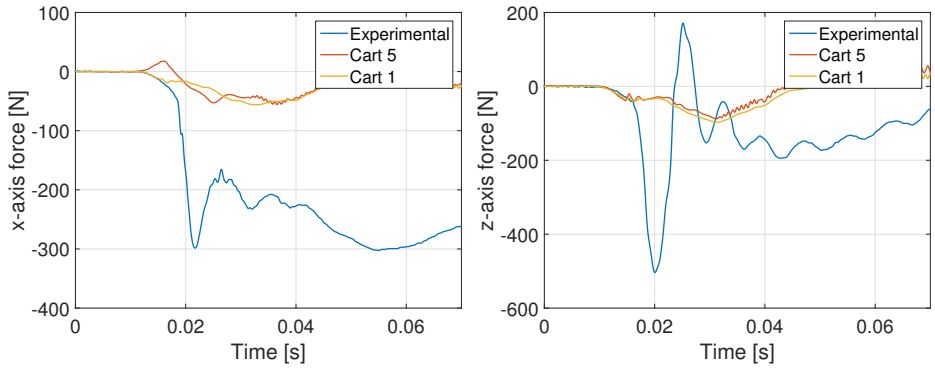

Figure 5.16: Comparison between cartilages and experimental axial forces; frontal impact.

The upper IDV cross section has been considered the most analogous to the Hybrid III load cell, also from the geometrical point of view. In Figure 5.17 the forces registered in THUMS neck cross sections have been compared with the experimental curves, applying a *scale factor* of 4.5. The Hybrid III resulted in fact stiffer than cadaver neck and since THUMS is a human model and not a dummy model, it resulted more similar to cadaver than to Hybrid III. With the scale factor of 4.5 the curves resulted similar in value.

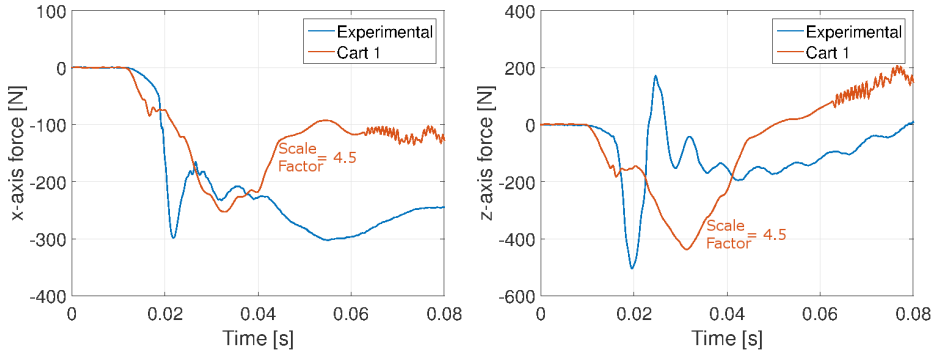

Figure 5.17: Comparison between cartilages and experimental axial forces scaled; frontal impact.

Lateral

In analogy with the frontal impact tests, also for the lateral tests, the upper neck and the bottom neck IDV cross section have been used for the evaluation of forces both in y-axis direction (impactor direction) and in z-axis direction (neck axial force).

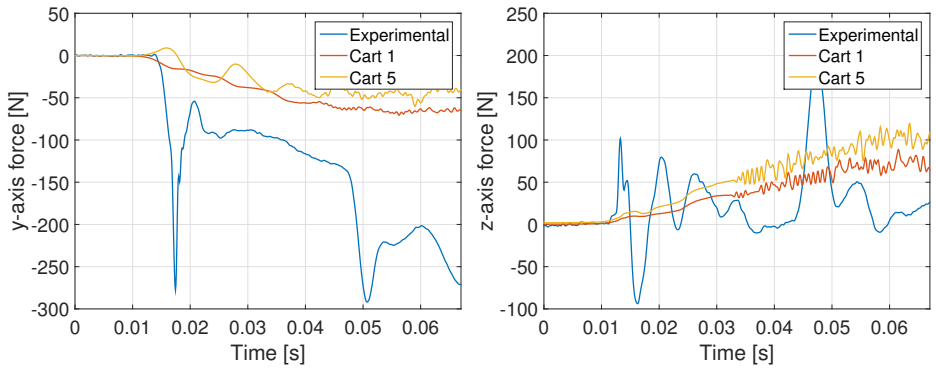

Figure 5.18: Comparison between cartilages and experimental axial forces; lateral impact.

The comparison with experimental data derived from Hybrid III, confirmed the necessity of a scale factor also in lateral impact test. For the sake of coherence, the same *scale factor* of 4.5 has been applied. In Figure 5.18 the experimental Hybrid III forces are compared with the scaled curved registered with neck IDV upper neck cross section (similar in position with the Hybrid III load cell).

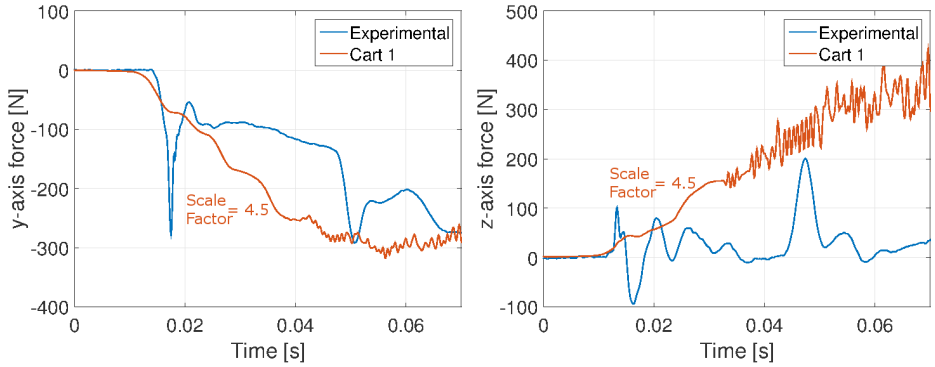

Figure 5.19: Comparison between cartilages and scaled experimental axial forces; lateral impact.

Upper

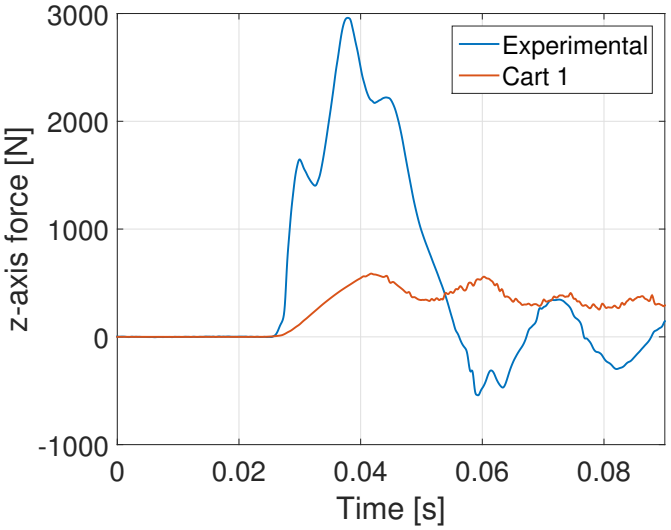

Figure 5.20: Comparison between cartilages and experimental z-axis forces; upper impact.

The upper impactor direction test confirmed the results previously obtained: a *scale factor* of 4.5 made possible the comparison between experimental and numerical z-axis forces.

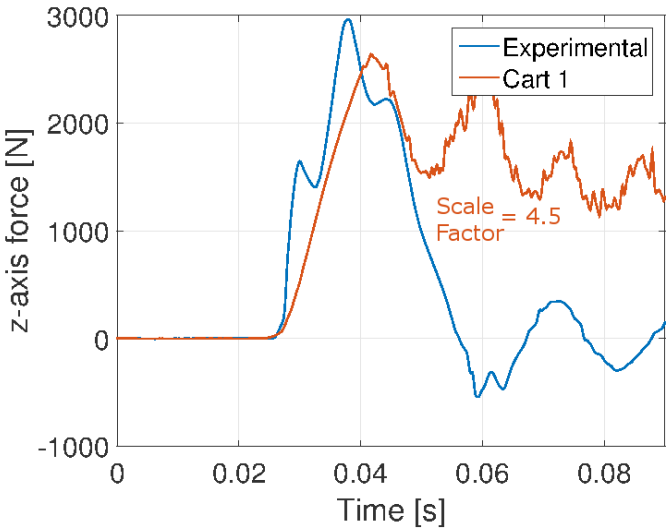

Figure 5.21: Comparison between cartilages and scaled experimental z-axis forces; upper impact.

5.3.2 Drop test

The frequency content and the time history of z-axis force and acceleration are reported in the following section for the drop tests. Analysis using different kind of CFC filter has been performed and a final configuration were selected in order to have the best correlation between experimental and numerical frequency content and in order to follow the same procedure adopted for *head test*. Due to the filters, also the time history resulted more related one to the other.

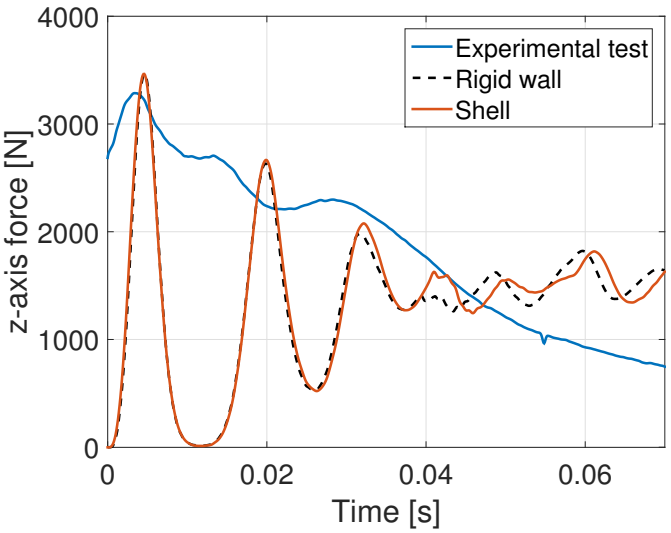

Figure 5.22: z-axis force in comparison with experimental on HIII.

0° drop, 0.08 m

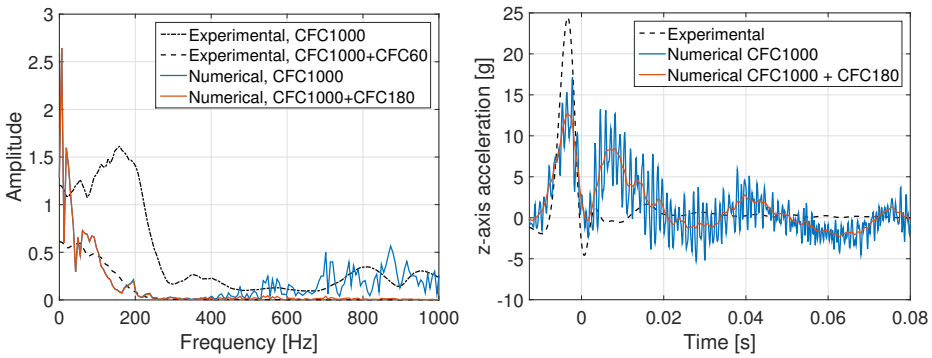

Figure 5.23: z-axis acceleration time history (left) and frequency content (right) in 0° drop test, 0.08 m.

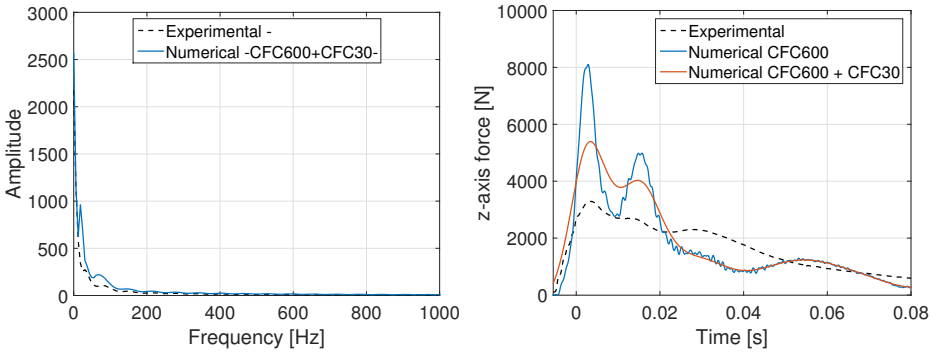

Figure 5.24: z-axis force time history (left) and frequency content (right) in 0° drop test, 0.08 m.

0° drop, 0.16 m

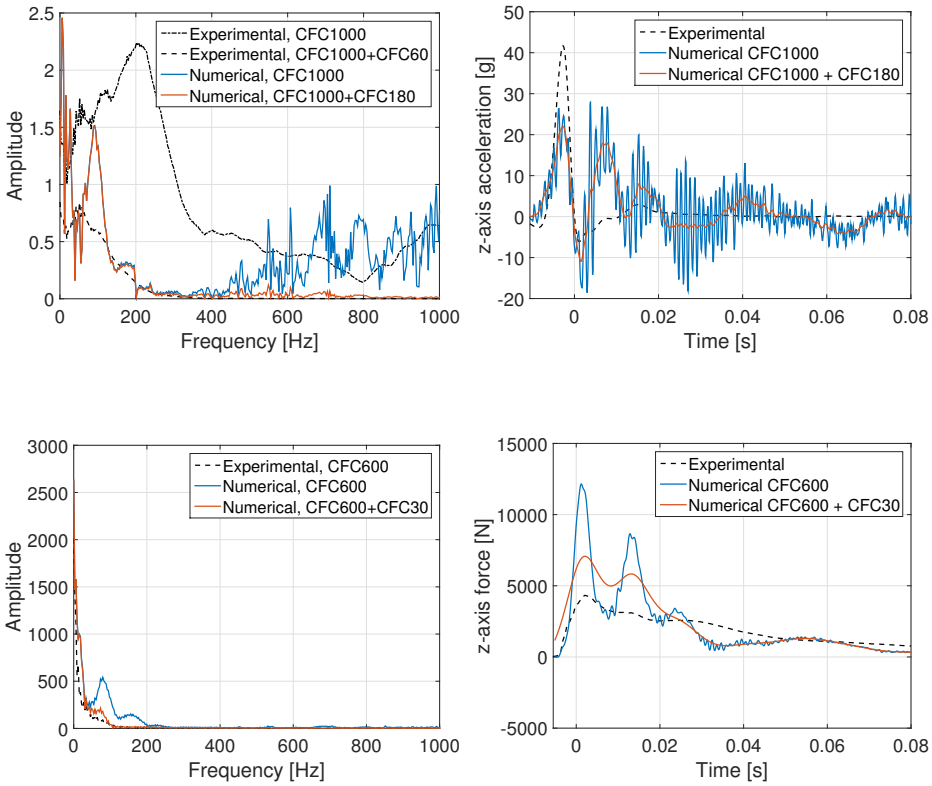

0° drop, 0.24 m

Since the frequency content characteristics of numerical acceleration and forces in comparison with experimental signal resulted similar for

every set-ups analysed, in the following sections only the signals time-history are presented.

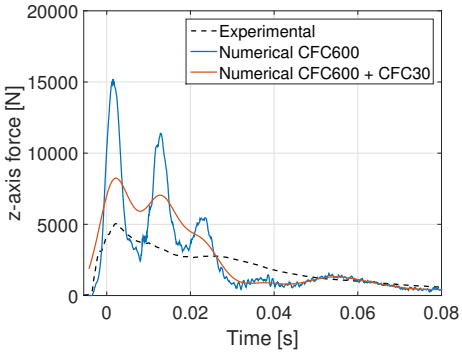

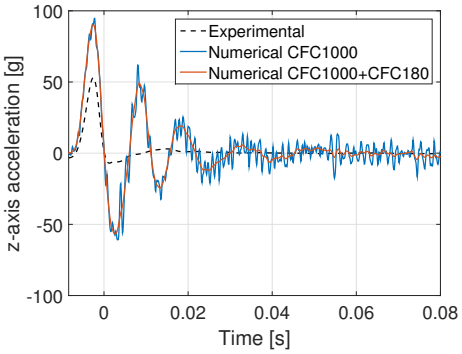

Inclined drop, 15°

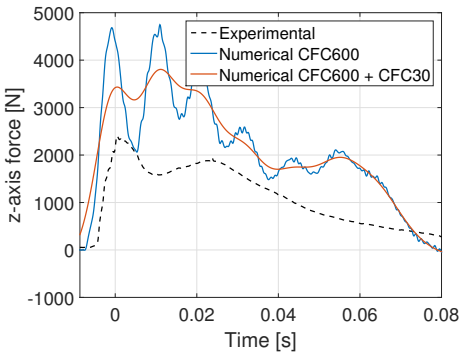

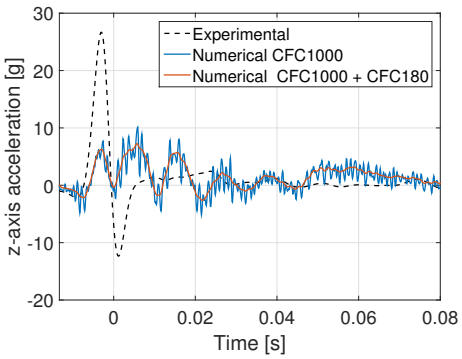

Some of the biofidelity issues of the Hybrid III are related to its high combined head-neck stiffness. In cadaver [35, 6] and volunteer tests [36], a human volunteer's neck flexed and its head escape the torso loading path, whereas the Hybrid III did not.

5.4 Numerical simulation comparison

5.4.1 Frontal head tests

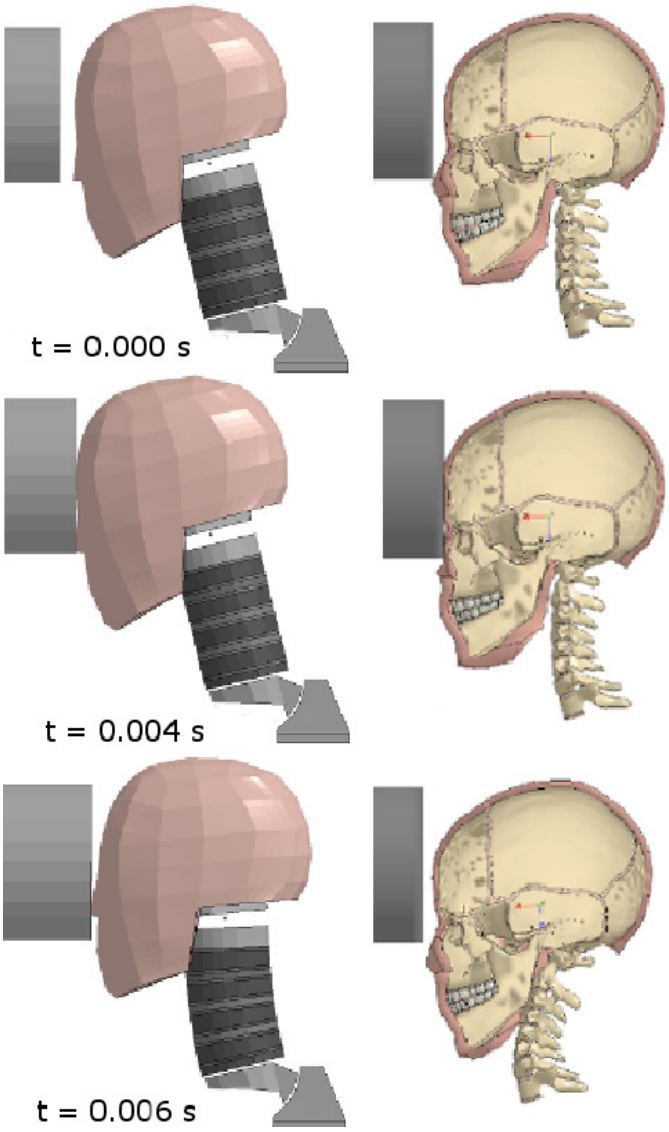

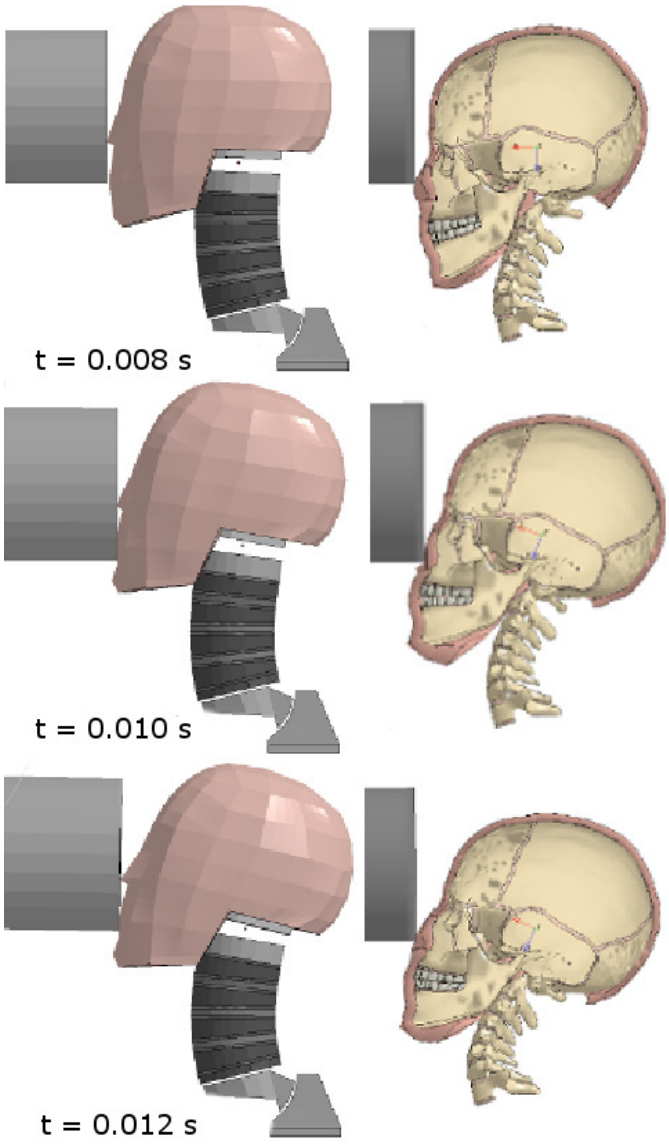

Figure 5.25: Simulation visualisation of frontal impact configuration: Hybrid III (left), THUMS (right).

5.4.2 0° drop test

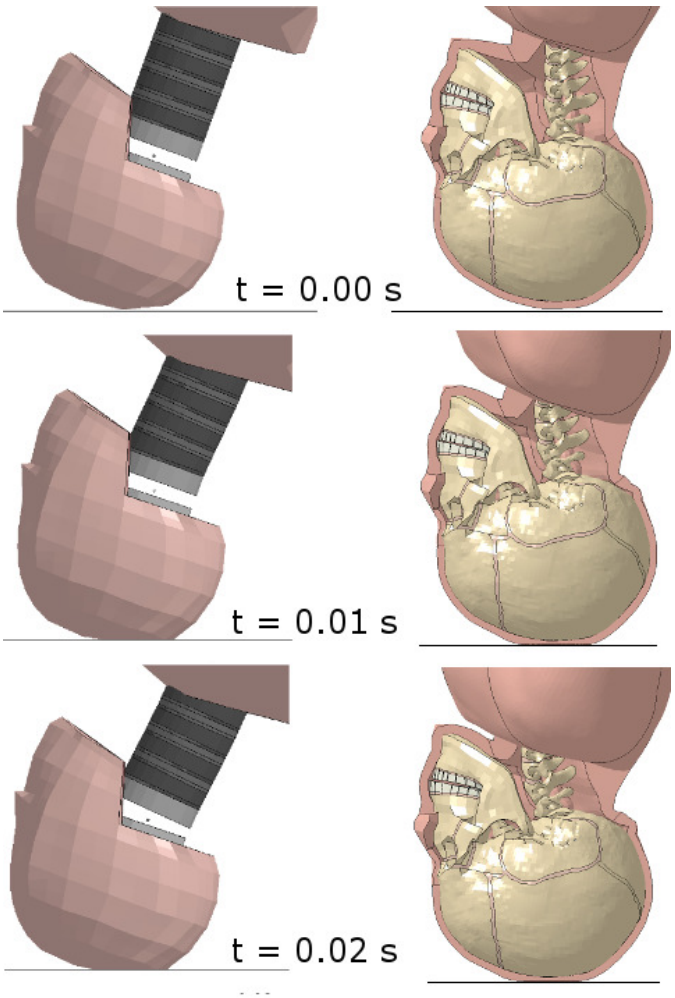

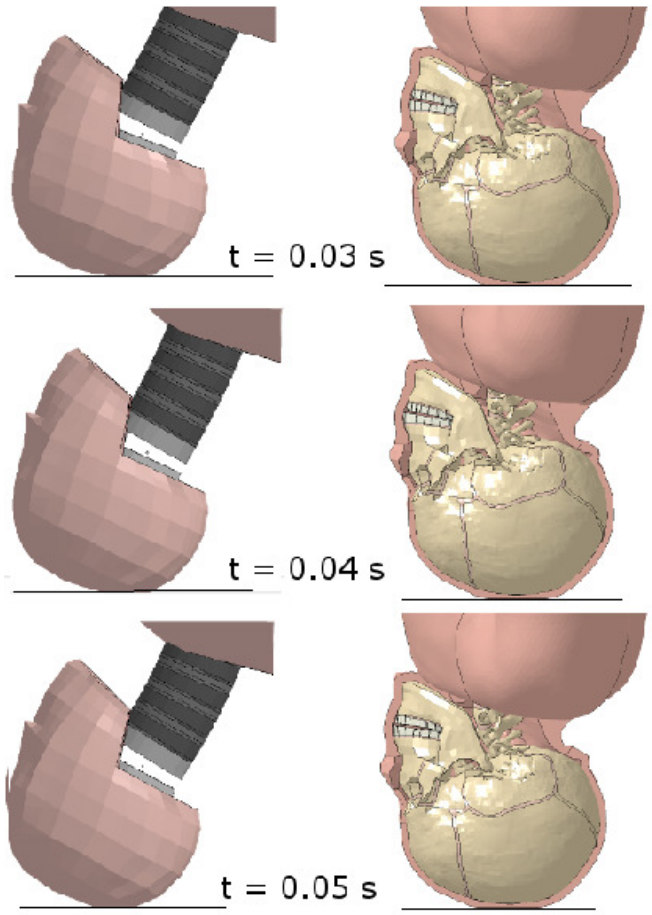

Figure 5.26: Simulation visualization of drop test: Hybrid III (left), THUMS (right).

Chapter 6

Conclusion, discussion and future development

6.1 Conclusion and discussion

The work presented in this thesis was focused on head and neck injury analysis in *head impact tests* and *drop tests*.
The initial part regarding the Antropomorphic Test Device (Hybrid III) gave additional proof ([28, 34]) of the high stiffness of the Hybrid III neck in comparison with real human neck. A scale factor of 4–5 is necessary to relate human being neck forces with the results obtained for the load cell in Hybrid III. Since THUMS is a human model, the comparison between its responses and Hybrid III's need the use of a scale factor.
No differences between upper neck and lower neck were registered with Hybrid III both in *head tests* and *drop tests*. Instead, different forces values were registered in different THUMS neck levels. Once again, THUMS responses are similar to the real human being behaviour.
The frontal, lateral and upper impact initially analysed happened at low velocity: no severity index were exceeded. Eventually, other three velocity conditions were analysed for *head impact tests* and higher severity index levels were registered.
This study demonstrated that drop height is an important factor influencing the response of the head.
In THUMS *head tests* simulation the importance of ligaments, tendons and flesh has been discussed and it has been observed that the pres-

ence of those part is fundamental for evaluating the force. However, THUMS reacts as a human cadaver –not a living human being– and its neck muscles do not have any active reaction as otherwise expected from a live human. This can be analysed in future development considering the possibility of introducing muscles activation in the model. Considering the forces in the THUMS neck recorded during *drop tests*, the lower neck level demonstrated lower magnitude than the upper neck level. This suggests a substantial decoupling between the head and the spinal column. This is confirmed also by the analysis of contact forces, which are higher than the force in the neck. In contrast, the Hybrid III tests indicated similar magnitude for upper neck and contact forces. These suggest more rigid coupling between the Hybrid III head and neck than those observed in THUMS. Further, the evaluation of the high speed films demonstrated –in the *head tests*– that the Hybrid III head followed the impactor excursion both in frontal, lateral and upper impact. This do not happen in THUMS, which has a similar behaviour to human specimens [28].

6.2 Future development

Even if the analysis of human behaviour have lot of aleatory parameters, the development of a human model as THUMS can be very useful in crashworthiness and in the analysis of human behaviour, also regarding the medical point of view. However the presence of instrumentation also in THUMS model would be necessary: in this way the injury criteria can be easily evaluated. In addition, the analysis and definition of new and/or updated threshold values should be evaluated because lot of the present threshold scores for injury criteria [11] are based on data recorded by Col John Paul Stapp (for more detail, refer back to Chapter 2) research, animal concussion tests, PMHS tests, low level exposed volunteers tests and dummy experimental tests, which cannot be considered totally reliable compared to real human being.
An interesting future development concerns the development of an ATD more comparable to the human body.

Appendix A

SAE J211 CFC Filter

The Society of Automotive Engineers J211 [14] describes guidelines and requirements for instrumentation for impact testing. J211 requires signals from impact tests to be filtered using one of four channel frequency classes (CFC) low-pass filters and it specifies acceptable frequency response for each filter class. The four filters are designated as CFC60, CFC180, CFC600, and CFC1000. It is clear from the J211 filter specifications that they were derived from analog Butterworth filters whose corner frequency (the frequency at which the signal loses ont half of its power) is equal to the CFC designation divided by 0.6.
The main characteristics of the CFC filters used in this work are presented hereby.

CFC 60 characteristics:

3db limit frequency	100 Hz
Stop damping	-30 dB
Sampling frequency	at least 600 Hz

Table A.1: CFC 60 characteristics.

CFC 180 characteristics:

3db limit frequency	300 Hz
Stop damping	-30 dB
Sampling frequency	at least 1800 Hz

Table A.2: CFC 180 characteristics.

CFC 600 characteristics:

3db limit frequency	1000 Hz
Stop damping	-40 dB
Sampling frequency	at least 6 kHz

Table A.3: CFC 600 characteristics.

CFC 1000 characteristics:

3db limit frequency	1650 Hz
Stop damping	-40 dB
Sampling frequency	at least 10 kHz

The output signal is given by the following difference equation:

$$Y(t) = a_0X(t)+a_1X(t-1)+a_2X(t-2)+b_1Y(t-1)+b_2Y(t-2) \quad \text{(A.1)}$$

in which the constants are calculated using the following equations:

$$\begin{aligned} w_d &= 2\pi CFC2.0775 \\ w_a &= \frac{sin(w_d) \times 0.5T}{cos(w_d) \times 0.5T} \\ b_0 &= \frac{w_a^2}{1+\sqrt{2}w_a + w_a^2} \\ b_1 &= 2b_0 \\ b_2 &= b_0 \\ a_1 &= 2\frac{w_a^2 - 1}{1+\sqrt{2}w_a + w_a^2} \\ a_2 &= -\frac{-1+\sqrt{2}w_a - w_a^2}{1+\sqrt{2}w_a + wa^2} \end{aligned}$$

and where

X(t) = input data sequence;

Y(t) = filtered data sequence;

T = sampling rate in seconds : 1/12500 s;

CFC = Channel frequency class constant (1000 or 600 in this work);

a, b = constant varying with class filter used.

Appendix B

Experimental data: maximum values and graphs

The maximum value of every acquired signal is presented hereby. Each graph shows the comparison between the maximum value reached in the first cable configuration and the maximum value in the second cable configuration. With the verification of tests repeatability, the graphs allow to analyse the cable influence in every impact configuration. The first cable configuration refers to the one with the black line (in frontal impact scenario, Figure 3.4) in horizontal position and 0.0101 m of axial cable out of the hex nut; the second cable configuration has the initial position of the black line (Figure 3.4) with an angle of about 7° and 0.0144 m of the length of the axial cable out of the hex nut.

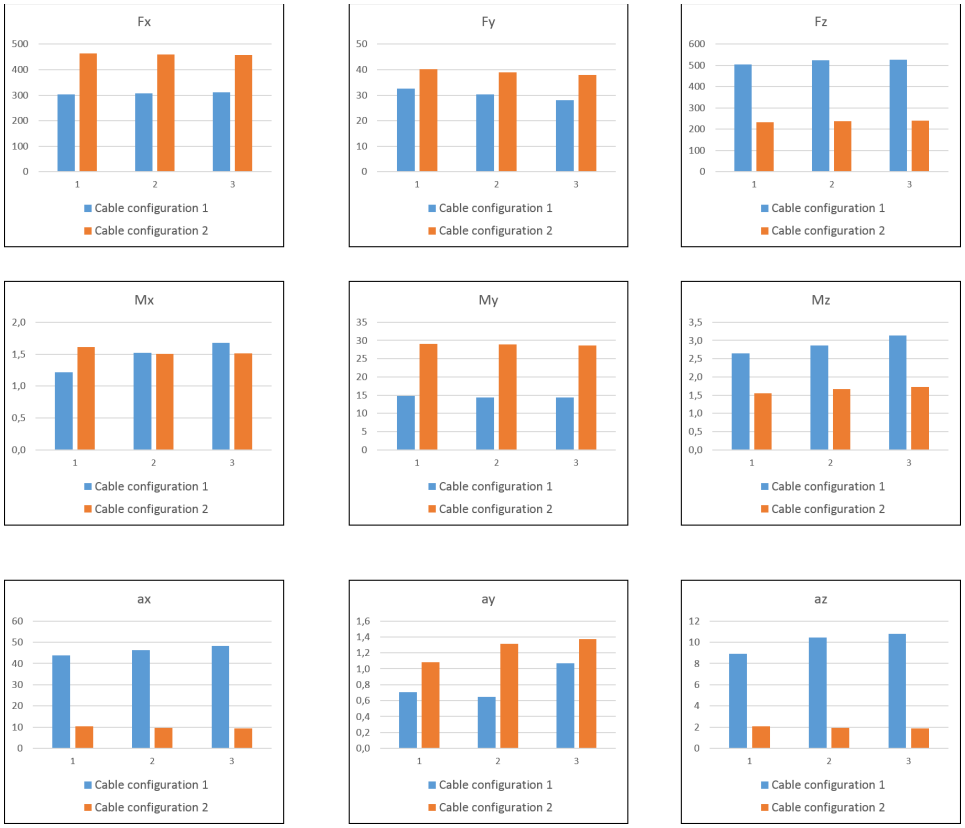

Figure B.1: DAS output in frontal impact.

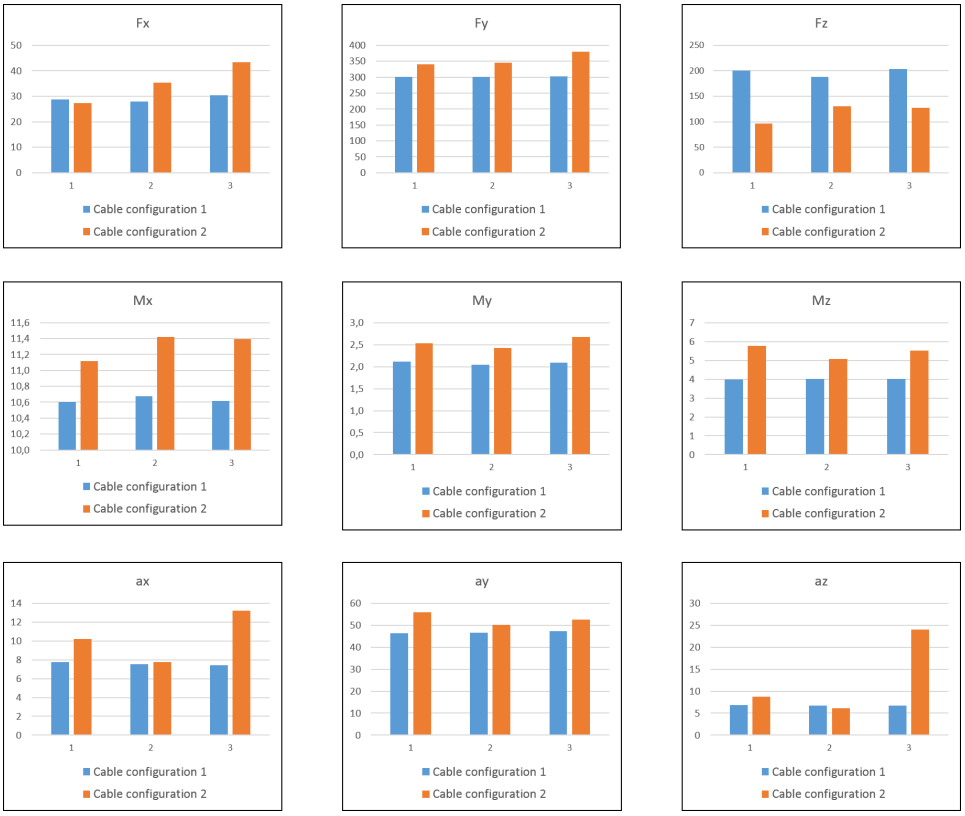

Figure B.2: DAS output in lateral impact.

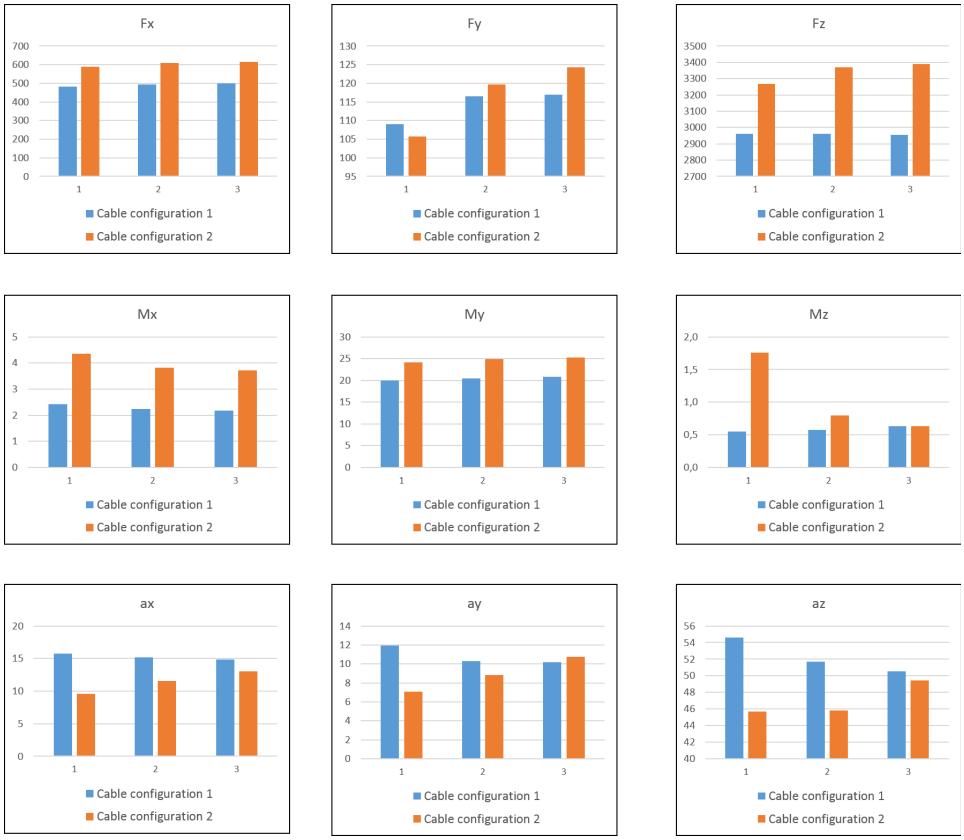

Figure B.3: DAS output in upper impact.

B.1 Axial forces

B.1.1 Head tests

Frontal impact

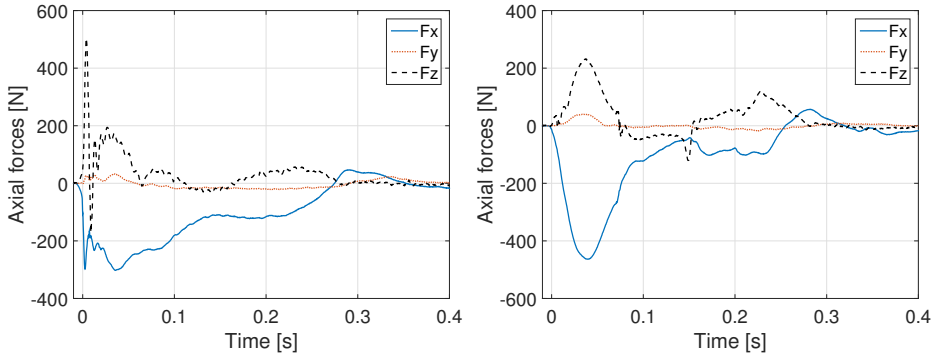

Figure B.4: x-forces in frontal impact in (left) first cable configuration and (right) in second cable configuration.

Lateral impact

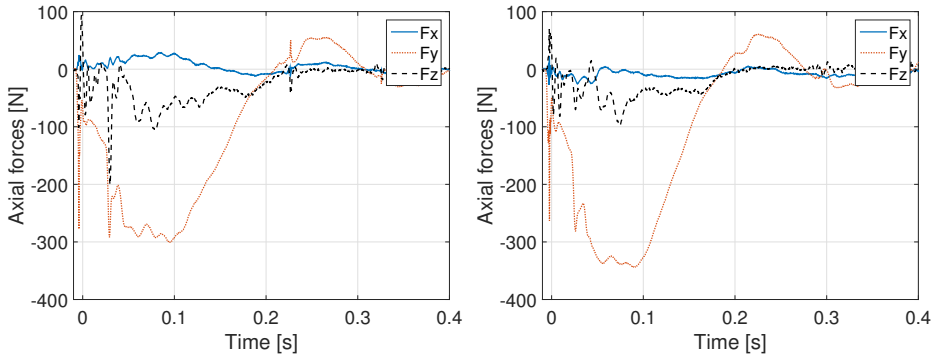

Figure B.5: y-forces in lateral impact in (left) first cable configuration and (right) in second cable configuration.

Upper impact

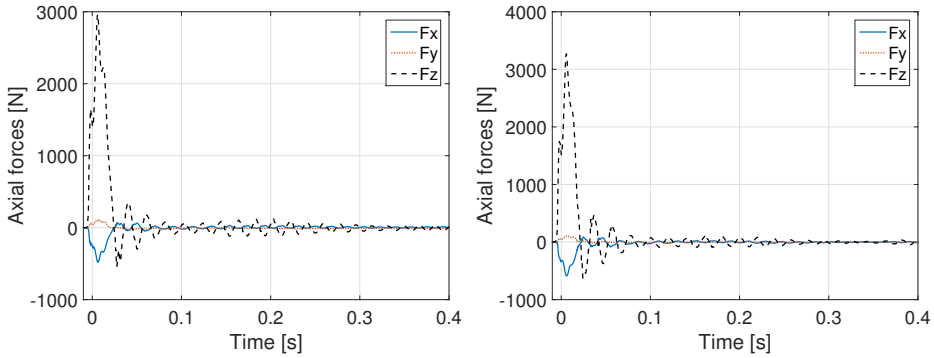

Figure B.6: z-forces in upper impact in (left) first cable configuration and (right) in second cable configuration.

B.2 Nij

B.2.1 Head tests

Frontal impact

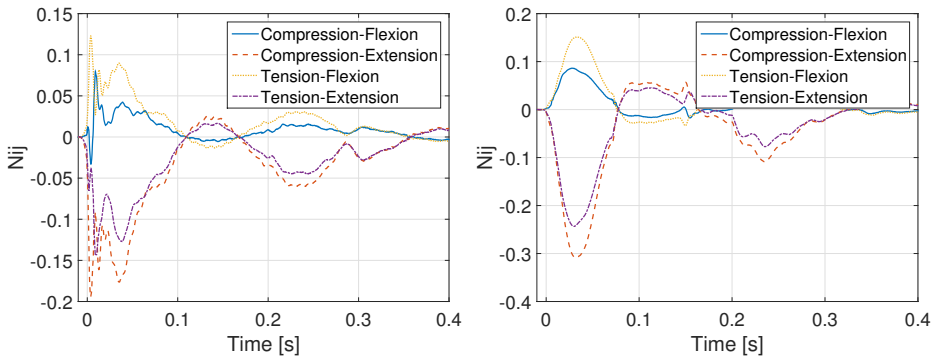

Figure B.7: Nij in frontal impact in first (left) cable configuration and in second (right) cable configuration.

Lateral impact

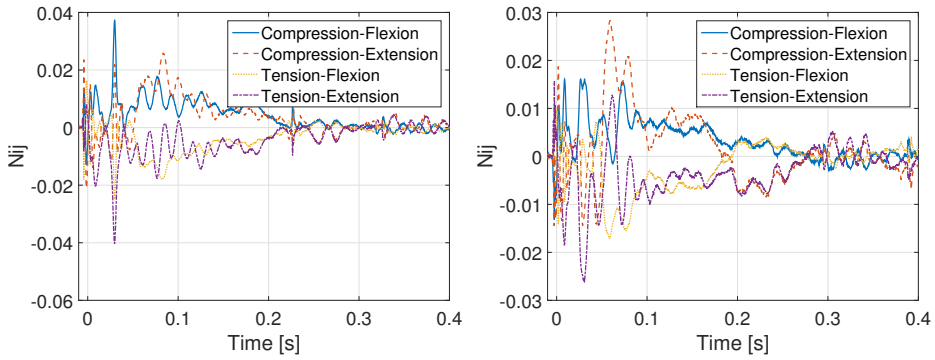

Figure B.8: Nij in lateral impact in first (left) cable configuration and in second (right) cable configuration.

Upper impact

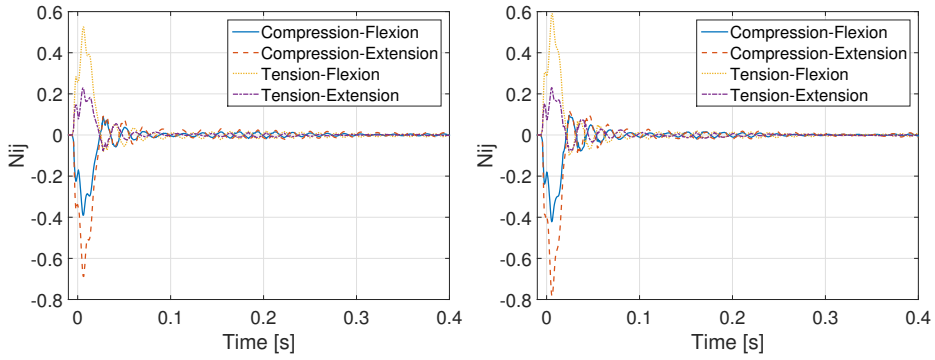

Figure B.9: Nij in upper impact in first (left) cable configuration and in second (right) cable configuration.

B.2.2 Drop tests

0° drop test

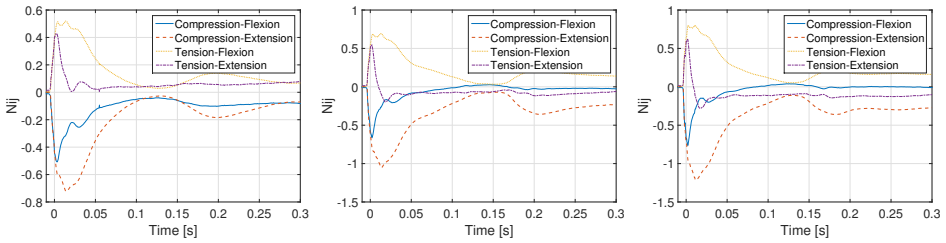

Figure B.10: Nij in 0° drop test at different heights.

15° drop test

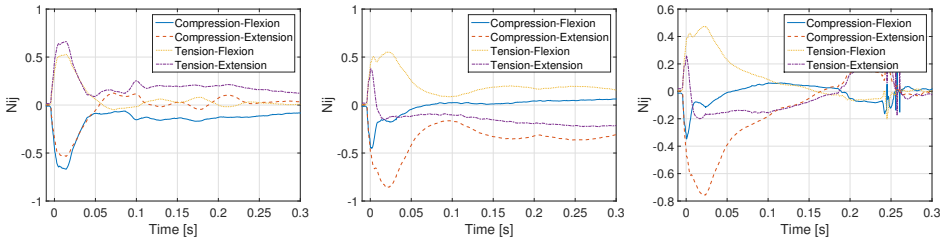

Figure B.11: Nij in 15 ° drop test in different orientation at 80 mm heights.

B.3 MOC

In the following sections are presented the total moment about occipital condyle calculated for the experimental tests.

B.3.1 Head tests

Frontal impact

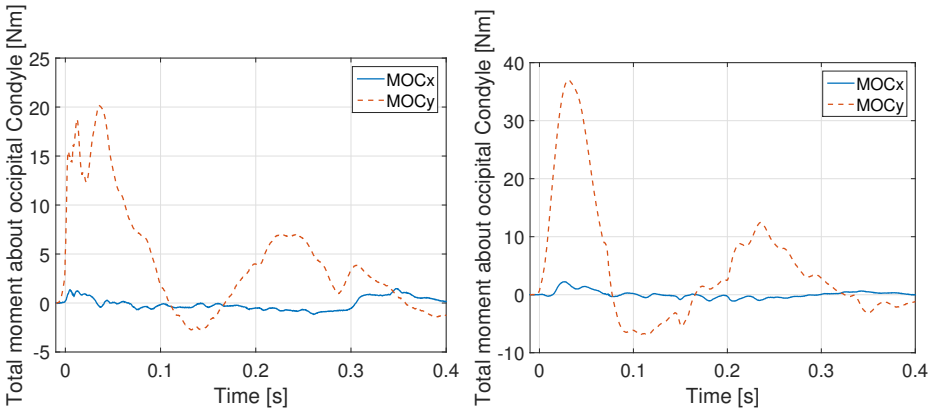

Figure B.12: Moc in frontal impact in first (left) cable configuration and in second (right) cable configuration.

Lateral impact

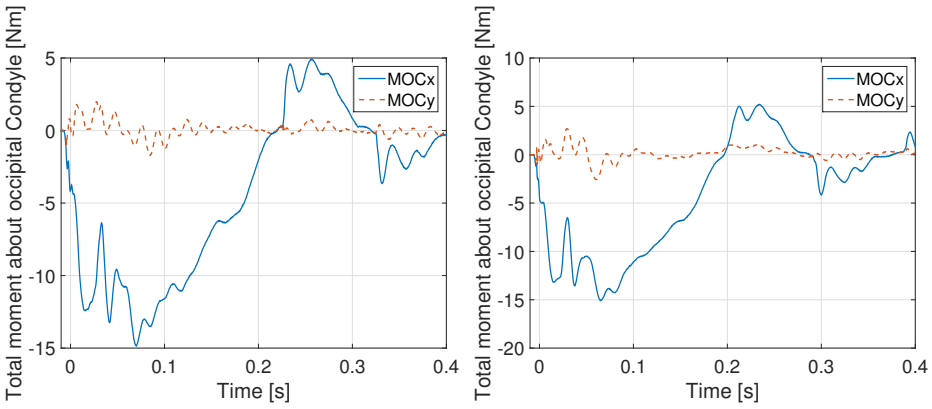

Figure B.13: Moc in lateral impact in first (left) cable configuration and in second (right) cable configuration.

Upper impact

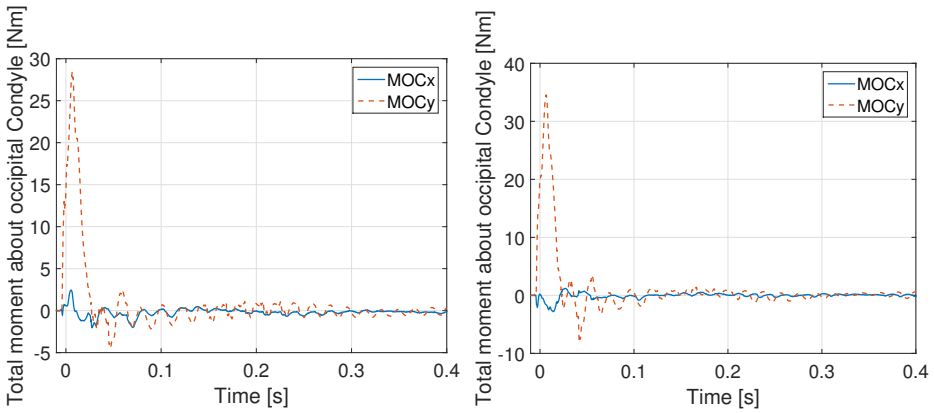

Figure B.14: Moc in upper impact in first (left) cable configuration and in second (right) cable configuration.

B.3.2 Drop tests

0° drop test

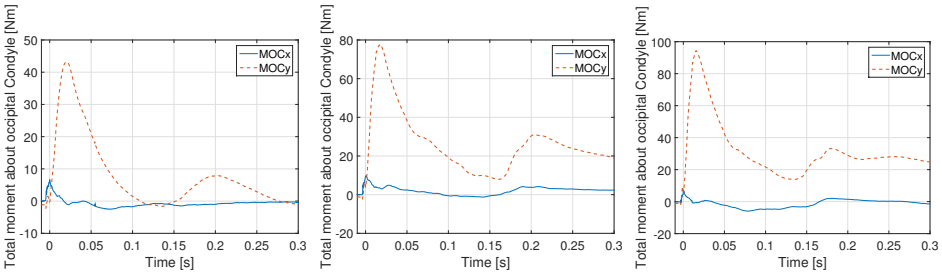

Figure B.15: Moc in 0° drop test at different heights.

15° drop test

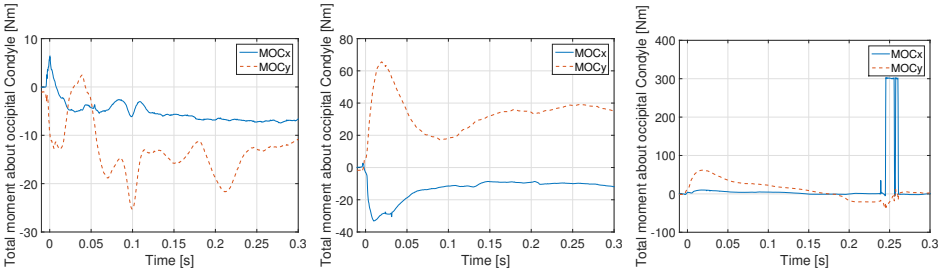

Figure B.16: Moc in 15° drop test in different orientation at 0.08 m height.

Appendix C

Brain Injuries

C.1 Intercranial Pressure

The pictures in this Appendix represent the trend of the Intercranial pressure on THUMS white and gray matter registered in frontal impact. The frames are reported with a time step of 0.002 s, starting from instant t = 0 s, to instant t = 0.012 s.
For the three directions the results presented the same trend: the higher the velocity of impact, the higher the pressure in the brain.

C.1.1 Frontal impact

Impactor velocity: 3 m/s

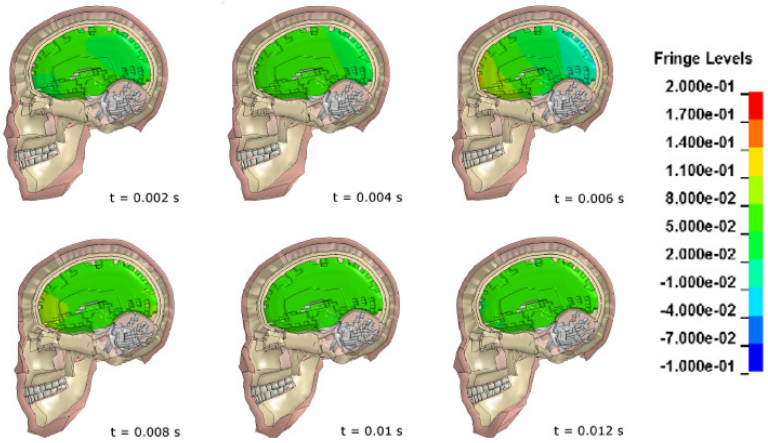

Figure C.1: Intercranial pressure; frontal impact at 3 m/s.

Impactor velocity: 3.5 m/s

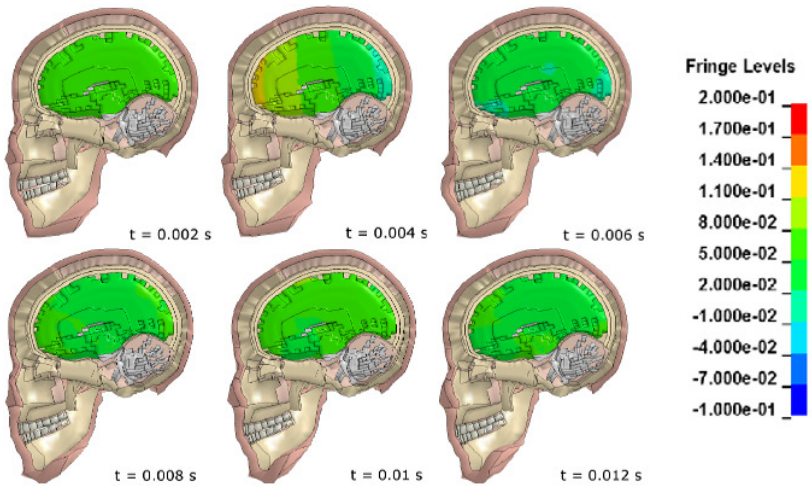

Figure C.2: Intercranial pressure; frontal impact at 3.5 m/s.

Impactor velocity: 4 m/s

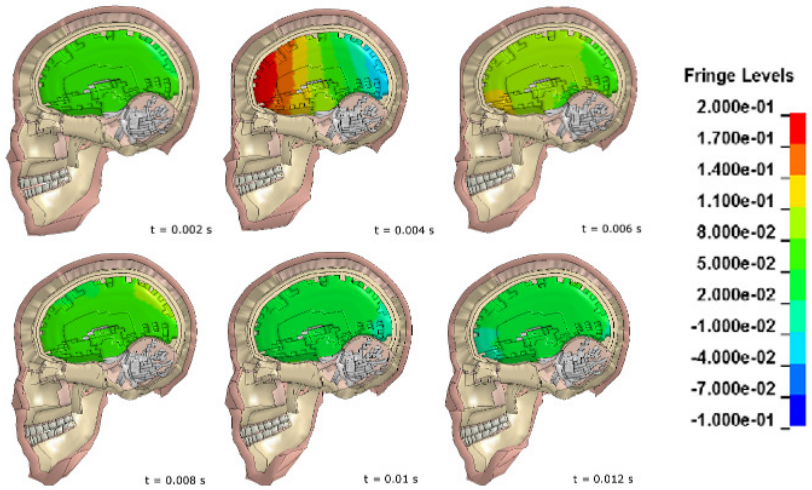

Figure C.3: Intercranial pressure; frontal impact at 4 m/s.

C.1.2 Lateral impact

3 m/s

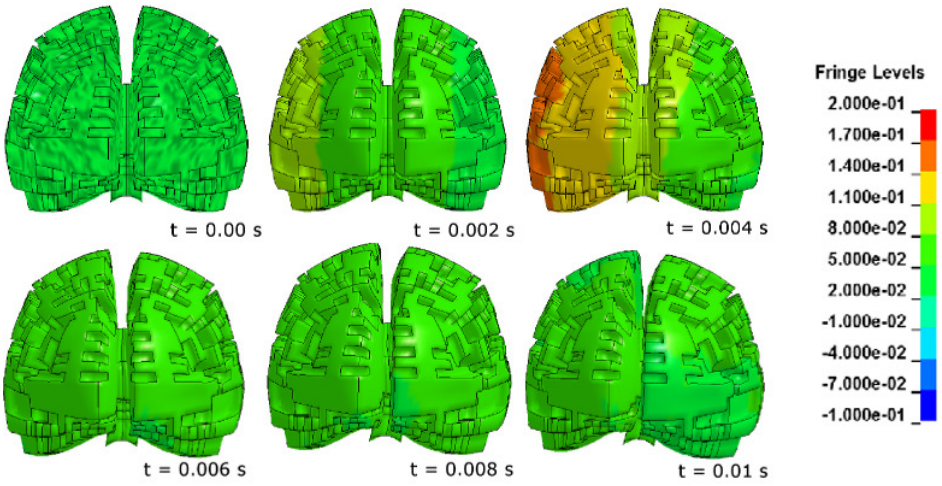

Figure C.4: Intercranial pressure; lateral impact at 3 m/s.

3.5 m/s

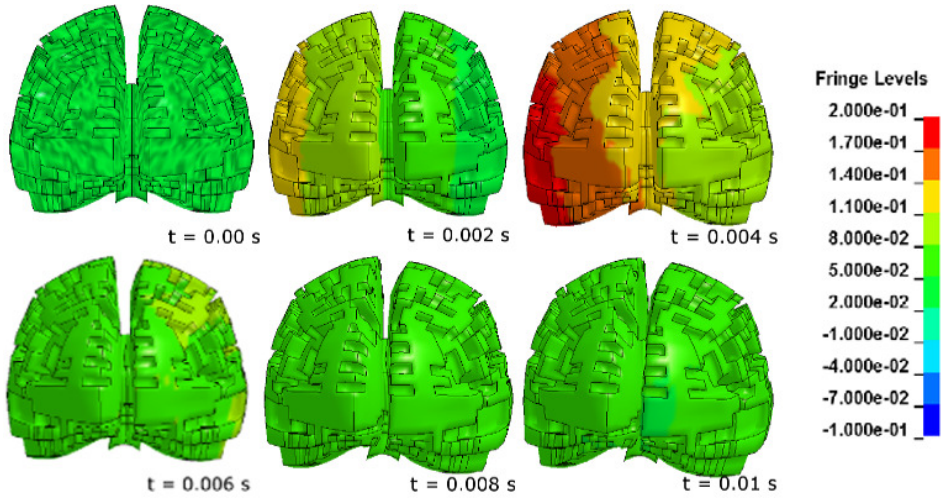

Figure C.5: Intercranial pressure; lateral impact at 3.5 m/s.

4 m/s

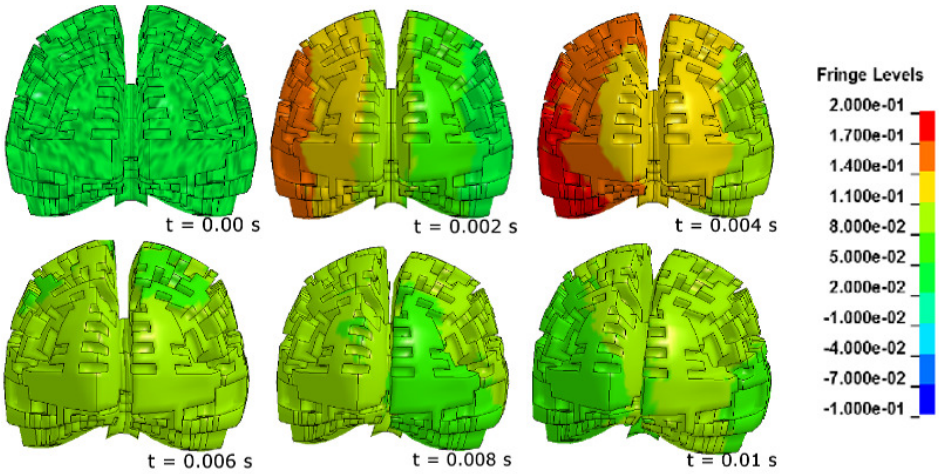

Figure C.6: Intercranial pressure; lateral impact at 4 m/s.

C.1.3 Upper impact

3 m/s

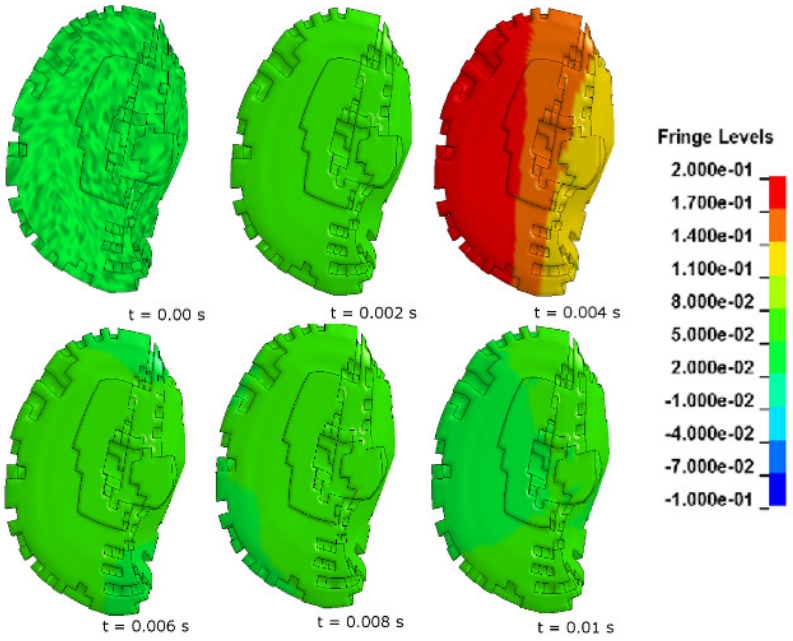

Figure C.7: Intercranial pressure; upper impact at 3 m/s.

3.5 m/s

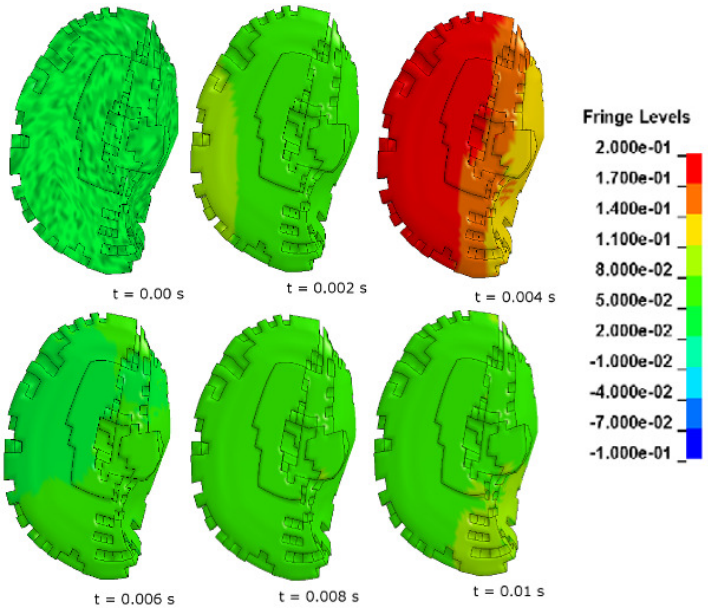

Figure C.8: Intercranial pressure; upper impact at 3.5 m/s.

4 m/s

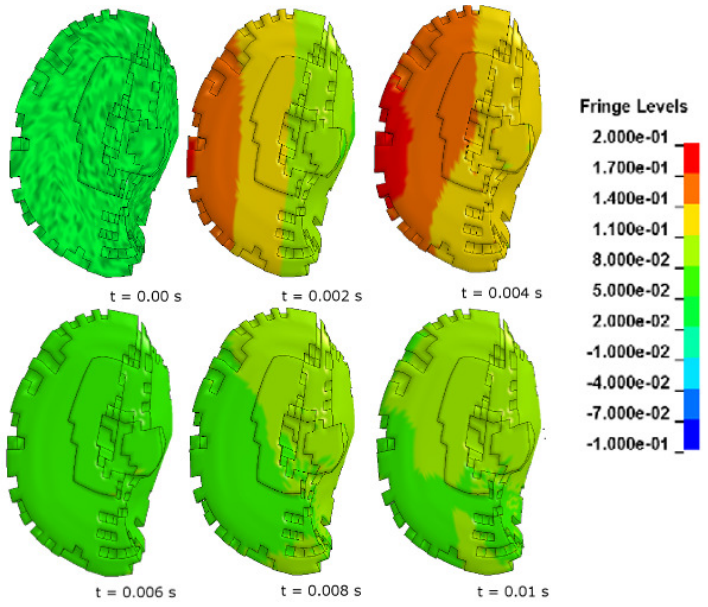

Figure C.9: Intercranial pressure; upper impact at 4 m/s.

C.2 CSDM

C.2.1 Frontal

3 m/s

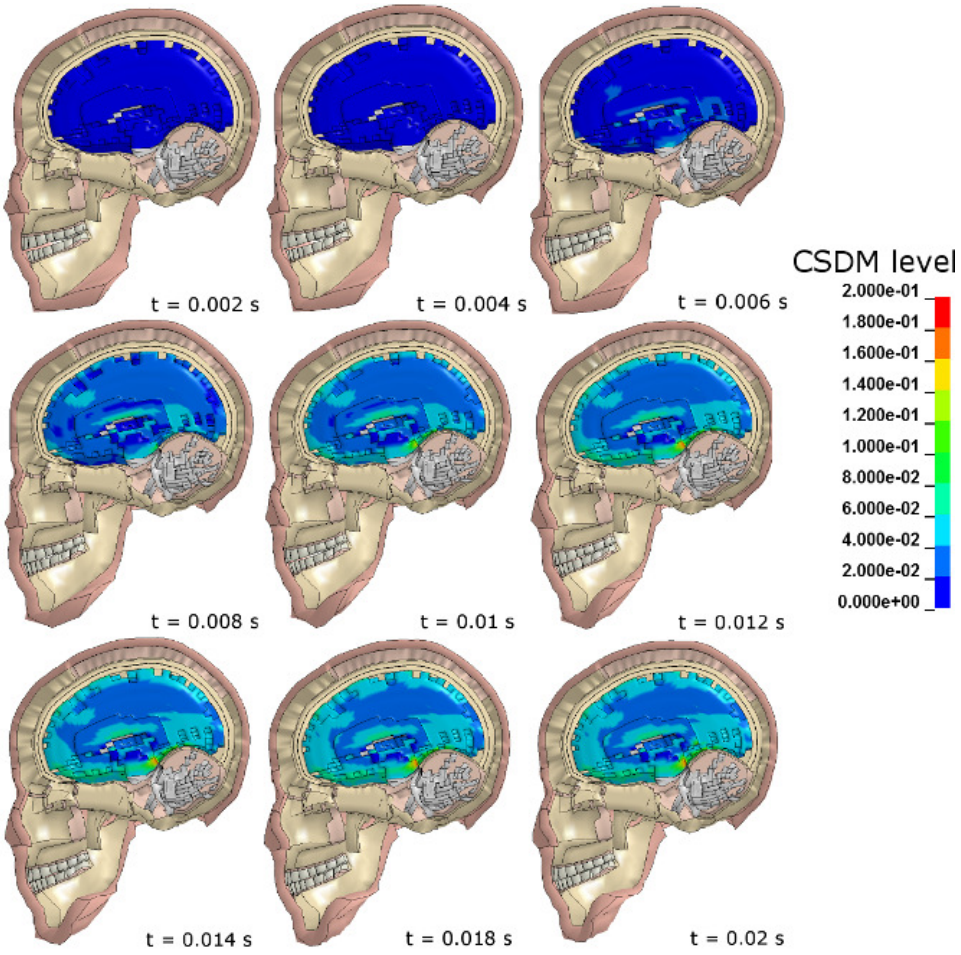

Figure C.10: CSDM; frontal impact at 3 m/s

3.5 m/s

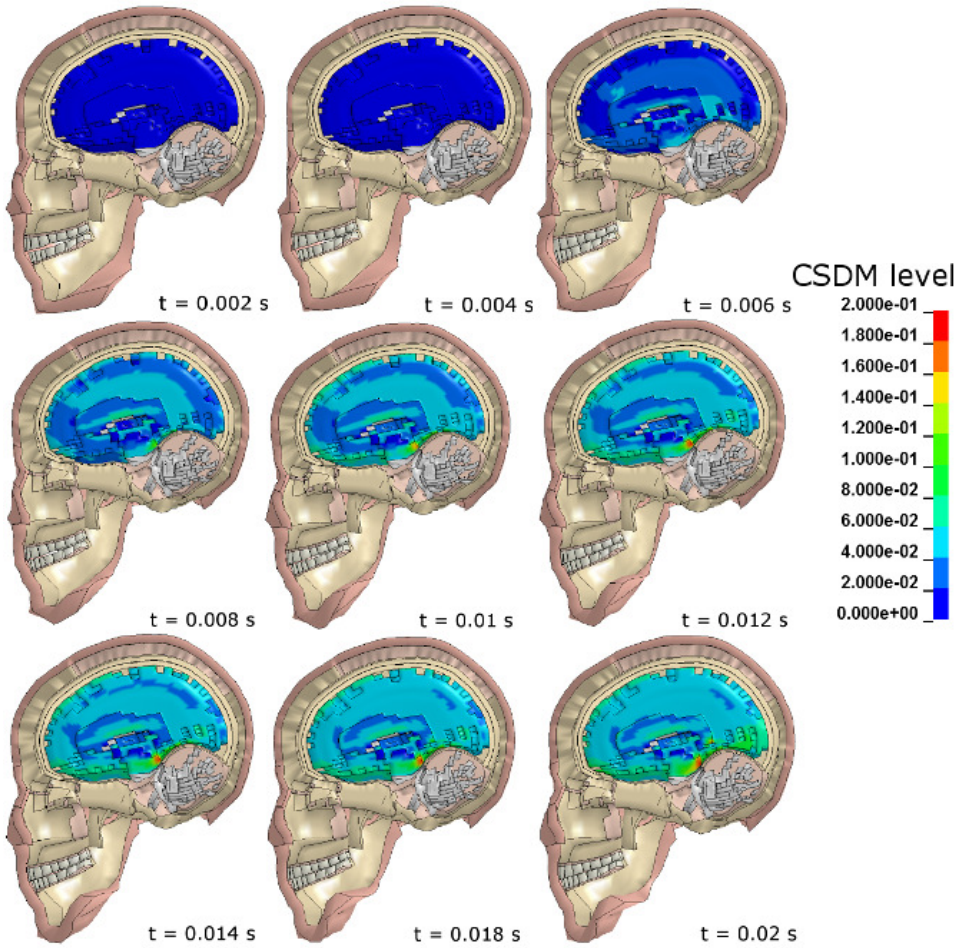

Figure C.11: CSDM; frontal impact at 3.5 m/s

4 m/s

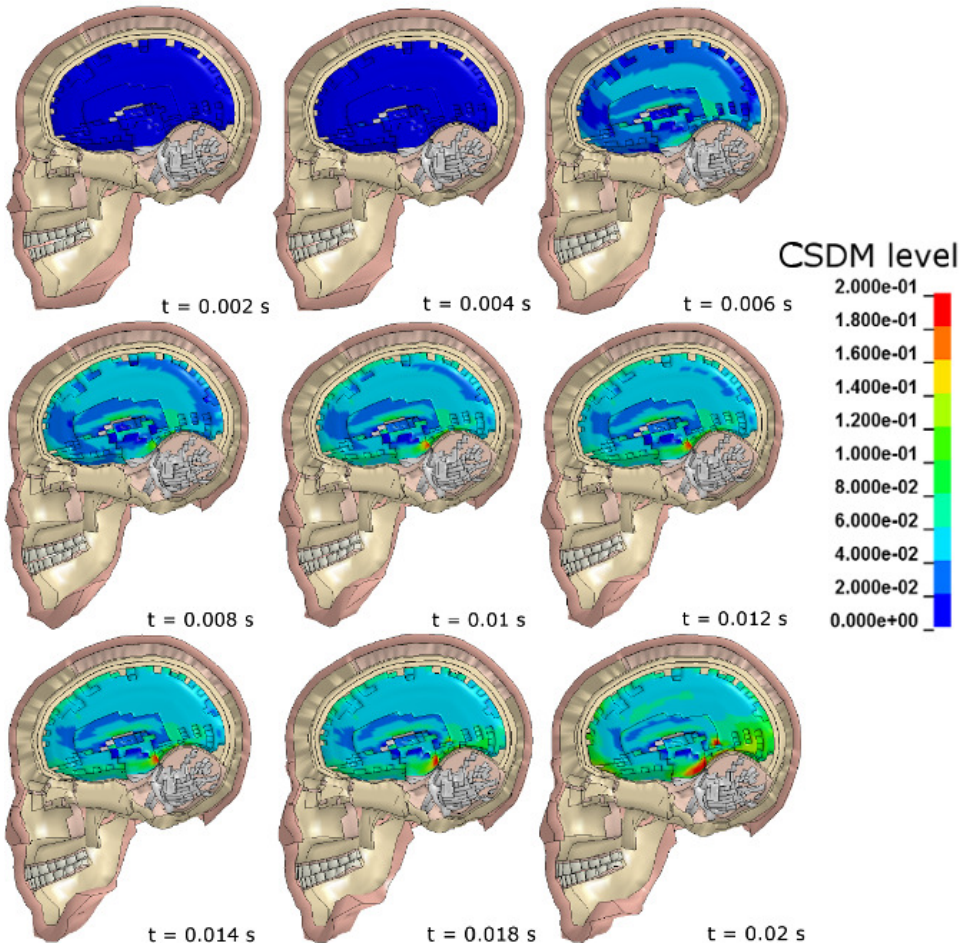

Figure C.12: CSDM; frontal impact at 4 m/s

C.3 Deformation

C.3.1 Frontal

3 m/s

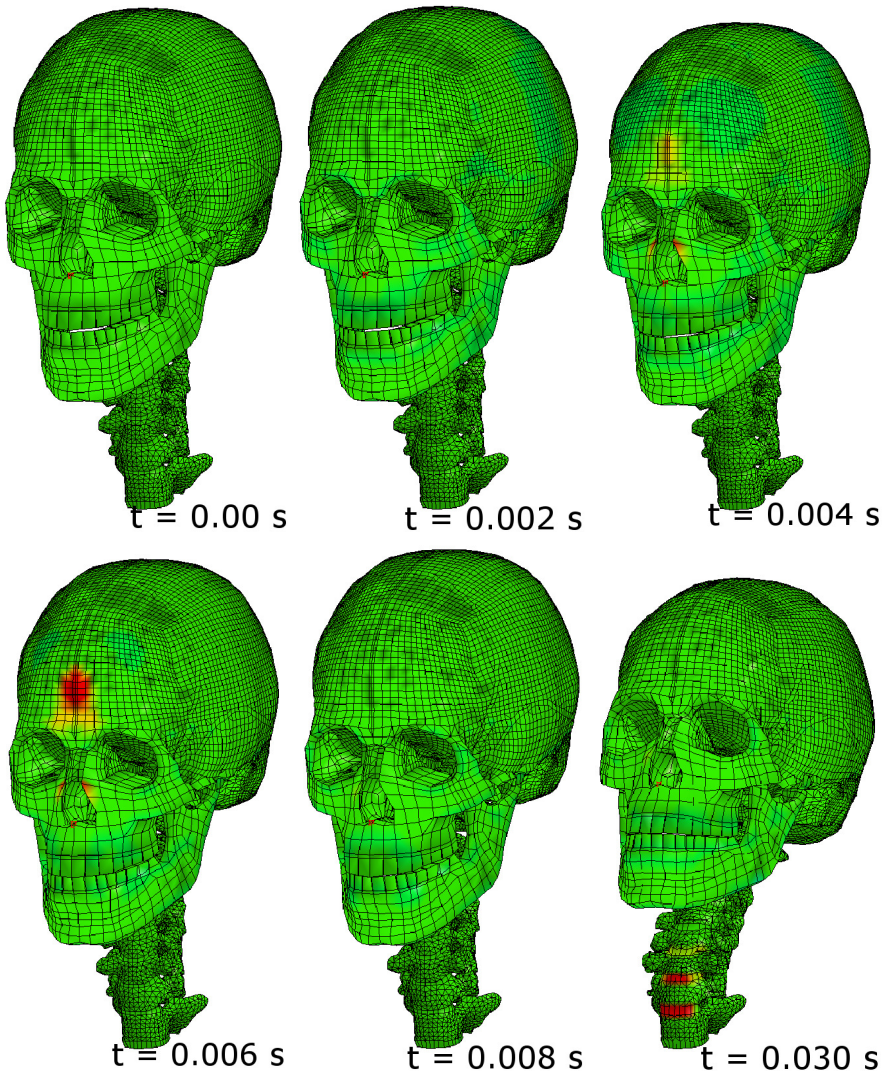

3.5 m/s

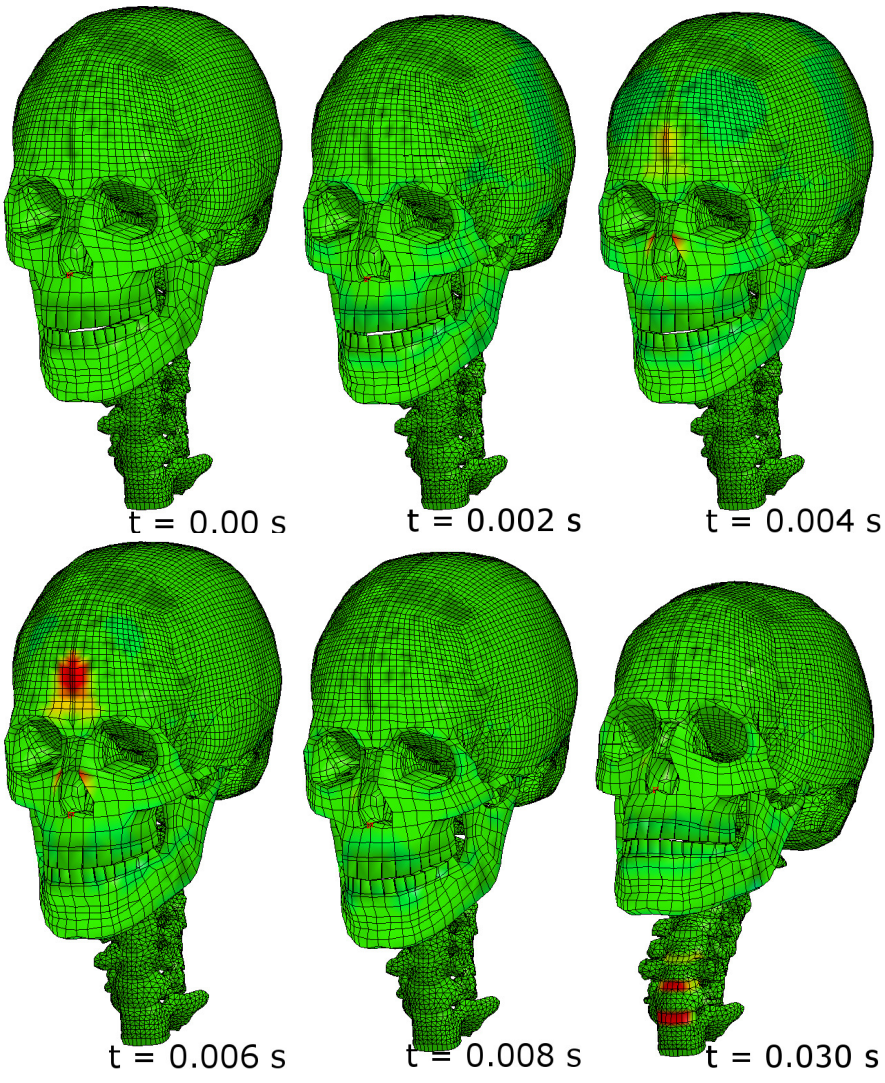

4 m/s

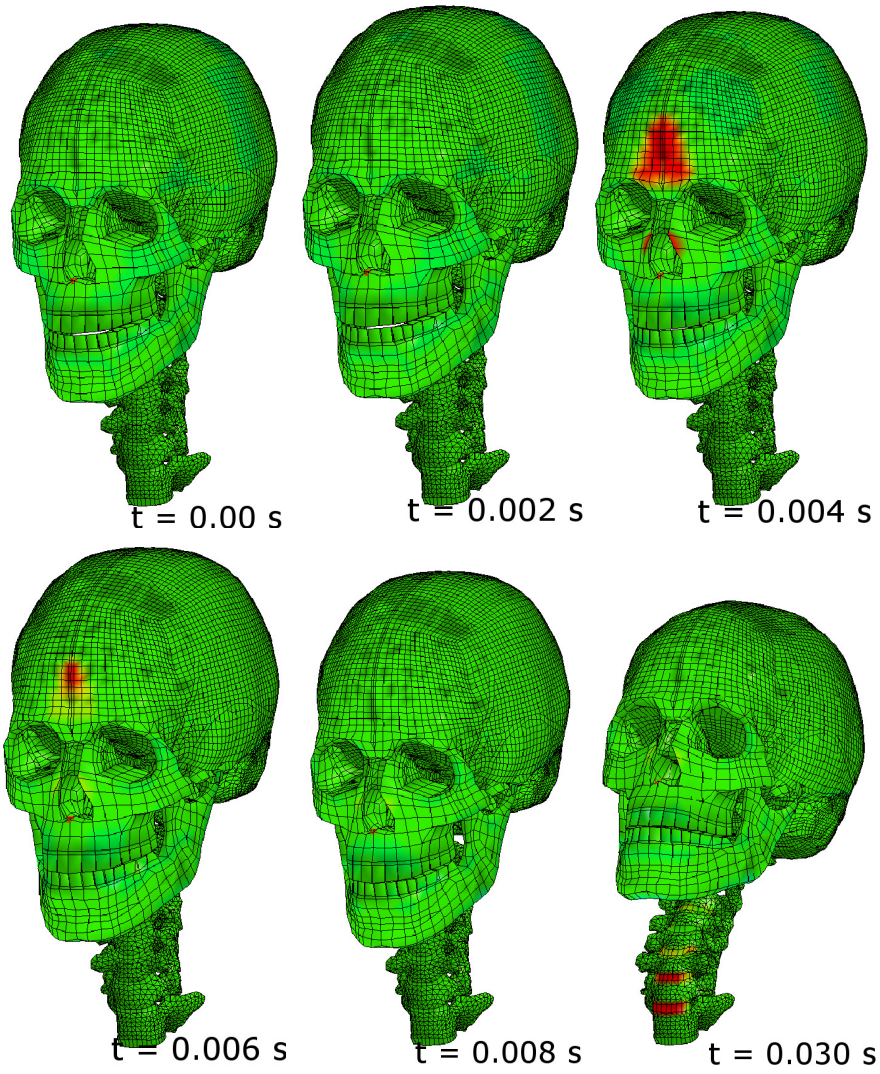

Nomenclature

AAAM	Association for the Advancement of Automotive Medicine
AIS	Abbreviated Injury Scale
ANOVA	ANalysis Of VAriance
ATD	Anthropomorphic Test Device
BC	Boundary Condition
BrIC	Brain Rotational Injury Criterion
CFR	Code of Federal Regulations
CG	Centre of Gravity
CSDM	Cumulative Strain Damage Measure
CSF	Cerebra Spinal Fluid
DAI	Diffuse Axonal Injury
DAS	Data Acquisition System
FE	Finite Element
FEHM	Finite Element Head Model
FMVSS	Federal Motor Vehicle Safety Standard
$\mathbf{G_0}$	Short-time Shear modulus
$\mathbf{G_\infty}$	Long-time Shear modulus
GAMBIT	Generalised Acceleration Model for Brain Injury Threshold
HIC	Head Injury Criterion
HRCT	High-Resolution Computer Tomography
ICP	InterCranial Pressure
IVD	InterVertebral Disc
LaST	Laboratorio Sicurezza dei Trasporti
MOC	Total Moment about Occipital Condyle
MPS	Maximum Principal Strain

NIJ	Normalized Neck Injury Criterion
PAC	Pia Arachnoid Complex
PMHS	Post Mortem Human Subject
SAE	Society for Automotive Engineers
SIMon	SIMulated Injury Monitor
TBI	Traumatic Brain Injury
THUMS	Total Human Model for Safety
WSTC	Wayne State Tolerance Curve

Bibliography

[1] SAE International. Sae j1733: Sign convention for vehicle crash testing. Technical Report 49 CFR 572.137, SAE International, October 7 1998.

[2] TOYOTA MOTOR CORPORATION. *THUMS, AM50 Pedestrian/Occupant Model, Academic Version 4.02*. Toyota Central RD Labs. Inc., May 2015.

[3] Humanetics. Humanetics online documentation. http://www.humaneticsatd.com/. Accessed: May 2015.

[4] Andre Matthew Loyd, Roger W. Nightingale, Yin Song, Jason F. Luck, Hattie Cutcliffe, Barry S. Myers, and Cameron 'Dale' Bass. The response of the adult and atd heads to impacts onto a rigid surface. *Accident Analysis and Prevention*, June 2014.

[5] N. Yoganandan, Jr. A, Sances, D. J. Maiman, J. B. Myklebust, P Pech, and S. J. Larson. Experimental spinal injuries with vertical impact. *Spine*, 11(9):855–860, 1986.

[6] G. S. Nusholtz and P. S. Kaiker. Kinematic of the human cadaver spine in response to superior-inferior loading of the head. Final UMTRI-86-31, Bioscience Division, University of Michigan, Transportation Research Institute, 2901 Baxter Road, Ann Arbor, Michigan, July 1986.

[7] A. Eichberger M. Darok, E. P. Leinsinger and H. Steffan. Neck injury criterion validation using human subjects and dummies. *Frontiers in Wiplash Trauma*, pages 409–434, 2000.

[8] N. Yoganandan, Jr. A. Sances, and F. Pintar. Biomechanical evaluation of the axial compressive responses of the human cadaveric and mankin necks. *Journal of biomechanical engineering*, 111(250), August 1989.

[9] David C. Viano and Chantal S. Parenteau. Analysis of head impacts causing neck compression injury. In *Traffic Injury Prevention*, pages 9:2, 144–152. Taylor and Francis, April 2008.

[10] LSTC. Lstc, livermore software technology corporation.

[11] Kleinberger M., Sun E., Eppinger R., Kuppa S., and Saul R. Development of improved injury criteria for the assessment of advanced automotive restraint systems. Technical report, National Highway Traffic Safety Administration, March 2000.

[12] Data Processing Vehicle Safety Workgroup. Crash analysis criteria description, October 2006. Arbeitskereis Messdatenverarbeitung Fahrzeugsicherheit.

[13] H. Mellander. Hic–the head injury criterion. In Sten Lindgren, editor, *Modern Concepts in Neurotraumatology*, volume 36 of *Acta Neurochirurgica*, pages 18–20. Springer Vienna, May 1986.

[14] SAE International. Sae j211-1: Instrumentation for impact test. Technical Report 49 CFR 571.202a, SAE International, May 4 2007.

[15] CEN. Road restraint systems - part 8: Motorcycle road restraint systems which reduce the impact severity of motorcyclist collisions with safety barriers. European Standard 1317-8 rev, European Committee for Standardization, August 2010. English Version, Draft.

[16] IIHS. Guidelines for rating injury measures. Frontal offset crashworthiness evaluation, Insurance Institute For Highway Safety, 1005 N. Glebe Road, Arlington VA 22201, May 2001.

[17] National Highway Traffic Safety Administration U.S. Department of Transportation. Test procedures for occupant crash pro-

tection. CFR FMVSS 208, Part 572, U.S. Department of Transportation, National Highway Traffic Safety Administration, Washinghton D.C., January 2003.

[18] Jeffrey H. Marcus. Dummy and injury criteria for aircraft crashworthiness. Technical Report DOT/FAA/AM-96/11, Civil Aeromedical Institute, Federal Aviation Administration, Oklahoma City, Oklahoma, U.S.A., April 1996.

[19] P. J. Bishop and R. Wells. The hybrid iii anthropometric neck in the evaluation of head first collisions. Technical Report 860201, SAE Technical Paper, Waterloo, Ontario, Canada, 1986.

[20] P. Rousseau and T. B. Hoshizaki. The influence of deflection and neck compliance on the impact dynamics of a hybrid iii headform. *Journal of Sports Engineering and Technology*, September 2009.

[21] S. Guha, D. Bhalsod, and J. Krebs. *LSTC Hybrid III Dummies, Positioning and Post-Processing*. LSTC, Michigan, dummy version: lstc.h3.103008 v1.0 edition, October 30 2008.

[22] Marco Anghileri, Luigi Casetelletti, and Emanuele Fracasso. Hybrid iii numerical model for aircraft seat crashperformance assessment. *Journal of Aircraft*, 44(5):1691– 1700, September-October 2007.

[23] Livermore Software Technology Corporation (LSTC), Livermore, California. *LS-DYNA® Keyword User Manual*, r8.0 edition, March 2015.

[24] Chawla A., Mukherjee S., Mohan D., and Jain S. Validation of the cervical spine model in thums. Technical Report 49 CFR 572.137, Department of Mechanical Engineering, Indian Institute of Technology, New Delhi-110016, India, May 2005.

[25] Garrett Anthony Mattos. *Characteristics of serious head injuries in pure rollover crashes and an evaluation of their replication in a dynamic rollover test*. PhD thesis, School of Aviation, Faculty of Science, UNSW University of New South Wales, March 2015.

[26] Mh. Lashkari, F. Frahmand, and K. Kangarlou. Finite elemet modeling of the humain brain under impact conditions. *IRJABS, International Research Journal of Applied and Basic Sciences*, 6:875–881, 2013.

[27] L. Zhang and A. I. King K. H. Yang. A proposed injury threshold for mild traumatic brain injury. *Journal of Biomechanical Engineering*, 126:226–236, April 2004.

[28] F. A. Pintar, A. Sances, N. Yoganandan, J. Reinartz, D. J. Maiman, J. K. Suh, G. Unger, J. F. Cusick, and S. J. Larson. Biodynamics of the total human cadaveric cervical spine. SAE Technical Paper 902309, SAE, October 1990.

[29] Nicholas Alan White. *Simulated automobile and rotary-wing aircraft impacts: dynamic neck response after surgical treatment for cervical spondylosis*. PhD thesis, Virginia Polytechnic Institute and State University, Blacksburg, VA, December, 9 2013.

[30] W.Fang, L. Guibing, and Y. Jikuang. A review of some available human neck finite element models in vehicle crash conditions. In IEE Computer Society, editor, *International Conference on Optoelectronics and Image Processing*, pages 104–107, 2010.

[31] Sances Jr. A, Carlin F., and Kumaresan S. Biomechanical analysis of head-neck force in hybrid iii dummy during inverted vertical drops. *Biomedical sciences instrumentation*, 38:459–464, 2001.

[32] E. G. Takhounts, R. H. Eppinger, J. Q. Campbell, R. E. Tannous, E. D. Power, and L. S. Shook. On the development of the simon finite element head model. *Stapp Car Crash Journal*, 47:107–133, October 2003.

[33] F. Bandak and R. Eppinger. A three-dimensional finite element analysis of the human brain under combined rotational and translational accelerations. *Stapp Car Crash Journal*, 38:145–163, 1995.

[34] J. G. Paver, D. Friedman, G. Mattos, and J. Caplinger. The developmento of iarv's for the hybrid iii neck modified for dynamic rollover crash testing. *ICRASH*, 121, 2010.

[35] R. W. Nightingale, J. H. McElhaney, D. L. Camacho, M. Kleinberger, B. A. Winkelstein, and B. S. Myers. The dynamic responses of the cervical spine: Buckling, end conditions, and tolerance in compressive impacts. Technical Report 973344, Duke University and National Highway Traffic Safety Administration, November 1997.

[36] K. Friedman, F. Gaston, J. Bish, D. Friedman, and Jr. A. Sances. An investigation of hybrid iii adn living human drop tests. *Critical Reviews in Biomedical Engineering*, 1, 2(28):219–223, 2000.